약학박사학위논문

Structural and functional studies of the DJ-1/ThiJ/*Pf*pI superfamily proteins from *Staphylococcus aureus*

포도상구균 유래의 DJ-1/ThiJ/*Pf*pI superfamily 단백질에 대한 구조와 기능 연구

2016 년 2 월

서울대학교 대학원

약학과 물리약학전공

김 효 정

Abstract

Structural and functional studies of the DJ-1/ThiJ/*Pf*pI superfamily proteins from *Staphylococcus aureus*

Hyo Jung Kim

Physical pharmacy

Department of pharmacy

The Graduate School

Seoul National University

Staphylococcus aureus is one of the most common pathogen that causes various diseases ranging from mild infections, such as skin infections and food poisoning, to life threatening infections, such as sepsis, endocarditis, and toxic shock syndrome. However, *S. aureus* has adapted to circumvent therapeutic strategies by developing resistance to antibiotics and becoming problems. The DJ-1/ThiJ/*Pf*pI superfamily is a group of proteins over diverse organisms. This superfamily includes versatile proteins, such as proteases, chaperones, heat shock proteins and human Parkinson's disease protein. SAV0551 and SAV1875, conserved proteins from *S. aureus*, are members of the DJ-1/ThiJ/*Pf*pI superfamily. However, their

structure and function remain unknown. Thus, to understand the function and activity mechanism of these proteins, the crystal structure of SAV0551 and SAV1875 from *S. aureus* was determined. Their conserved cysteine residue forms a catalytic triad with histidine and aspartate. In particular, cysteine in SAV1875 is spontaneously oxidized to Cys105-SO_2H in the crystal structure. To study the oxidative propensity of Cys105 in SAV1875 and the corresponding functional differences with changes in cysteine oxidation state, the crystal structures of SAV1875 variants, E17N, E17D, C105D, and over-oxidized SAV1875 were determined. The overall fold of SAV1875 and SAV0551 is similar to that observed for the DJ-1/ThiJ/*Pf*pI superfamily. We identified SAV1875 as a novel member of the YhbO-type subfamily exhibiting chaperone function and SAV0551 as a member of Hsp-type subfamily that has chaperone and glyoxalase function. The chaperone activity was based on the surface structure, but if SAV1875 is over-oxidized further with H_2O_2, its chaperone activity is eliminated.

Key words: DJ-1/ThiJ/*Pf*pI superfamily, *Staphylococcus aureus*, cysteine, oxidation, chaperone

Student Number: 2011-30503

Table of Contents

Abstract·····i

Contents·····iv

List of Tables·····viii

List of Figures·····ix

Contents

Chapter I. Introduction

1.1. *Staphylococcus aureus*

1.1.1. Features of *Staphylococcus aureus*·····1

1.1.2. Antibiotic resistance of *Staphylococcus aureus*·····2

1.2. DJ-1/ThiJ/*Pf*pI superfamily

1.2.1. Introduction of DJ-1/ThiJ/*Pf*pI superfamily·····3

1.2.2. Classification of DJ-1/ThiJ/*Pf*pI superfamily·····3

1.2.3. Protein members of DJ-1/ThiJ/*Pf*pI superfamily·····5

1.3. Research goals·····5

Chapter II. The structure and function of SAV0551

2.1. Introduction·····9

2.2. Materials and Methods

2.2.1. Cloning, protein expression, and purification·····11

2.2.2. Crystallization and data collection·····12

2.2.3. Structure determination and refinement·····13

2.2.4. Determination of chaperone activity·····13

2.2.5. Determination of glutathione independent glyoxalase activity·····14

2.3. Results

2.3.1. Structure of SAV0551·····15

2.3.2. Oligomeric state of SAV0551·····17

2.3.3. Catalytic triad of SAV0551·····20

2.3.4. SAV0551 has chaperon activity·····22

2.3.5. SAV0551 has glutathione independent glyoxalase activity·····23

2.4. Discussion·····26

Chapter III. The structure and function of SAV1875

3.1. Introduction·····29

3.2. Materials and Methods

3.2.1. Cloning, protein expression, and purification·····31

3.2.2. Crystallization and data collection·····33

3.2.3. PAGE·····34

3.2.4. Mass spectrometry·····34

3.2.5. Protein oxidation·····35

3.2.6. Circular Dichroism (CD)·····35

3.2.7. Protease activity assay and zymogram·····36

3.2.8. Determination of chaperone activity·····37

3.3. Results

3.3.1. Structure of SAV1875·····37

3.3.2. Oligomeric state of SAV1875·····40

3.3.3. Comparison of SAV1875 with DJ-1 superfamily proteins·····43

3.3.4. Stabilization of oxidized Cys105·····45

3.3.5. Oxidation propensity of Cys105 in SAV1875·····51

3.3.6. Protease activity of SAV1875 was not detected·····55

3.3.7. SAV1875 has chaperon activity·····57

3.4. Discussion·····59

Chapter IV. Summary·····62

References·····63

Korean Abstract (국문초록)·····71

List of Tables

Table 1. Classification of DJ-1/ThiJ/*Pf*pI superfamily·····4

Table 2. Primer design of SAV1875 mutants·····31

List of Figures

Figure 1. Micrograph of *S. aureus*·····1

Figure 2. Comparison of SAV0551 amino acid sequence to other members of the DJ-1/ThiJ/*Pf*pI superfamily·····10

Figure 3. Expression, purification, and crystallization of SAV0551·····15

Figure 4. Ribbon diagram of SAV0551·····17

Figure 5. The SAV0551 dimer·····18

Figure 6. Catalytic triad of SAV0551·····19

Figure 7. Surface structure of SAV0551·····20

Figure 8. The configuration of catalytic triad·····21

Figure 9. No significant difference in chaperone activity in wild type SAV0551 and cysteine mutants·····23

Figure 10. Remaining amount of methylglyoxal at 100 sec of time point·····25

Figure 11. Narrow active site cleft of SAV0551·····26

Figure 12. Comparison of SAV1875 amino acid sequence to other members of DJ-1/ThiJ/*Pf*pI superfamily·····30

Figure 13. Expression, purification, and crystallization of SAV1875·····38

Figure 14. Ribbon diagram of SAV1875·····39

Figure 15. Dimer structure of SAV1875·····40

Figure 16. Ribbon diagram of constrained hexamer SAV1875·····42

Figure 17. Surface structure of SAV1875·····43

Figure 18. The superposition of SAV1875 (cyan) with other members of the DJ-

1/ThiJ/*Pf*pI superfamily YhbO (pink), *Ph*pI (blue), DR1199 (orange), Ton1285 (green), and DJ-1 (Grey)·····44

Figure 19. A hydrogen bond·····46

Figure 20. Oxidation state of cysteine at residue 105·····48

Figure 21. Hydrogen bonds around Cys105·····49

Figure 22. Local difference around the reactive cysteine in DJ-1 (left) and SAV1875 (right)·····50

Figure 23. The geometry of cysteinesulfinic acid is not the same as aspartate··51

Figure 24. MS spectrometry and PAGE of SAV1875·····53

Figure 25. Over-oxidized SAV1875 does not lead to loss of secondary structure·····55

Figure 26. Comparison of oligomeric state in solution of YhbO-type DJ-1 superfamily·····56

Figure 27. Chaperone activity of SAV1875 depending on cysteine oxidation state·····58

Chapter I. Introduction

1.1. *Staphylococcus aureus*

Staphylococcus aureus is a gram positive bacterium that is usually found in the nasal passages and on the skin. This organism is part of the human normal flora, and is primarily found in the nose and skin. However, *S. aureus* is either one of the most common opportunistic pathogen that causes various diseases ranging from mild infections, such as skin infections and food poisoning, to life threatening infections, such as sepsis, endocarditis, and toxic shock syndrome [1]. Several exotoxins, which are secreted from *S. aureus*, are associated with specific diseases [2].

1.1.1. Features of *Staphylococcus aureus*

S. aureus belongs to the *Staphylococcaceae* family. It appears as grape-like clusters when viewed through a microscope, and has large, round, golden-yellow colonies. The spherical cells of *S. aureus* are up to 1 μm in diameter, non-motile, non-spore forming, facultative anaerobes that usually form in clusters [3].

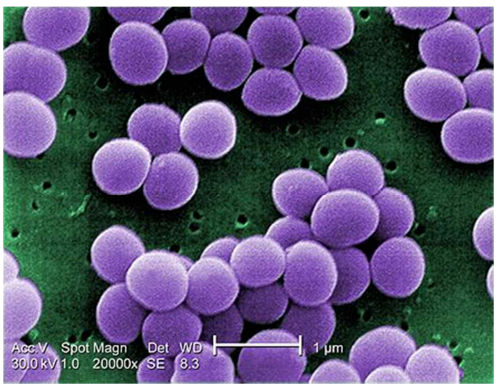

Figure 1. Micrograph of *S. aureus* (Matthew J. Arduino, DRPH Photo Credit)

1.1.2. Antibiotic resistance of *Staphylococcus aureus*

The treatment of choice for *S. aureus* infection was penicillin. Penicillin inhibits the formation of peptidoglycan cross-linkages that provides the rigidity and strength in a bacterial cell wall. However, soon after the advent of penicillin in 1946, 80% of hospital *S. aureus* isolates were penicillin-resistant by 1960 [4]. Nowadays, penicillin resistance is extremely common, and first-line therapy is most commonly a penicillinase-resistant β-lactam antibiotics (oxacillin or flucloxacillin). In many cases, treatment faces difficulties because of the evolution of resistant strains. MRSA, methicillin resistant *S. aureus* emerged. Today, MRSA accounts for over 60% of *S. aureus* infection, including nosocomial and community acquired infection [5]. Combination therapy can be used to treat serious infections, but its use is controversial because of the possibility of kidney damages. Recently, there are even newly emerging strains such as vancomycin resistant *S. aureus* (VRSA). More specifically, vancomycin resistant *S. aureus* bacteria are classified as VISA (vancomycin-intermediate *S. aureus*) if the minimum inhibitory concentration (MIC) against vancomycin is 4-8 μg/ml and classified as VRSA if the MIC is more than 16 μg/ml [6]. For example, *S. aureus* Mu50 (ATCC 700699), which was first isolated from a sternal abscess in a child who had received a prolonged course of vancomycin treatment [7], is classified as VISA because the MIC against vancomycin is 8 μg/ml [8, 9]. Because of this bacterial resistance, the prognosis of a *S. aureus* infection is still poor despite early diagnosis and appropriate treatment [10]. Currently, the spread of resistance in bacterial populations is a major health challenge. Therefore, understanding the detailed mechanism of how bacteria adapt to environmental changes is essential for developing better therapeutics. Thus, researches on the bacterial system under environmental stress condition are emerging as important issues.

1.2. DJ-1/ThiJ/*Pf*pI Superfamily

1.2.1. Introduction of DJ-1/ThiJ/*Pf*pI Superfamily

The DJ-1/ThiJ/*Pf*pI superfamily (DJ-1 superfamily hereafter) is a group of proteins over diverse organisms. This superfamily includes versatile proteins, such as proteases, chaperones, heat shock proteins and human Parkinson's disease protein. Mainly, DJ-1 superfamily proteins function as specific stress response proteins: *Escherichia coli* Hsp31, which is involved in thermal stress protection, acid resistance, and glyoxalase activity [11-13]; *Ph*pI and *Pf*pI, which are heat-endurable proteases from *Pyrococcus horikoshii* [14] and *Pyrococcus furious* [15], respectively; *Deinococcus radiodurans* DR1199, which is a general stress resistance protein [16]; and *E. coli* YhbO, a protein highly sensitive to oxidative, thermal, UV, and pH stresses [17].

Structurally, DJ-1 superfamily proteins share a common fold. Most members of DJ-1 superfamily proteins are oligomers from dimer to hexamer. Each monomer consists of the antiparallel β-strands surrounded by α-helices. This fold is called "α/β sandwich fold". In the core structure, there is a "nucleophilic elbow" is present, a sharp turn of a β-strand and an α-helix, which is common to several hydrolytic enzymes. On its extremely sharp turn, cysteine is located. This cysteine usually is a part of catalytic triad in DJ-1 superfamily proteins.

1.2.2. Classification of DJ-1/ThiJ/*Pf*pI superfamily

The DJ-1 superfamily proteins can be classified into subfamilies based on their quaternary structure; DJ-1-type, YhbO-type, and Hsp-type. Alternative oligomerization modes are a method of generating functional diversity in homologs

with a similar tertiary structure. Each subfamily has different characteristics in the oligomeric state and a catalytic dyad/triad conformation. The DJ-1-type proteins (DJ-1 and YajL) form a dimeric interface consisting of α-helices, β-strands, and loops. The YhbO-type proteins (YhbO, *Ph*pI, DR1199, and Ton1285) interact with the other subunits by three helices. The Hsp-type proteins (Hsp31) form a unique dimerization surface consisting of N terminal β strands and loops [18, 19]. DJ-1, YajL, and YdeA are the members of DJ-1-type DJ-1 subfamily. YhbO, *Pf*pI, DR1199, and Ton1285 are known proteins for YhbO-type DJ-1 subfamily. Hsp31 proteins from *E. coli, Candida albicans, Vibrio cholerae,* and *Saccharomyces cerevisiae* are categorized as Hsp-type DJ-1 subfamily members. In addition to the difference in dimerization modes among these subfamilies, there is also a difference in the architecture of catalytic triad. The DJ-1-type DJ-1 forms catalytic dyad with nearby histidine. The cysteine in the DJ-1-type YajL does not form catalytic dyad/triad. The YhbO-type proteins constitute a catalytic triad with cysteine, the histidine next to cysteine, and an acidic residue from the other subunit [11, 16]. The Hsp-type proteins form a catalytic triad using cysteine, the histidine next to cysteine, and an acidic residue from an intrasubunit from the other domain (cap domain). Consequently, these commonalities and distinctive features suggest that the oligomeric state and the reactive cysteine of DJ-1 superfamily proteins appear to be crucial in the functions of these proteins [20, 21].

	DJ-1-type DJ-1 superfamily	**YhbO-type DJ-1 superfamily**	**Hsp-type DJ-1 superfamily**
Examples	DJ-1	YhbO	*E. coli* Hsp31
	YajL	*Pf*pI	*V. cholerae* Hsp31
		Ton1285	*S. cereviseae* Hsp31
		DR1199	*C. albicans* Hsp31

Dimerization modes		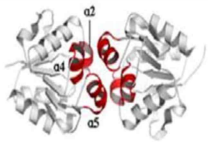	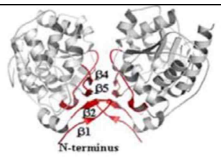

Table 1. Classification of DJ-1/ThiJ/*Pf*pI superfamily. DJ-1 superfamily can be divided into three distinct subfamilies depending on their dimeric interfaces. The DJ-1 dimer, YhbO dimer, and Hsp31 dimer are shown.

1.2.3. Protein members of DJ-1/ThiJ/*Pf*pI superfamily

Many of DJ-1 family proteins are of unknown function, and also are examples of proteins with both sequence and fold similarity that has multiple classes. DJ-1, a representative member of DJ-1-type DJ-1 subfamily protein is associated with Parkinson's disease and cancers. Deletion or mutations in DJ-1 are reported to be responsible for recessive early onset of Parkinson disease. However, the detailed mechanisms are still not fully revealed. DJ-1 plays a protective role against oxidative stress. It functions as a redox sensitive regulator of suppressing the JNK signaling pathways or interacts with Daxx and sequesters in within the nucleus, preventing the initiation of apoptotic signals [22, 23]. It also acts as a chaperone that helps folding of α-syneclin. YhbO-type DJ-1 subfamily members are stress response proteins that protect cells from oxidative, thermal, and pH stresses. Some proteins (*Pf*pI, *Ph*pI, and Ton1285) of YhbO-type DJ-1 subfamily revealed proteolytic activity. Hsp-type DJ-1 proteins are mostly 31 kDa of chaperones and also have glyoxalase III activity.

1.3. Research goals

Bacteria are designed to be adaptable to their circumstance. In the changes in temperature, pH, radiation, oxidation, and other nature of the surrounding support, bacteria adapt to environment. Bacterial surrounding layers, genetic information for resistance, and other structures associated with a bacterium are capable of alteration. Some alterations are reversible, disappearing when the particular pressure is lifted. Other alterations are maintained and can even be passed on to succeeding generations of bacteria. This adaptation is under tight genetic control, involving the expression of multiple genes. The examples are the responses shown by *Helicobacter pylori* to growth in an acidic environment of stomach and *Deinococcus radiodurans* to growth in a harsh radiation. Bacteria also react to sudden changes in their environment by expressing or repressing the expression of a whole list of genes. A well-known example of this adaptation is the heat shock response of *E. coli*. The name derives from the fact that the response was first observed in bacteria suddenly shifted to a higher growth temperature. Another adaptation exhibited by *Vibrio parahaemolyticus* is the formation of adherent populations on solid surfaces. This mode of growth is called a biofilm, involving the expression of previously unexpressed genes. In addition, deactivation of actively expressing genes can occur.

Some harmful bacteria are adapting to drugs faster than cures can be developed. Resistance is an example of adaptation of the bacteria to environment. The introduction of first antibiotic is followed by the development of resistance to the agent. The adaptation of bacteria to an antibacterial agent can occur in two ways. The first method is known as inherent resistance. For example, gram-negative bacteria are often naturally resistant to penicillin. This is because bacteria have another outer membrane, which makes the penetration of penicillin to its target more difficult. The second method is called acquired resistance due to a change in the genetic information of the bacterial genome. Acquired adaptation can occur because of mutation or as a response by the bacteria to the selective pressure

imposed by the bacterial agent. Once the genetic alteration that confers resistance is present, it can be passed on to the subsequent generations.

S. aureus is notorious for its ability to become resistant to many antibiotics. Methicillin-resistant *Staphylococcus aureus* (MRSA) isolates soon after the introduction of methicillin. First, MRSA isolates have been associated with nosocomial infections and rapidly developed resistance to multiple drug classes. In recent years, reservoir of community associated MRSA is rapidly expanding. Compared to nosocomial strains, community-associated MRSA isolates are associated with increased virulence and currently are more likely to be susceptible to a variety of antibiotics. Vancomycin non susceptibility in *S. aureus* is on the increase, requires further complicating therapy. Study of early isolates of MRSA showed that a key genetic component responsible for resistance, *mecA*, is not native to the *S. aureus* genome. This genetic element confers resistance to most currently available β-lactam antibiotics. However, not all *mecA* clones are resistant to methicillin, modulated by a variety of chromosomal factors. In the early MRSA that has the *mecA* gene do not express methicillin resistance, but soon after, mutations on control regulator genes occur and the strains become resistant to methicillin. Today, most MRSA strains are resistant to multi drugs including vancomycin.

S. aureus is one of the well-known pathogens causing many forms of infection ranging from mild to life threatening. The bacteria tend to infect the skin, often cause superficial skin lesions such as boil, furuncle, abscess, and styes. However, the bacteria can travel through the bloodstream and infect organs in the body, particularly lung (pneumonia), heart valves (endocarditis), and bones (osteomyelitis). Among many strains of *S. aureus*, some strains produce toxins that can cause toxic shock syndrome. *S. aureus* infection is an important infection with an incidence rate ranging from 20 to 50 cases/100,000 population per year. The mortality rate due to *S. aureus* infection is between 10% and 30%. Comparatively,

this accounts for a greater number of deaths than for AIDS, tuberculosis, and viral hepatitis combined [24].

Previously, researches have concentrated on developing more powerful antibiotics to cope with the increased resistance. But developing more powerful antibiotics contributes to concerns about antibiotic-resistant bacteria. Researches about fundamental mechanisms of bacterial physiology to adapt varying environment are currently ongoing, but still remain elusive. Thus, our research focused on the alteration of bacterial proteins under stress conditions. Since DJ-1 superfamily proteins are known as stress-response proteins, we expected that these proteins would show defensive roles under stress condition.

Herein, we elucidated the crystal structures of SAV0551, SAV1875, mutants of wild type proteins, and over-oxidized SAV1875. To gain insight on the function, chaperone, protease, and glyoxalase activity tests were conducted. These functional tests revealed SAV0551 and SAV1875 as multi-functional proteins. Since the wild type SAV1875 is oxidized in the crystal structure, this protein is predicted to be related to oxidative stress defense system. The three mutants, E17N, E17D, and C105D, and over-oxidized SAV1875 containing Cys105-SO_3H (cysteinesulfonic acid) were designed to identify the oxidative propensity of Cys105 as well as the corresponding structural and functional differences. The structural and functional research under oxidative condition will promote a better understanding of bacterial physiology and how bacteria defend against oxidative stress.

Chapter II. The structure and function of SAV0551

2.1. Introduction

From the sequence homology among Hsp-type DJ-1 subfamily members, SAV0551 is predicted to be classified into Hsp-type DJ-1 subfamily: Hsp31 from *E.coli* (54% sequence identity), Hsp31 from *Vibrio cholerae* (49% sequence identity), and Hsp31 from *Saccharomyces cerevisiae* (12% sequence identity). A structure-based sequence alignment was acquired using the ClustalW web server tool [25] and viewed using the ESPript web server tool [25]. The sequence alignment of SAV0551 with Hsp31 proteins from *E. coli*, *V. choleae*, and *S. cerevisiae* is shown in Figure 2. Form the sequence information, SAV0551 is predicted to have chaperone and glyoxalase function as well based on similarity to others of Hsp-type DJ-1 subfamily proteins. SAV0551 gene codes 292 amino acids. The estimated molecular weight is 32 kDa and calculated pI is 4.90.

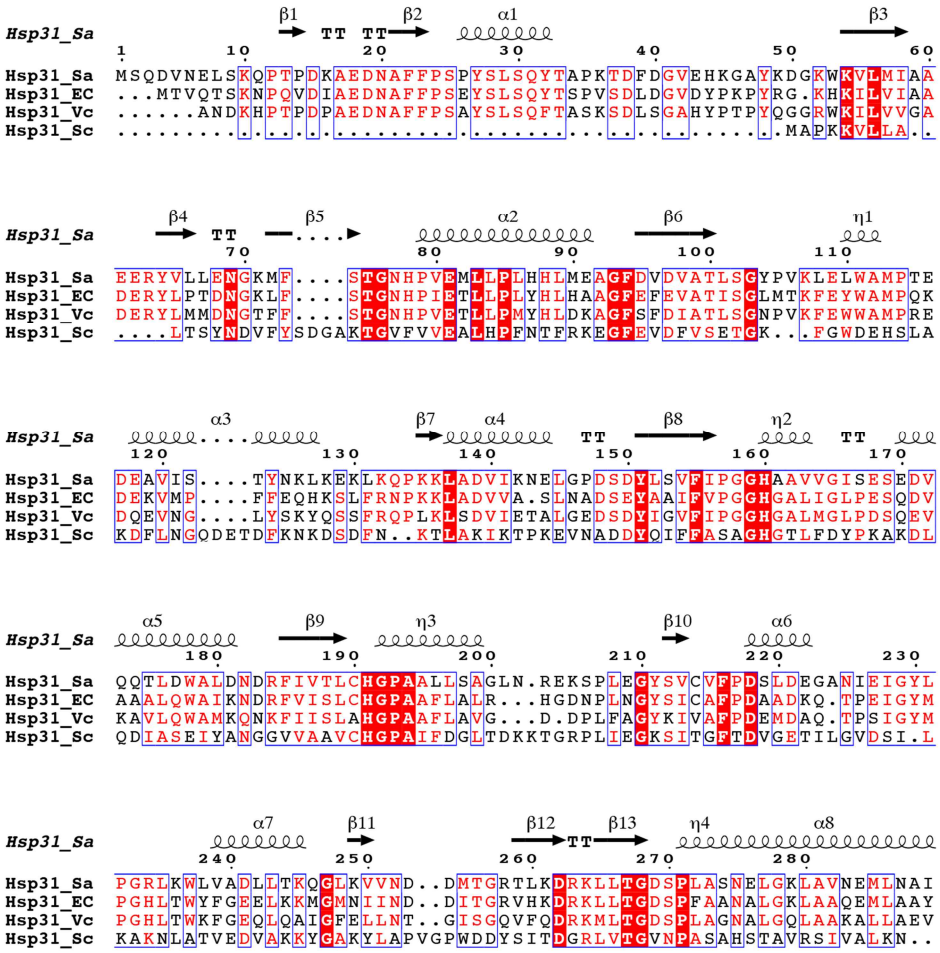

Figure 2. Comparison of SAV0551 amino acid sequence to other members of Hsp-type DJ-1/ThiJ/*Pf*pI superfamily.

Sequence alignment of SAV0551 with *E.coli* Hsp31 (54% sequence identity), *Vibrio cholerae* Hsp31 (49% sequence identity), and *Saccharomyces cerevisiae* Hsp31 (12% sequence identity). Identical residues are colored white on a red background and similar residues are red on a white background. Secondary structure elements (springs, α-helices; arrows, β-strands) are represented above the sequences and are numbered. The figure was constructed using ESPript [25].

2.2. Materials and Methods

3.2.1. Cloning, protein expression, and purification

The predicted ORF of Hsp31 (SAV0551) was amplified from *S. aureus* MU50 genomic DNA using standard PCR methods. The forward and reverse oligonucleotide primers designed using the published genome sequence were 5'-GACTGCATATGTCACAAGATGTAAATGAATTAAG and 5'- GTCACTCGAGT TTATTTTGTATTGCATTTAACAT, respectively, where the bases underlined represent the NdeI and XhoI restriction enzyme cleavage sites. The amplified DNA was inserted into the NdeI/XhoI-digested expression vector pET-21a(+) expression vector (Novagen Inc., USA). The resulting construct contains eight nonnative residues at the C-terminus (LEHHHHHH) that facilitate protein purification. The accuracy of the cloning was confirmed by DNA sequencing. The resulting expression plasmid was then transformed into *E. coli* BL21(DE3) cells (Novagen Inc., USA).

To prepare mutants, the EZchange Site-directed Mutagenesis kit (Enzynomics Inc., Republic of Korea) was used to generate point mutations in the SAV0551 recombinant pET-21a(+) plasmid. The point mutations resulted in separate multiple recombinant plasmids, specifically C190A and C190D. The sequences of the reconstructed mutants were confirmed by DNA sequencing (data not shown).

Wild type and SAV0551 mutants (C190A and C190D) cells were grown at 37°C until the OD600 reached 0.6 and expression was induced by the addition of isopropyl-β-D-thiogalactopyranoside (IPTG) to a final concentration of 0.5 mM. After an additional 4 hr of growth at 37°C, cells were harvested by centrifugation and resuspended in 50 mM Tris-HCl, pH 7.5, 0.5 M NaCl and 20 mM imidazole buffer. Cells were lysed by sonication at 4°C and the supernatant was loaded to Ni^{2+}-NTA column (Qiagen; 3 ml of resin per liter of cell culture) previously

equilibrated with the same buffer. The column was washed extensively with wash buffer (50 mM Tris-HCl, pH 7.5, 0.5 M NaCl, and 50 mM imidazole); then the bound protein was eluted with elution buffer (50 mM Tris-HCl, pH 7.5, 0.5 M NaCl, and 500 mM imidazole) until there was no detectable absorbance at 280 nm in the elutant. Fractions containing protein were concentrated to about 2 ml and applied to a Superdex 75 (10/300 GL) column (GE Healthcare Life Sciences, Germany) column that had been equilibrated with the final buffer (50 mM Tris-HCl, pH 7.5 and 0.15 M NaCl). Purified protein was judged to be over 95% pure by SDS-PAGE. The protein solution was concentrated using 10,000 MWCO spin columns (Millipore, USA). The protein concentration was estimated by measuring the absorbance at 280 nm, employing the calculated extinction coefficient of 35,535 $M^{-1}cm^{-1}$.

2.2.2. Crystallization and data collection

Crystallization was performed at 293 K by the hanging-drop vapor diffusion method using 24-well VDX plates (Hampton Research, USA). Initial crystallization conditions were established using screening kits from Hampton Research (Crystal Screens I and II, Index, PEG/Ion, and MembFac) and from Emerald BioSystems (Wizard I, II, III and IV). For the optimal growth of the SAV0551 crystals, each hanging drop was prepared on a siliconized cover slip by mixing 1 µl of protein solution and 1 µl of precipitant solution (23% (w/v) PEG3350, 100 mM BisTris, pH 6.0), and this drop was equilibrated against a 1 ml reservoir of precipitant solution. These conditions yielded needle-shaped crystals for each protein that grew to dimensions of 1.0 × 0.3 × 0.2 mm in two days. All crystals belonged to space group P212121 and contain eight molecules per asymmetric unit.

For crystal freezing, the crystals were transferred to a cryoprotectant solution with 30% (v/v) ethylene glycol in the crystallization condition for several minutes

before being flash-frozen in a stream of nitrogen gas at 100 K. Diffraction data were collected on beam-lines 5C at the Pohang Light Source, South Korea. The raw data were processed and scaled using the HKL2000 program suite [26]. Further data analysis was carried out using the CCP4 suite [27].

2.2.3. Structure determination and refinement

To determine the structure of wild type SAV0551, molecular replacement was used with the program Molrep [28] within the CCP4 suite [27] using the homologous structure of Hsp31 from *V. cholerae* (PDB code 4I4N) as a search model. Refinement of each crystal structure was done through iterative cycles of model building using COOT [29], followed by refinement of the models with Refmac5 [30]. A 5% portion of the data were set aside prior to refinement for the Rfree calculations for each data set [31]. Solvent molecules became apparent in the later stages of refinement and were added into the model. Further refinement was pursued until no further decrease in Rfree was observed. Structural alignments were carried out using the program PyMOL and Chimera [32], which were then used for the construction and generation of all figures. Protein interfaces, surfaces and assemblies were calculated using the PISA server at the European Bioinformatics Institute [33].

2.2.4. Determination of chaperone activity

To monitor the chaperone activity of wild type and the SAV0551 mutants, citrate synthase was employed as a substrate [34, 35]. Initially, to identify chaperone activity, 75 μg of citrate synthase (Sigma-Aldrich Inc., USA) was mixed with a solution of 100 mM Tris-HCl, pH 8.0, 20 mM dithiothreitol (DTT), 6 M guanidine chloride (GnCl). The citrate synthase mixture (75 μg of citrate synthase, 100 mM Tris-HCl, pH 8.0, 6 M GnCl, 20 mM DTT) was incubated for 1 hr at 25°C; consequently, the citrate synthase in this solution was denatured. After incubation,

refolding of citrate synthase was achieved by 100-fold dilution with a solution of 100 mM Tris-HCl (pH 8.0) containing 5 μM wild type and the SAV0551 mutants. The diluted solution was mixed with acetyl-CoA, oxaloacetate, $MnCl_2$ and 5,5'-dithiobis-(2-nitrobenzoic acid) (DTNB) to detect the activity of citrate synthase (100 mM Tris-HCl, pH 8.0, 1 mM DTNB, 0.2 mM $MnCl_2$, 0.4 mM oxaloacetic acid, 0.3 mM acetyl-CoA). After mixing, only the active, refolded enzyme will break acetyl-CoA into the acetyl group and CoA. The CoA reacts with DTNB, which acts as a coloring agent, and this produces a yellow TNB-CoA-SH compound that is detectable at 412 nm using a Multi-Mode microplate reader (SpectraMax M5e, USA). After a 48 min reaction period, the highest specific activity value obtained for TNB-CoA-SH was considered 100% and the lowest was 0%. The calculated specific activities of the wild type and the SAV0551 mutants were expressed as a percentage of this value.

2.2.5. Determination of glutathione independent glyoxalase activity

The glyoxalase activity assay of wild type and the SAV0551 mutants was performed using the methylglyoxal (Sigma, 40% solution). The reaction was initiated by adding enzyme in reaction buffer (100 mM HEPES, pH 7.5, 50 mM KCl, 2 mM DTT) with 6 mM methylglyoxal. The reaction mixture of methylglyoxal and protein (wild type and the SAV0551 mutants) were incubated at 20°C. The final concentration of protein was 10 μM. The remaining methylglyoxal at each time point was determined by reaction with 2,4-dinitrophenylhydrazine (DNPH) to generate the purple chromophore mehtylglyoxal-bis-2,4,-dinitrophenylhydrazone after alkali treatment.

The assay was performed by removing a 50 μl sample of the reaction at fixed time points after enzyme addition (0 sec, 20 sec, 40 sec, 60 sec, 80 sec, 100 sec, and 120 sec) and rapidly mixing with 0.9 ml of distilled water. To this solution, 0.33 ml of a freshly prepared stock of DNPH reagent (0.2% DNPH dissolved in 2 N HCl) was

immediately added and incubated at 37°C for 15 min. This highly acidic solution stops the enzymatic reaction, whose rate was already greatly diminished by the initial 19-fold dilution into water. The purple color of the hydrazine was developed by addition of 1.67 ml of 3.8 M NaOH and incubation for 5-10 min at room temperature followed by measurement of absorbance at 550 nm in a SpectraMax M5e. All measurements were made in triple times.

2.3. Results

2.3.1. Structure of SAV0551

The SAV0551 sample was prepared as a concentration of 10 mg/ml (Figure 3).

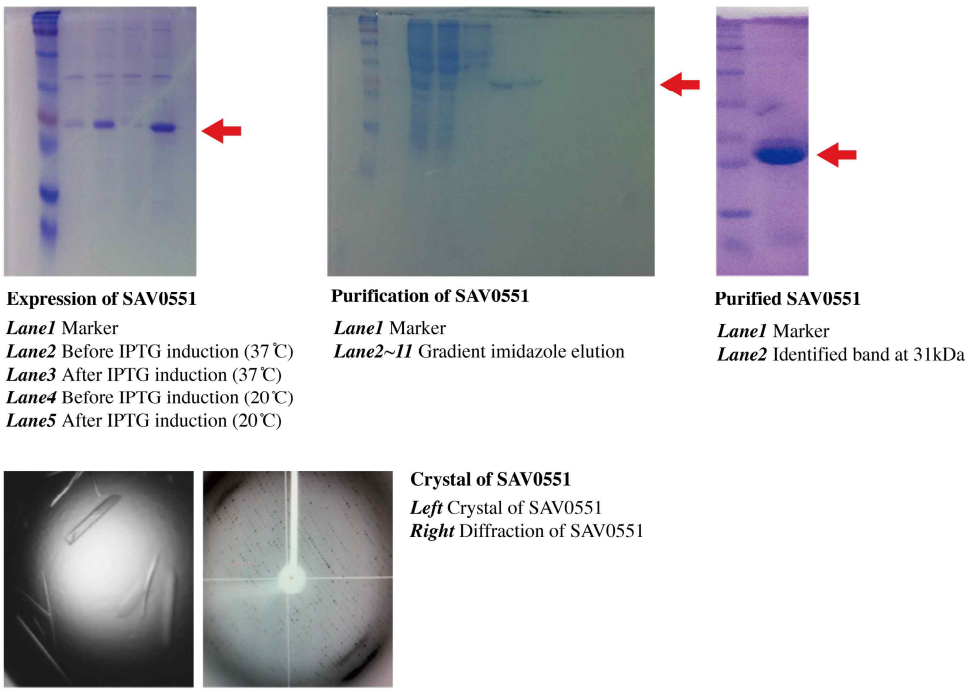

Figure 3. Expression, purification, and crystallization of SAV0551.

SAV0551 sample was prepared to determine the structure and function. The SAV0551 was over expressed by IPTG induction system, and purified using Ni^{2+}-NTA affinity column. Protein purity is measured over 95% based on SDS-PAGE. SAV0551 crystallizes in a condition of 23% (w/v) PEG3350, 100 mM BisTris, pH 6.0. The crystal diffracted to a 2.6 Å of resolution.

SAV0551 crystallizes in a space group P212121, with four dimers in the asymmetric unit. The crystal structure of SAV0551 was determined at 2.6 Å resolution including the additional C-terminal histidine tag. The protein consists of two domains: a core domain whose similarity to DJ-1 superfamily proteins had been expected, and a cap domain, which has also called "P" region. The core domain consists of an α/β sandwich fold with eleven α-helices and eight β-strands. Six β-strands, β4 (residues 93-97), β1 (residues 52-56), β5 (residues 149-154), β6 (residues 183-187), β8 (residues 263-266), and β7 (residues 257-260), are aligned in the center, wherein the latter β7 strand is anti-parallel to the central β-strands. Nine helices surround the core of β-strands. α11 (residues 269-287), α2 (residues 77-89), α3 (residues 108-110), α4 (residues 116-125), α5 (resides 135-142), α6 (residues 158-161), α7 (residues 168-179), α8 (residues 190-196), and α10 (237-243) are around the core in a clockwise direction. In addition, two short α-helices (α1 (resides 135-142) and α9 (resides 135-142)) and two β-strands (β2 (resides 135-142) and β3 (resides 135-142)) form cap domain. These core domain and cap domain are linked via a 22-residue-long-linker (residues 31-51) (Figure 4).

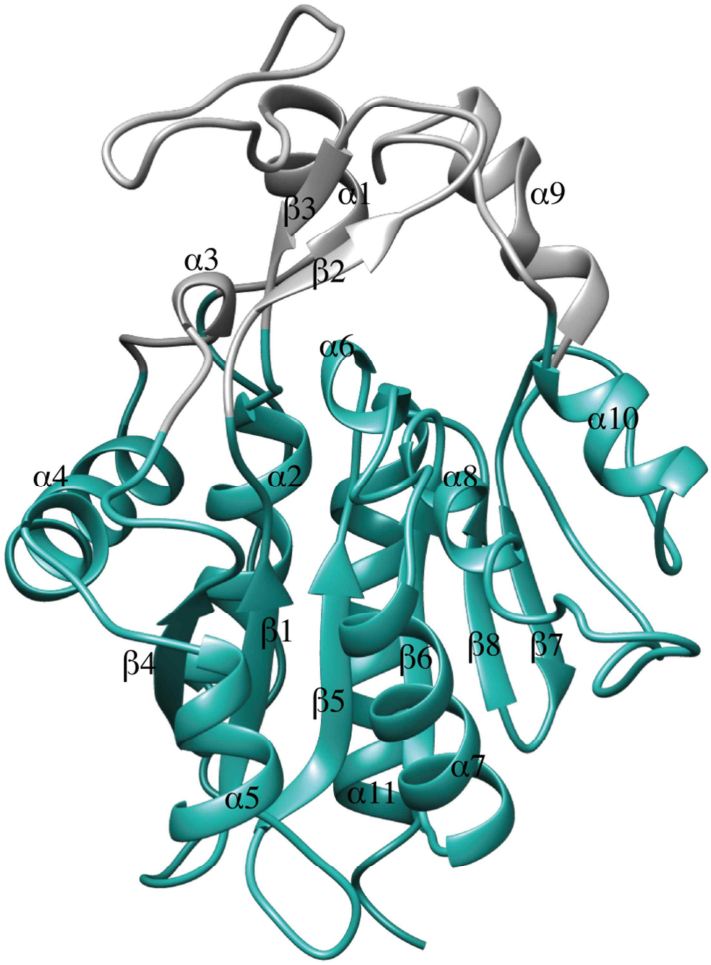

Figure 4. Ribbon diagram of SAV0551.

Ribbon representation of the SAV0551 monomer. Main domain is colored in cyan and additional cap domain is colored in grey. SAV0551 shows a sandwich structure with a α1-β1-β2-β3-α2-β4-α3-α4-β5-α6-α7-β6-α8-α9-α10-β7-β8-α11 topology.

2.3.2. Oligomeric state of SAV0551

The dimer structure of SAV0551 is consistent with the results of size exclusion chromatography indicating an apparent molecular mass of 65 kDa, which is double the size of the monomer. The loops and β-strands from cap domain are responsible

for dimer formation (Figure 5). Each monomer contains catalytic triad consisting of Cys190 and His191 from the core domain and Asp221 from the cap domain. The Cys190 S^{γ} interacts with His191 $N^{\delta 1}$, while the Asp221 carboxylate hydrogen bonds with His191 $N^{\varepsilon 2}$ (Figure 6). This catalytic triad is well conserved in Hsp-type DJ-1 superfamily proteins. In the crystal structure, oxygen atoms are modeled near the S^{γ} atom of Cys190 in chain A, B, D and G. This result is not consistent with the structure of SAV1875, another DJ-1 superfamily protein from the same organism. Although we have identified two oxygen atoms are covalently bound to Cys105 S^{γ} in the crystal structure of two chains in SAV1875 previously, the oxidation state of Cys190 in SAV0551 is not consistent among eight chains. Since this catalytic triad is predicted to have a catalytic function, cysteine mutant C190A was designed. To mimic the oxidized cysteine, C190D mutant was also designed.

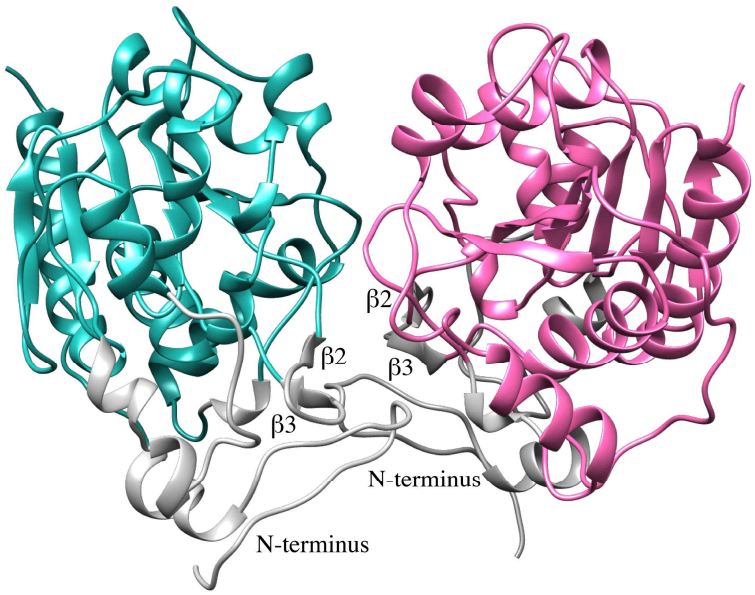

Figure 5. The SAV0551 dimer.

β2, β3, and N-terminus loop of cap domain are mainly involved in dimeric conformation.

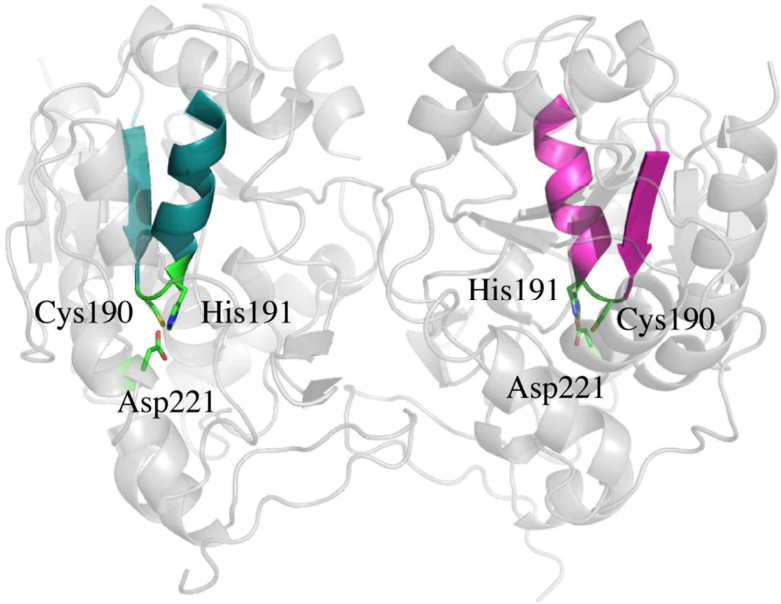

Figure 6. Catalytic triad of SAV0551.

The nucleophilic elbow (strand-nucleophile-helix motif) in each domain is shown in cyan and magenta. The catalytic triad is shown as sticks (Cys190, His191, and Asp221). The catalytic triad is located on the cleft region between main domain and cap domain.

When viewing the surface area, the majority of the surface is negatively charged with the exception of hydrophobic patches. The dimer results in a large concave structure and canyon structure, a hydrophobic bowl that measured ~20 Å in diameter and a canyon ~10 Å in depth. The catalytic triad is exposed toward the solvent accessible area, but the opening is restricted (measured ~6 Å in a diameter) (Figure 7).

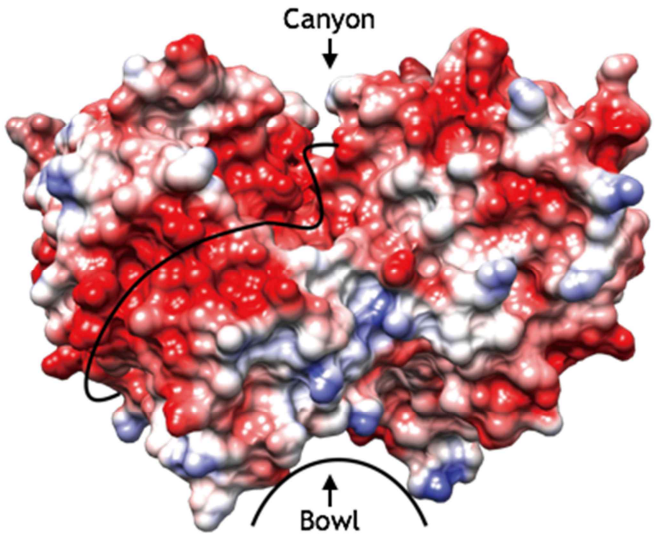

Figure 7. Surface structure of SAV0551.

Potential surface charge of the crystal structure of SAV0551, calculated with Chimera [32], where surfaces are colored between -10 kcal/mol·e (red) and +10 kcal/mole·e (blue). Canyon and bowl are labeled.

2.3.3. Catalytic triad of SAV0551

All the DJ-1 superfamily proteins share the reactive cysteine residue at a sharp turn between a β-strand and an α-helix, a "nucleophilic elbow". Mostly, the cysteine at the nucleophilic elbow forms catalytic triad together with a histidine and an acidic residue. Although the nucleophilic elbow and a cysteine are absolutely conserved in DJ-1 superfamily members, catalytic triad is not strictly conserved. Many of DJ-1-type DJ-1 subfamily proteins dose not contain catalytic triad. DJ-1-type DJ-1 lacks histidine residue next to Cys106, but His126 was found within 5 Å to Cys106, instead, forming catalytic dyad. DJ-1-type YajL lacks histidine residue around reactive cysteine. YhbO-type and Hsp-type DJ-1 subfamily proteins have conserved catalytic triad, but the architecture of the catalytic triad is different.

YhbO-type DJ-1 subfamily has catalytic triad with a cysteine, histidine next to cysteine, and an acidic residue from adjacent subunit. The catalytic triad that was found in Hsp-type DJ-1 subfamily protein consists of cysteine and histidine from the core domain and an acidic residue (Glu/Asp) from cap domain. Furthermore, even though the overall topology is similar, the configuration of the catalytic triad results in an opposite "handedness" between the two subfamilies (Figure 8).

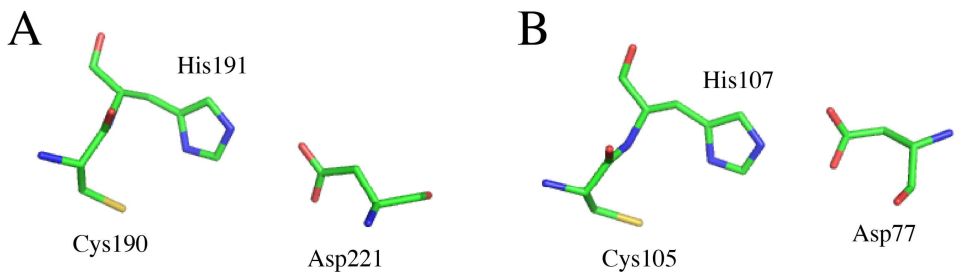

Figure 8. The configuration of catalytic triad.
The configuration of the catalytic triad results in an opposite "handedness".
(A) Catalytic triad in Hsp-type DJ-1 subfamily protein SAV0551. (B) Catalytic triad in YhbO-type DJ-1 subfamily protein SAV1875. This shows an opposite handedness of catalytic triad.

SAV0551 is a Hsp-type DJ-1 subfamily member and it shares the same structural arrangement of catalytic triad as other members of Hsp-type DJ-1 subfamily. Residues 183-196 (α8 and β6) of SAV0551 form the nucleophilic elbow. Cys190 at the nucleophilic acid forms catalytic triad together with His191 and Asp221. One of the dissimilarity in catalytic triad of Hsp31-type proteins is shown for the acidic residue. It can be substituted to glutamate if the origin of Hsp31 protein is yeast. Taken together, the presence of cap domain, the oligomeric interface that is consisted of cap domain loops, and the features of catalytic triad prove SAV0551 is

a member of Hsp-type DJ-1 subfamily [11].

2.3.4. SAV0551 has chaperon activity

Hsp-type DJ-1 subfamily proteins are highly conserved and function as molecular chaperones which facilitate the synthesis and folding of proteins. Under the stress conditions such as heat shock, pH shift, or oxidation, increased expression of chaperone proteins protect cells by stabilizing unfolded proteins, giving cell time to repair or re-synthesize damaged proteins. Molecular chaperones have been divided into three functional subclasses based on their mechanism of action. “Folding” chaperones (DnaK and GroEL) rely on ATP-driven conformational changes to mediate the net refolding of their substrates [36]. “Holding” chaperones (Hsp31, Hsp33, and IbpB) stabilize partially partially folded proteins on their surface and rapidly release them in an active form once the stress has abated. It plays an important role in protecting cells from severe stress condition [37, 38]. The third class of chaperone, “disaggregating” (ClpB) promotes the solubilization of proteins that have been aggregated as a result of stress [39]. Hsp31 proteins are kwon as holdase, a holding molecular chaperone. To hold unfolded substrates, the surface structure of Hsp31 is crucial. Hsp31 from *E.coli*, work as dimers by forming a deep acidic canyon and bowl on their dimeric interface [11]. When the surfaces of Hsp31 from *E. coli* were viewed, hydrophobic patches were detected around the canyon for the binding of unstructured proteins [40]. SAV0551 expresses similar surface patterns of a canyon and bowl as Hsp31 from *E. coli*. SAV0551 has a deep acidic canyon that winds from the dimeric interface to each side of the subunit, and bowl structure is located on the bottom side. The hydrophobic patches are detected around the canyon. This characteristic surface structure is well conserved in other Hsp-type DJ-1 subfamily members. The wild type and the SAV0551 mutants were tested for chaperone activity using citrate synthase. The observed data shows a chaperone-facilitated renaturation of citrate synthase in the wild type and the

SAV0551 mutants. There are no significant differences in the chaperone activity between the wild type and the SAV0551 mutants. From this study, we identified SAV0551 as a chaperone protein from *S. aureus* and that the presence of cysteine is not the key elements for the chaperone function (Figure 9).

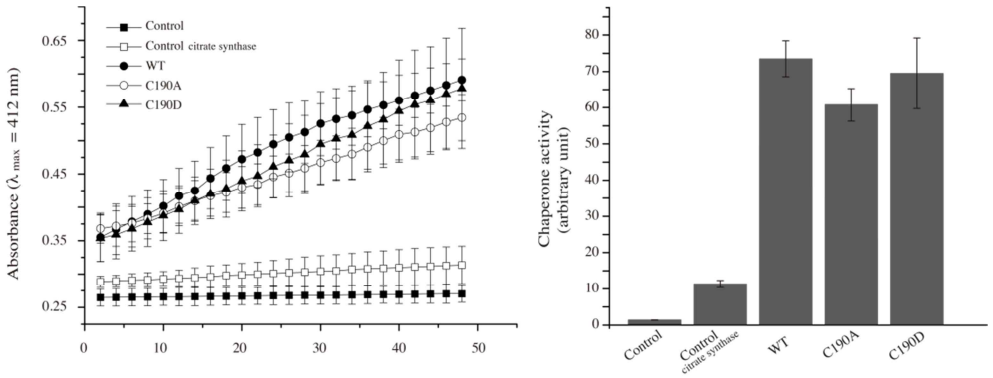

Figure 9. No significant difference in chaperone activity in wild type SAV0551 and the cysteine mutants.

SAV0551 exerts a chaperone function. The chaperone activity was assayed by monitoring an increase in absorbance at 412 nm. (A) The control (■) contained 50 µl of the reaction mixture only, which was 1 mM DTNB, 0.2 mM $MnCl_2$, 0.4 mM oxaloacetic acid, 0.3 mM acetyl-CoA in 100 mM Tris-HCl buffer (pH 8.0). The control with citrate synthase (□) contained an additional 0.75 µg of denatured citrate synthase. A final concentration of 5 µM was used for the wild type (●), C190A (○) and C190D (▲). (B) The calculation of chaperone activity at the 48 minutes time point. The data from three scans were averaged.

2.3.5. SAV0551 has glutathione independent glyoxalase activity

Endogenous methylglyoxal is generated as an unavoidable consequence of glycolysis. It also formed by lipid peroxidation systems, metabolism of acetone,

and the degradation of DNA [41]. Methylglyoxal is a known endogenous and environmental mutagen, which can modify both DNA and proteins. To detoxify methylglyoxal, there is glyoxalase system that converts methylglyoxal to non-toxic D-lactate. The glyoxalase system is accomplished by the sequential action of two thiol-dependent enzymes: glyoxalase I and II in the presence of glutathione (GSH) [42]. Recently, a GSH-independent glyoxalase system of Hsp31 was identified in *E. coli*. In this system, the *E. coli* Hsp31 converts methylglyoxal directly to D-lactate in a single step, independent of GSH [12]. The reactive cysteine and catalytic triad are shown to be responsible for the function, but the detailed mechanism of how Hsp31 executes these functions remains to be determined. To determine the glyoxalase III activity, wild type, the SAV0551 mutants, and SAV1875 were used. SAV1875 is also DJ-1 superfamily protein, which has a catalytic triad and reactive cysteine. The level of methylglyoxal is reduced substantially by the time when it was mixed with wild type SAV0551. However, cysteine mutants C190A and C190D do not show any difference in remaining amount of methylglyoxal. This result indicates that reactive cysteine is crucial for glyoxalase III function. Moreover, SAV1875 shows half of SAV0551's glyoxalase activity (calculated from the amount of remaining methylglyoxal at 100 second time point) (Figure 10). Considering cysteine on catalytic triad is the key component for its action, this result may be due to the local structure of catalytic triad. The surface structure of SAV1875 around catalytic triad is of a great different shape from SAV0551. In the crystal structure of SAV1875, the catalytic triad is exposed to solvent area with about 6 Å in width. On the other hand, the catalytic triad of SAV0551 is positioned deep inside of the surface with narrow opening (3 Å). This structure shows SAV0551 allows only small molecules to access its catalytic triad. Methylglyoxal is a small molecule, which could be a perfect fit inside restricted pocket of SAV0551 (Figure 11). From this study, we can figure out not only just presence of catalytic triad, but the approach to catalytic triad is important for its glyoxalase

function.

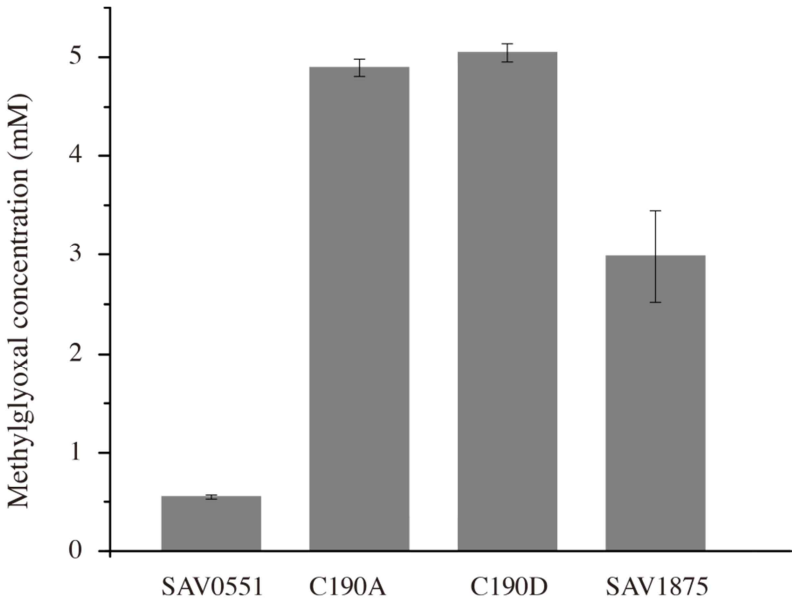

Figure 10. Remaining amount of methylglyoxal at 100 sec of time point.

SAV0551 exerts glyoxalase activity. It degrades methylglyoxal. 6 mM methylglyoxal was used initially. The remaining amount of methylglyoxal at 100 second time point is indicated as a graph.

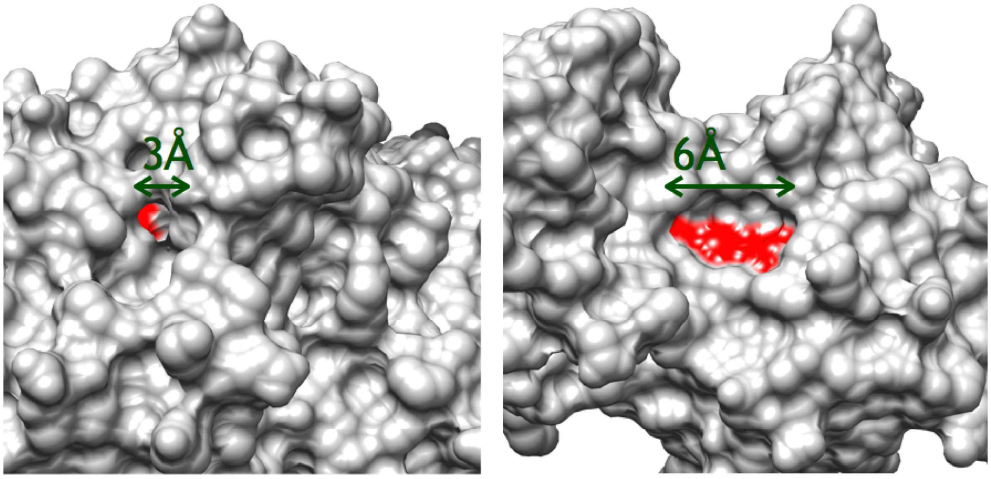

Figure 11. Narrow active site cleft of SAV0551.

The narrow opening of active site is selective for small substrate such as methylglyoxal.

2.4. Discussion

Chaperone is a class of proteins that assist folding or assemble of other macromolecular structures. Chaperones assist folding of newly synthesized proteins, repairing misfolded proteins, and eliminating aggregated proteins. Hsp31, holding chaperone, is known to repair misfolded protein by holding unfolded protein on its surface area. This chaperone function becomes more crucial when the cells are exposed to a harsh condition, such as heat, radiation, and oxidative stress. Chaperones help misfolded proteins, which are damaged by various stresses, to retrieve their normal biological function. Heat shock proteins are expressed when cells are under stress conditions. The structural studies herein confirmed SAV0551 as a member of the Hsp-type DJ-1 superfamily and is has all the pertinent traits of

this group, including the shape of dimerization interface using cap domain and the architecture of catalytic triad. For the interaction of unfolded proteins, hydrophobic bowl, a deep canyon, and hydrophobic patches are known as important characteristics of *E. coli* Hsp31. Similar to Hsp31 of *E. coli*, the quaternary structure of SAV0551 has analogous features. The dimer structure contains about 20 Å width hydrophobic bowl and a deep acidic canyon that winds from one subunit to another. The highly conserved hydrophobic patches are also detected on the surface of SAV0551. Because the Hsp-type DJ-1 superfamily members are well-known as Hsp31, holding chaperone, SAV0551 is also predicted to perform similar biological function. We discovered that the wild type and cysteine mutants of SAV0551 assisted in the folding of citrate synthase regardless of the presence of cysteine. Further detailed studies on diverse substrates and *in vivo* tests are needed to verify the exact mechanism of the SAV0551 chaperone activity.

A recent report indicates that Hsp31 displays glyoxalase III function, a GSH-independent glyoxalase. Accumulation of methylglyoxal, also called dicarbonyl stress, causes endogenous damage by reacting with proteins and DNA. DNA modification results in frameshift mutations and proteins modification is often directed to functional sites. Hsp31 protects cell against methylglyoxal toxicity. Glyoxalase activity was detected in wild type SAV0551, and SAV1875 shows less than half of SAV0551's activity, while cysteine mutants of SAV0551 did not. As predicted, cysteine is revealed as a key residue for the glyoxalase activity. Moreover, compared to the catalytic triad of SAV1875, which has a similar overall structure with SAV0551, the catalytic triad in SAV0551 is more occluded by neighboring α-helices. This may be responsible for the substrate affinity. Small molecules such as methylglyoxal would have high selectivity for active site of SAV0551.

Altogether, the crystal structure of Hsp-type DJ-1 subfamily protein SAV0551 was determined. It shows an activity of chaperone through its surface structure and

glyoxalase III through catalytic triad, which are crucial functions for stress response system of a damaged cell.

Chapter III. The structural and functional study of SAV1875

3.1. Introduction

From the sequence homology among YhbO-type DJ-1 subfamily members, SAV1875 is predicted to be classified into YhbO-type DJ-1 subfamily: YhbO (49% sequence identity), *Ph*pI (42% sequence identity), DR1199 (40% sequence identity), Ton1285 (39% sequence identity), and DJ-1 (29% sequence identity). A structure-based sequence alignment was acquired using the ClustalW web server tool [43] and viewed using the ESPript web server tool [25]. The sequence alignment of YhbO, *Ph*pI, DR1199, Ton1285 and DJ-1 is shown in Figure 12. SAV1875 is an uncharacterized protein coding 171 amino acids. The estimated molecular weight is 19 kDa and calculated pI is 4.59.

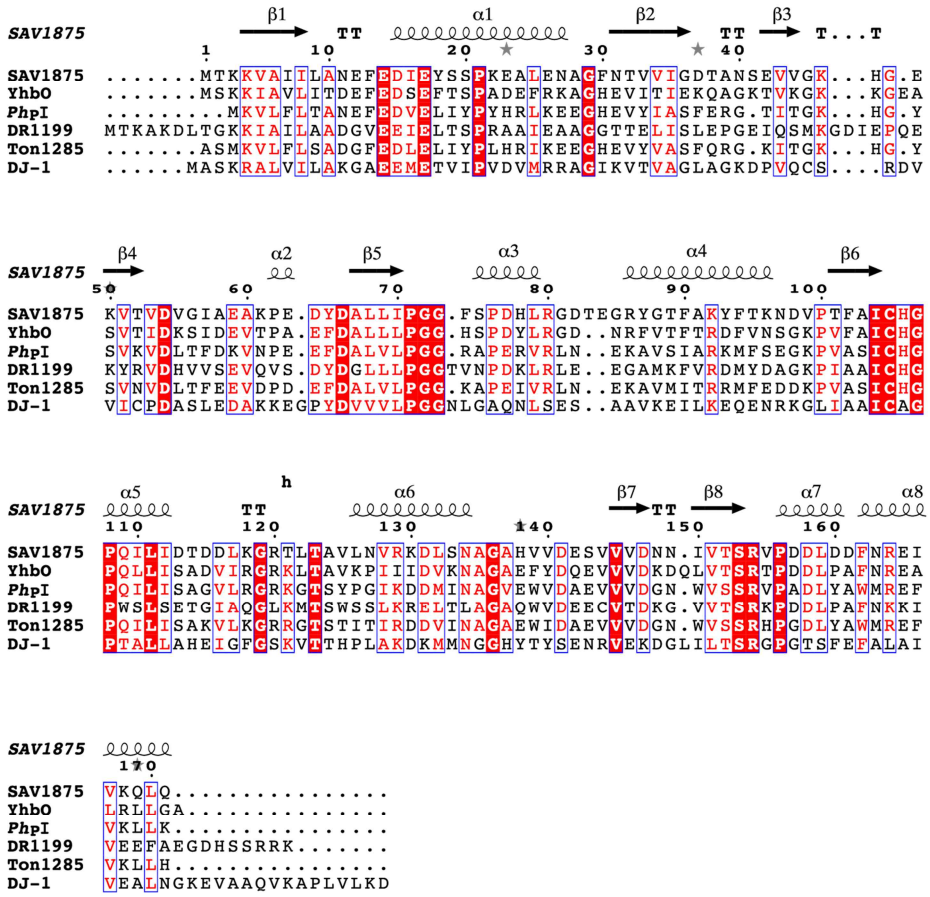

Figure 12. Comparison of SAV1875 to other members of DJ-1/ThiJ/*Pf*pI superfamily.

Sequence alignment of SAV1875 with YhbO (49% sequence identity), *Ph*pI (42% sequence identity), DR1199 (40% sequence identity), Ton1285 (39% of sequence identity) and DJ-1 (29% sequence identity) proteins. Identical residues are colored white on a red background and similar residues are red on a white background. Secondary structure elements (springs, α-helices; arrows, β-strands) are represented above the sequences and are numbered. The figure was constructed using ESPript [25].

3.2. Materials and Methods

3.2.1. Cloning, protein expression, and purification

The ORF encoding SAV1875 was amplified from *S. aureus* Mu50 genomic DNA by PCR using 5'-GACTGCATATGACTAAAAAAGTAGCAATTATTC as the forward primer and 5'-GTACACTCGAGTTGTAATTGTTTAACGATTTCT as the reverse primer. The NdeI and XhoI restriction sites are underlined and were used for cloning into the pET-21a(+) vector (Novagen Inc., USA). The resulting construct has eight additional residues (LEHHHHHH) that encode a C-terminal hexa-histidine tag. For removal of hexa-histidine tag, SAV1875 gene is inserted into a pET-28a(+) (Novagen Inc., USA) vector. The resulting construct in pET-28a(+) comprised residues 1-171 with an additional 20 residues (MGSSHHHHHHSSGLVPRGSH) containing thrombin cleavage site. The sequence of the cloned gene was confirmed by DNA sequencing (data not shown).

To prepare mutants, the EZchange Site-directed Mutagenesis kit (Enzynomics Inc., Republic of Korea) was used to generate point mutations in the SAV1875 recombinant pET-21a(+) plasmid. SAV1875 gene was amplified from recombinant plasmid DNA with the following primer pairs (Table 2).

Mutants	Primer sequence	
E17D	Forward	5'GCAAACGAATTTGAAGATATAGATTATTCAAGTCCTAAAG AGGC-3'
	Reverse	3'GCCTCTTTAGGACTTGAATAATCTATATCTTCAAATTCTGC-5'
E17N	Forward	5'-GCAAACGAATTTGAAGATATAAACTATTCAAGTCCTAAAGA GGC-3'

	Reverse	3'-GCCTCTTTAGGACTTGAATAGTTTATATCTTCAAATTCGTTTGC-5'
C105D	Forward	5'-GATGTACCAACATTTGCCATTGATCATGGGCCACAAATACTAATAG-3'
	Reverse	3'-CTATTAGTATTTGTGGCCCATGATCAATGGCAAATGTTGGTACATC-5'

Table 2. Primer design of SAV1875 mutants.

After digestion of the methylated and non mutated parental DNA template with DpnI, the circular dsDNA was transformed to competent cell. The point mutations resulted in separate multiple recombinant plasmids, specifically E17D, E17N, and C105D. The sequence of the cloned gene were confirmed by DNA sequencing (not shown).

Wild type and SAV1875 mutants (E17D, E17N, and C105D) in pET-21a(+) were overexpressed in *E. coli* BL21(DE3) cells (Novagen Inc., USA) and grown at 37°C in Luria-Bertani (LB) medium supplemented with ampicillin (50 μg/ml) until the OD600 reached 0.5. Recombinant protein expression was induced by the addition of 0.5 mM isopropyl β-D-1-thiogalactopyranoside (IPTG), and the cells were allowed to grow for an additional 4 hr at 37°C. The cells were harvested by centrifugation at 4°C. The cell pellet was resuspended in lysis buffer (50 mM Tris-HCl, pH 7.5, 500 mM NaCl) and disrupted at 4°C using an Ultrasonic processor (Cole Parmer, USA). The cell lysate was centrifuged at 18,000 rpm for 1 hr at 4°C. The cleared supernatant was purified by binding to a Ni^{2+}-NTA affinity column (Qiagen, USA; 3 ml of resin per liter of cell lysate) and eluted with binding buffer

containing 100 mM imidazole. Further purification and buffer exchange were achieved by size exclusion chromatography using a Superdex 75 (10/300 GL) column (GE Healthcare Life Sciences, Germany) that was previously equilibrated with buffer (50 mM Tris-HCl, pH 7.5, 200 mM NaCl). The purities of the hexa-histidine tagged wild type and SAV1875 mutants were estimated to be over 95% by SDS-PAGE. The purified proteins were concentrated to 10 mg/ml by ultrafiltration in 10,000 MWCO spin columns (Millipore, USA). The absorbance at 280 nm was measured, and the calculated extinction coefficient of 5960 $M^{-1}cm^{-1}$ was employed to determine the protein concentration.

3.2.2. Crystallization and data collection

Crystallization was performed at 293 K by the hanging-drop vapor diffusion method using 24-well VDX plates (Hampton Research, USA). Initial crystallization conditions were established using screening kits from Hampton Research (Crystal Screens I and II, Index, PEG/Ion, and MembFac) and from Emerald BioSystems (Wizard I, II, III and IV). For the optimal growth of the SAV1875 crystals, each hanging drop was prepared on a siliconized cover slip by mixing 1 μl of protein solution and 1 μl of precipitant solution (29% (w/v) PEG MME 2000, 100 mM BisTris, pH 6.5), and this drop was equilibrated against a 1 ml reservoir of precipitant solution. The SAV1875 mutants (E17D, E17N, and C105D), and over-oxidized SAV1875 crystals were prepared in the same manner but with different precipitant solutions: for E17D, 44% (w/v) PPG400, 100 mM BisTris, pH 6.0; for E17N, 47.5% (w/v) PPG400, 0.2 M guanidine hydrochloride, 100 mM BisTris, pH 6.0; for C105D, 37.5% (w/v) PPG400, 100 mM BisTris, pH 6.0; and for over-oxidized SAV1875, 47.5% (w/v) PPG400, 100 mM BisTris, pH 5.5. These conditions yielded needle-shaped crystals for each protein that grew to dimensions of 1.0 × 0.4 × 0.4 mm in three days. All crystals belonged to space group P21212 and contain two molecules per asymmetric unit.

For crystal freezing, the crystals were transferred to a cryoprotectant solution with 30% (v/v) glycerol in the crystallization condition for several minutes before being flash-frozen in a stream of nitrogen gas at 100 K. Diffraction data were collected on beam-lines 6C and 5C at the Pohang Light Source, South Korea and BL-17A at the Photon factory, Japan. The raw data were processed and scaled using the HKL2000 program suite [26]. Further data analysis was carried out using the CCP4 suite [27].

3.2.3. PAGE

SDS-PAGE was conducted according to the Laemmli method [44] using a 12% (w/v) polyacrylamide gel. The samples were treated with 1% (w/v) SDS and 5% (v/v) 2-mercaptoethanol at 100°C for 5 min before electrophoresis in a vertical Mini Gel system (Bio-Rad Laboratories, Republic of Korea). The proteins were stained with Coomassie Brilliant Blue R250 (Thermo Scientific, USA). Additionally, for the separation of SAV1875 depending on the charge-to-mass ratio between oxidized and reduced state, native PAGE was performed, and analysis was conducted using a 10% (w/v) polyacrylamide gel with neither SDS nor 2-mercaptoethanol. Native PAGE was performed in a buffer (25 mM Tris-HCl, pH 8.3, 192 mM glycine). The staining was performed as described above for SDS-PAGE.

3.2.4. Mass spectrometry

Mass analyses were performed on a nano-HPLC system (Dionex Ultimate 3000 RSLCnano System, Thermo Scientific, USA) coupled with a hybrid quadrupole-obitrap mass spectrometer (Q-Exactive, Thermo Scientific, USA) at the NICEM (National Instrumentation Center for Environmental Management, Seoul National University, Seoul, Republic of Korea). Protein samples (10 μl) were loaded onto a C8 reverse phase column (INNO5, Young Jin Biochrom., Republic of Korea). A

HPLC was used for room temperature gradient elution at a flow rate of 150 µl/min by using a linear gradient from 0.1% (v/v) formic acid in water (Solvent A) to 0.1% (v/v) formic acid in acetonitrile (Solvent B). The total run time for each sample was 20 min. The molecular mass of protein was generated from several multiply charged peaks using the Xcalibur 2.2 Software (Thermo Scientific, USA).

3.2.5. Protein oxidation

For the complete oxidation of cysteine, the wild type and SAV1875 mutants at 20 mg/ml (1 mM) were incubated for 30 min at room temperature in H_2O_2 (Sigma-Aldrich Inc., USA) with a molar ratio of protein: H_2O_2 of 1:50. After treatment, excess H_2O_2 was removed by extensive dialysis with buffer (50 mM Tris-HCl, pH 7.5). The control consisted of the same protein with H_2O, which was incubated under the same conditions. The oxidation states of Cys105 were determined by mass spectrometry and native PAGE.

3.2.6. Circular Dichroism (CD)

Circular dichroism (CD) spectra were collected with a Chirascan Series spectrometer equipped with a temperature controller (Applied Photophysics, UK). The protein samples were prepared in a buffer (50 mM Tris-HCl, pH 7.5, 200 mM NaCl). The CD Spectra were recorded with a step size of 1.0 nm, a bandwidth of 1 nm and an averaging time of 2.0 sec. Measurements were performed in a 1 mm path length quartz SUPRASIL cell (Hemlla, Germany) using a 10 µM concentration of proteins at room temperature. Three scans were applied continuously and the data were averaged. CD spectra were smoothed and processed after blank subtraction using Pro-Data Viewer software (Applied Photophysics, UK). Furthermore, the secondary structure was analyzed using the K2D3 software (data not shown) [45]. The change in molar ellipticity [θ] was calculated using the following equation [46], where θ is in degrees, length (l) is in millimeters and C is

the molar concentration of protein:

$$[\theta] = \theta / (l \times C \times \text{number of residues})$$

3.2.7. Protease activity assay and zymogram

The protease activity assay of wild type, the SAV1875 mutants, and over-oxidized SAV1875 was performed using the MGT protease assay kit (Marker Gene Technologies, Inc., USA). Fluorescein isothiocyanate (FITC)-labeled casein was cleaved into smaller fragments and highly fluorescent-labeled peptides were released [47]. Fluorescence increase is proportional to protease activity, and this fluorescence was measured in a continuous assay format using a Multi-Mode microplate reader (SpectraMax M5e, USA) with excitation and emission wavelength of 485 and 528 nm, respectively. The FITC-casein was diluted to 1 mg/ml with reaction buffer (100 mM sodium phosphate, pH 7.6, 150 mM NaCl). By mixing FITC-casein with a gradient of protein concentrations (final protein concentration from 1 μM to 15 μM, separately), the protease activity was monitored. The proteins were diluted into the reaction buffer immediately before conducting the test. The mixture of FITC-casein and protein (wild type, the SAV1875 mutants and over-oxidized SAV1875) were sealed and incubated for 2 hr at 37 °C under protection from UV light.

For zymogram analysis, 0.1% (v/v) gelatin copolymerized with the acrylamide gels were used. Electrophoresis was performed at 4 °C at a constant voltage of 100 V. The gels were washed in 2.5% (w/v) Triton X-100 solution at room temperature for 40 min. Following washing, gels were incubated for 20 hr at 37°C in a buffer (50 mM Tris-HCl, pH 8.0, 5 mM $CaCl_2$, 0.02% NaN_3) for proteolytic activity. Staining with Coomassie Brilliant Blue shows the proteolytically cleaved sites as a clear band on a dark background [48].

3.2.8. Determination of chaperone activity

To monitor the chaperone activity of wild type, the SAV1875 mutants and over-oxidized SAV1875, citrate synthase was employed as a substrate [34, 35]. Initially, to identify chaperone activity, 75 μg of citrate synthase (Sigma-Aldrich Inc., USA) was mixed with a solution of 100 mM Tris-HCl, pH 8.0, 20 mM dithiothreitol (DTT), 6 M guanidine chloride (GnCl). The citrate synthase mixture (75 μg of citrate synthase, 100 mM Tris-HCl, pH 8.0, 6 M GnCl, 20 mM DTT) was incubated for 1 hr at 25°C; consequently, the citrate synthase in this solution was denatured. After incubation, refolding of citrate synthase was achieved by 100-fold dilution with a solution of 100 mM Tris-HCl (pH 8.0) containing 5 μM wild type, the SAV1875 mutants or over-oxidized SAV1875. The diluted solution was mixed with acetyl-CoA, oxaloacetate, $MnCl_2$ and 5,5'-dithiobis-(2-nitrobenzoic acid) (DTNB) to detect the activity of citrate synthase (100 mM Tris-HCl, pH 8.0, 1 mM DTNB, 0.2 mM $MnCl_2$, 0.4 mM oxaloacetic acid, 0.3 mM acetyl-CoA). After mixing, only the active, refolded enzyme will break acetyl-CoA into the acetyl group and CoA. The CoA reacts with DTNB, which acts as a coloring agent, and this produces a yellow TNB-CoA-SH compound that is detectable at 412 nm using a Multi-Mode microplate reader (SpectraMax M5e, USA) [49]. After a 70 min reaction period, the highest specific activity value obtained for TNB-CoA-SH was considered 100% and the lowest was 0%. The calculated specific activities of the wild type, the SAV1875 mutants, and over-oxidized SAV1875 were expressed as a percentage of this value.

3. 3. Results

3.3.1. Structure of SAV1875

The SAV0551 sample was prepared as a concentration of 10 mg/ml (Figure 13).

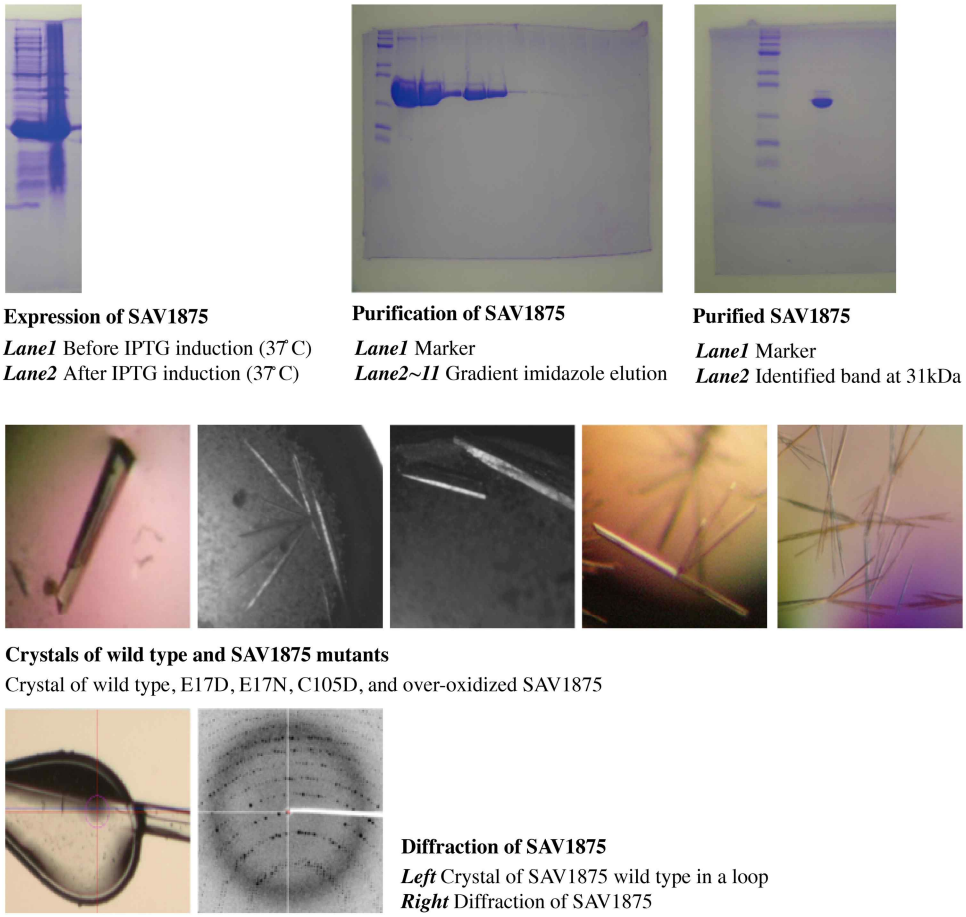

Figure 13. Expression, purification, and crystallization of SAV1875.

Wild type and mutants SAV1875 samples were prepared to determine the structure and function. The wild type and mutants SAV1875 were over expressed by IPTG induction system, and purified using Ni^{2+}-NTA affinity column. Protein purity is measured over 95% based on SDS-PAGE. SAV1875 wild type crystallizes in a condition of 29% (w/v) PEG MME 2000, 100 mM BisTris, pH 6.5. The crystal diffracted to a 1.8 Å of resolution.

The 2.1 Å crystal structure of SAV1875 has clear electron density for 171 amino

acids including the additional C-terminal tag and lacks the methionine residue at position 1. The protein consists of an α/β sandwich fold with eight α-helices and eight β-strands. Six β-strands, β2 (residues 31-35), β1 (residues 4-8), β5 (residues 67-70), β6 (residues 101-104), β8 (residues 150-153), and β7 (residues 145-147), are aligned in the center, wherein the latter β7 strand is anti-parallel to the central β-strands. Eight α-helices surround the core of β-strands. Both sides of the β-strands are covered with α-helices (α1 (residues 15-27), α7 (residues 156-158), and α8 (residues 160-171) are located on one side and α2 (residues 62-64), α3 (residues 75-81), α4 (residues 86-96), α5 (residues 107-113), and α6 (residues 126-134) are on the other side). Additionally, anti-parallel strands β3 (residues 42-44) and β4 (residues 50-52) are located on top of the sandwich structure (Figure 14).

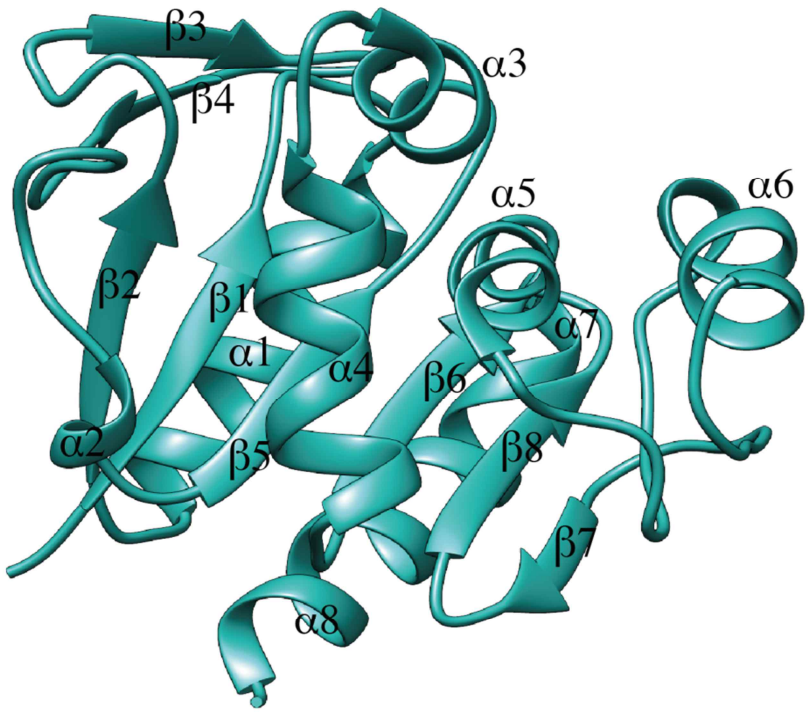

Figure 14. Ribbon diagram of SAV1875.

Ribbon representation of the SAV1875 monomer.

3.3.2. Oligomeric state of SAV1875

The crystal structure revealed that SAV1875 exists as a compact homodimer with an interface that buries about 828 $Å^2$ per subunit (12.3% of the subunit surface). The dimer involves contacts between three helices (α3, α5, and α6) on each monomer (Figure 15). On its dimeric interface, there are 3 salt bridge pairs between Asp77 and His106, Asp115 and Lys130, and Asp131 and Arg80. Numerous hydrophobic residues are also found in the dimeric interface, including Gly73, Phe74, His78, Gly81, Ile112, Leu126, Val128, and Leu132. On the basis of its quaternary structure, SAV1875 was classified as a new member of YhbO-type subfamily.

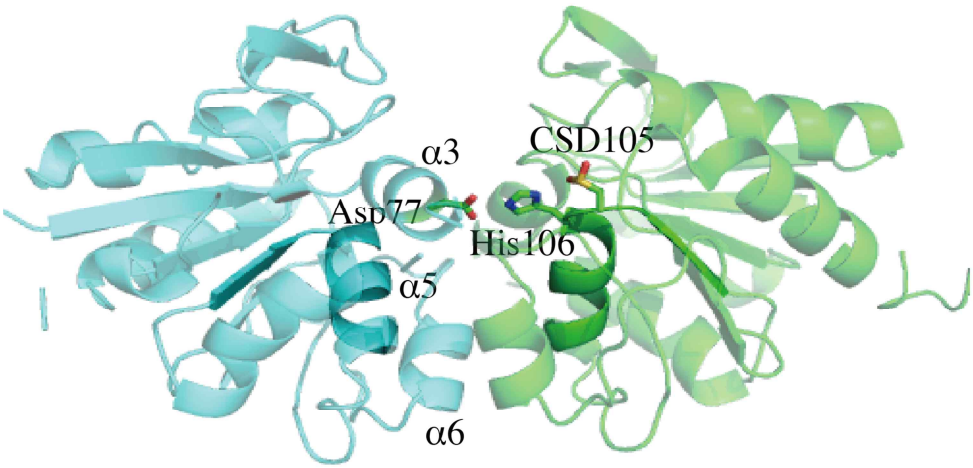

Figure 15. Dimer structure of SAV1875.

The SAV1875 dimer is shown in a ribbon representation from side view. Chain A is colored in cyan and chain B is in green. Three helices (α3, α5, and α6) are involved in dimeric interface. The nucleophilic elbow (strand-nucleophile-helix motif) in each domain is shown in darker color. Cysteine is positioned in the turn of the

nucleophilic elbow, and the catalytic triad is shown as sticks (CSD105, His106, and Asp77 from the adjacent monomer). The oxidized Cys105 is denoted as CSD105.

The dimer crystal structure of SAV1875 is consistent with the results of size exclusion chromatography, which indicates a dimeric state of SAV1875 with an apparent molecular mass of 39 kDa in solution. However, the YhbO-type dimer proteins can form a ring-like hexamer in solution by trimerization. With the exception of DR1199, which has a long protruded loop toward the center, other YhbO-type proteins, including *Ph*pI, YhbO, and Ton1285, can exist as hexamers in a solution [18, 50]. Because an additional terminal amino acid extension alters the oligomerization modes of YhbO, we prepared a variant of SAV1875, a histidine-tag removed SAV1875. Both forms of histidine-tagged and tag-removed SAV1875 proteins form only dimers in a solution. This may be because of the wider dimerization mode of the two subunits in SAV1875 compared with *Ph*pI. If SAV1875 were to make the same trimerization as *Ph*pI, the helices and loops, which form DJ-1-type dimeric interface, would sterically inhibit each other (Figure 16).

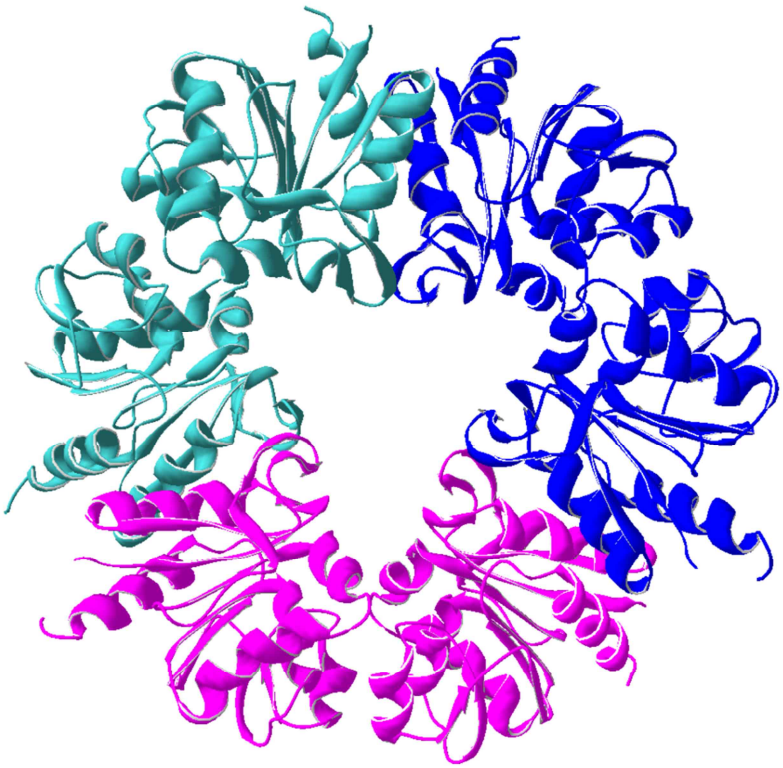

Figure 16. Ribbon diagram of constrained hexamer SAV1875.

If SAV1875 makes the same hexamerization, helices and loop would crash each other. This is because of the wide dimerization mode of two subunits in SAV1875.

When viewing the surface area, the electrostatic distribution of SAV1875 reveals several characteristics. The majority of the surface is negatively charged with several exceptions that indicate hydrophobic patches on the surface area which are dominated by Ile16, Ala28, Gly29, Ala39, Val44, His47, Gly48, Ala58, His78, Gly85, Gly119, Leu126, Arg129, His138, Val146, Ala148, and Pro156. The dimeric interface of SAV1875 shows a deep canyon and this spans over the dimer (Figure 17). These characteristics are similar to those of Hsp31 [11], known chaperone proteins in the DJ-1 superfamily. Therefore, these findings suggest that SAV1875 may function as a chaperone.

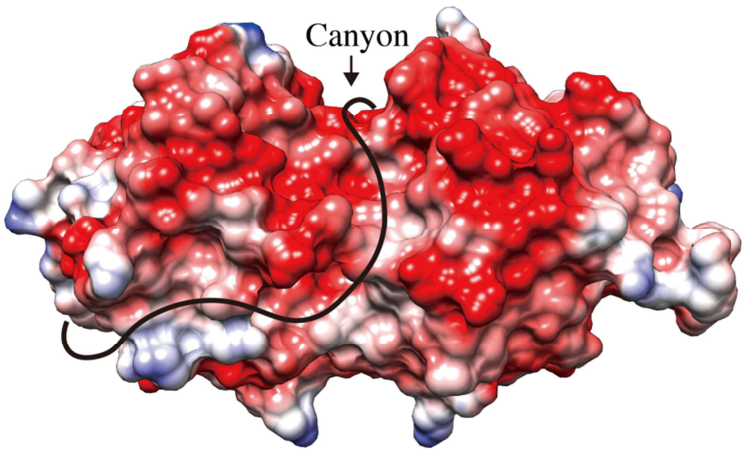

Figure 17. Surface structure of SAV1875.

Potential surface charge of the crystal structure of SAV1875, calculated with Chimera [32], where surfaces are colored between -10 kcal/mol•e (red) and +10 kcal/mole•e (blue). Most of the surface is negatively charged. Canyon is labeled.

3.3.3. Comparison of SAV1875 with DJ-1 superfamily proteins

The overall fold of SAV1875 shows structural similarity to other members of DJ-1 superfamily proteins, as predicted by sequence homology. The superposition of SAV1875 with the structures of YhbO, *Ph*pI, DR1199, Ton1285, and DJ-1 are shown in Figure 18.

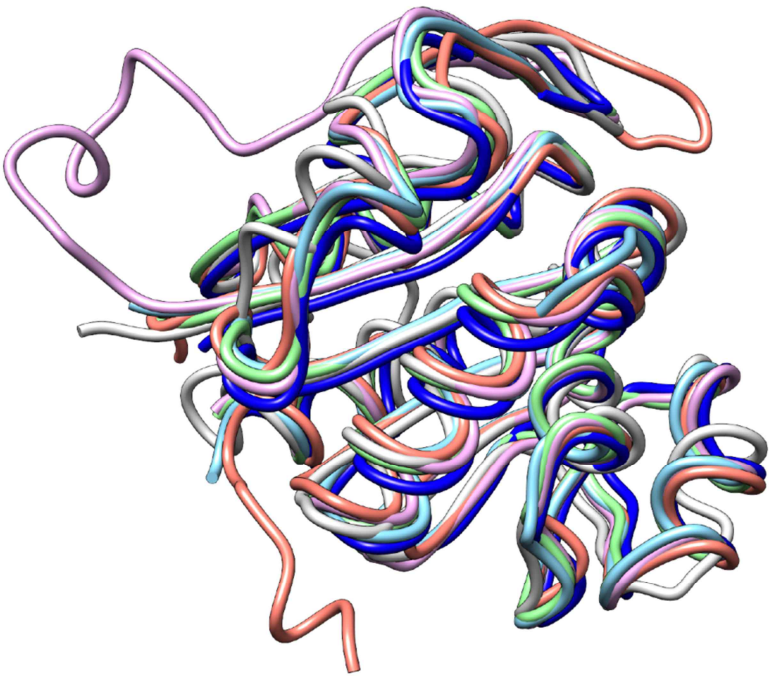

Figure 18. The superposition of SAV1875 (cyan) with other members of the DJ-1/ThiJ/*Pf*pI superfamily YhbO (pink), *Ph*pI (blue), DR1199 (orange), Ton1285 (green), and DJ-1 (Grey).

The overall fold of the core domain of SAV1875 is similar to other members of the DJ-1/ThiJ/*Pf*pI superfamily.

In addition to the similarity of the overall fold within the DJ-1 superfamily proteins, all the DJ-1 superfamily proteins share the reactive cysteine residue at a sharp turn between a β-strand and α-helix. This strand-nucleophile-helix motif is defined as a "nucleophilic elbow". Residues 101-113 (α5 and β6) of SAV1875 form the nucleophilic elbow. Cys105 lies at the sharp turn between the α5 helix and the β6 strand (Figure 15). In nearly all the DJ-1 superfamily proteins, except the DJ-1-type subfamily, the cysteine forms a catalytic triad with a neighboring histidine and an acidic residue. However, the structural features of the catalytic triad vary between the different DJ-1 subfamilies. The YhbO-type proteins constitute a

catalytic triad with cysteine, the histidine next to cysteine, and an acidic residue from the other subunit [14, 16]. The Hsp-type proteins form a catalytic triad using cysteine, the histidine next to cysteine, and an acidic residue from an intrasubunit from the other domain (cap domain) [11, 51].

The catalytic triad that was found in SAV1875 consists of Cys105, His106, and Asp77 (from the adjacent monomer) and was located in its dimeric interface, specifically on the depressed area (Figure 15). The catalytic triad shares the same handedness with the YhbO-type proteins. Cys105 interacts with N^{δ} His106, and Asp77 interacts with N^{ε} of His106. However, Cys105 is oxidized to Cys105-SO_2H in the crystal structure of SAV1875 and is denoted as CSD105. Similar results were previously observed in the homologous cysteine residues from the DJ-1 superfamily proteins, in which the involved cysteine residue was very sensitive to oxidation, forming either Cys-SOH or Cys-SO_2H. In the crystal structure of DJ-1 (DJ-1-type), the cysteine is oxidized to Cys-SO_2H. YajL (DJ-1-type) exhibits both Cys-SOH and Cys-SO_2H modification on each subunit. The crystal structure of DR1199 (YhbO-type) shows a Cys-SOH modification, and the cysteine in YDR533Cp (Hsp-type) exists as Cys-SO_2H [16, 51-53]. These oxidized cysteines are stabilized by specific surrounding residues near the cysteine, including an acidic residue which is analogous to Glu17 in SAV1875.

3.3.4. Stabilization of oxidized Cys105

The cysteine residue at the nucleophilic elbow is absolutely conserved in the DJ-1 superfamily proteins, and is considered a critical residue for their catalytic function [54]. In addition to the cysteine, another highly conserved acidic residue in the DJ-1 superfamily is glutamate, which donates hydrogen bonds to the oxidized cysteine. A hydrogen bond is formed between and electronegative atom (the hydrogen acceptor) and a hydrogen atom that attaches with another electronegative atom (the hydrogen donor) (Figure 19). The hydrogen atom in a hydrogen bond is shared by

two electronegative atoms such as oxygen and nitrogen. The hydrogen bond plays very important roles in protein structure because it stabilizes the tertiary and quaternary structure. In protein structure, the most usual cases of hydrogen bond are between two alcohols, an alcohol and an acid, two acids, or and alcohol and an amine or amide.

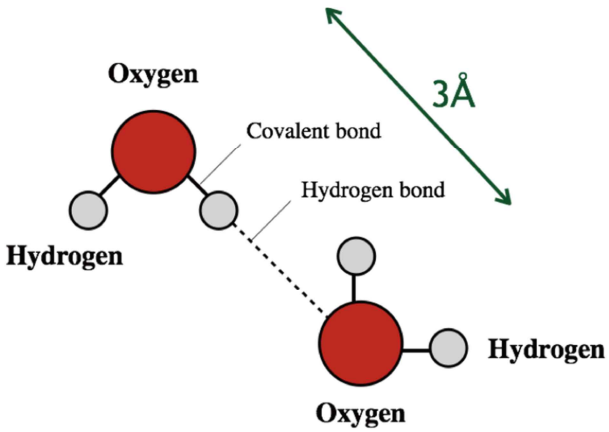

Figure 19. A hydrogen bond.

A single hydrogen atom bound to a electronegative oxygen atoms. The mean donor-acceptor distance in protein is about 3.0 Å.

SAV1875 has a conserved acidic glutamate residue at residue 17. In the crystal structure of SAV1875, oxidized Cys105 acts as another acidic residue and makes hydrogen bonds with Glu17 (2.71 Å), His106 (2.69 Å), and the Gly73/His106 amide pocket (3.02 Å and 2.96 Å, respectively; Figure 21A). Considering the mean donor-acceptor distance in protein is close to 3.0 Å, these hydrogen bonds are responsible for stabilization of oxidized Cys105. Because the O^{δ} of oxidized Cys105 and the O^{ε} of Glu17 form hydrogen bonds, we speculated that a glutamate substitution at position 17 would alter the cysteine oxidation status without disturbing the catalytic triad. Thus, aspartate and asparagine mutants (E17D and E17N, respectively) were designed because these amino acids have shorter carbon chains (one carbon) than glutamate. In particular, asparagine is the amide of

aspartate, which does not carry a formal charge under biologically relevant pH conditions. Cys105 was mutated to aspartate, which mimics Cys-SO_2H, to generate the solely oxidized form of SAV1875. The crystal structure of each mutant was identified and showed distinct differences in their cysteine oxidation states (Figure 20). In the crystal structure of wild type and E17D SAV1875, Cys105 is oxidized to Cys105-SO_2H, and Cys-SOH is observed in E17N SAV1875. In the crystal structure of E17D, the hydrogen bond between oxidized Cys105 and Asp17 is retained, showing a distance of 2.81 Å (Figure 21B). The E17N crystal structure showed a disruption of the hydrogen bonds between Cys105 and Asn17 (Figure 21C). However, the oxidized cysteines of the SAV1875 mutants still maintain hydrogen bonds with His106 and with the Gly73/His106 amide pocket.

These results are not consistent with a similar study on the DJ-1 protein [52, 55]. To stabilize the oxidation state of Cys106 in the DJ-1 protein, Glu18 and the Gly75/Ala107 amide pocket are required. In the crystal structures, Cys106 of the DJ-1 E18N mutant is oxidized to Cys106-SO_2H, and Cys106 of DJ-1 E18D mutant is modified to Cys106-SOH, which indicates minor oxidation toward the Gly75/Ala107 amide pocket (Figure 21). The opposite behavior was observed in the SAV1875 mutants and is due to the local structural difference around Cys105. In detail, Gly73 and His106 are shown to form an amide pocket as Gly75/Ala107 in DJ-1 (Figure 22).

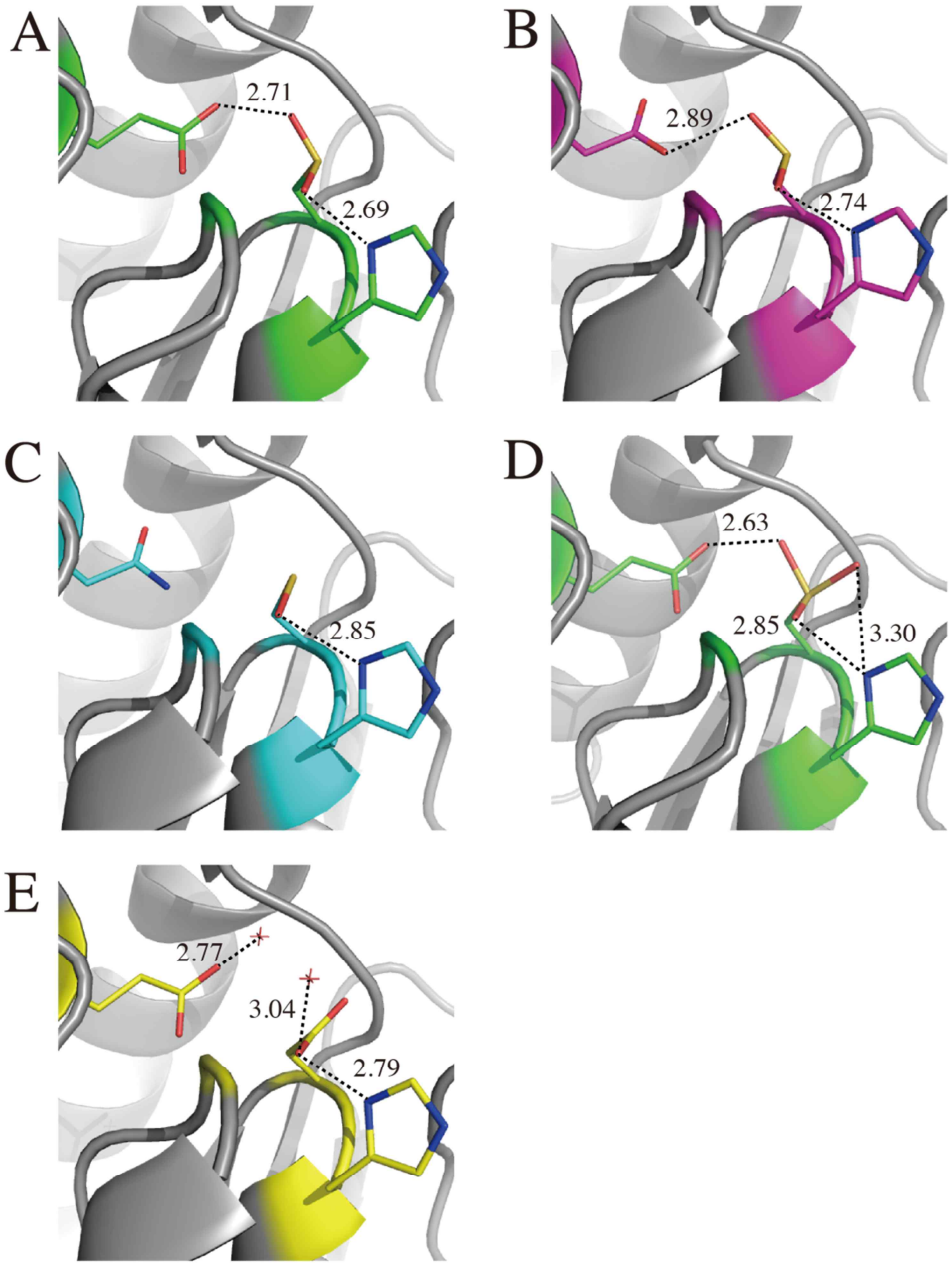

Figure 20. Oxidation state of cysteine at residue 105.

(A) Cys105 in wild type SAV1875 is oxidized to Cys105-SO_2H in the crystal structure. (B) Cys105 in E17D SAV1875 is oxidized to Cys105-SO_2H in the crystal structure. (C) Cys105 in E17N SAV1875 is oxidized to Cys105-SOH in the crystal structure. (D) Cys105 in over-oxidized SAV1875 is oxidized to Cys105-SO_3H in

the crystal structure. (E) In the crystal structure of C105D, two water molecules are inserted. Asp105 and Glu17 form hydrogen bond with each of water molecules.

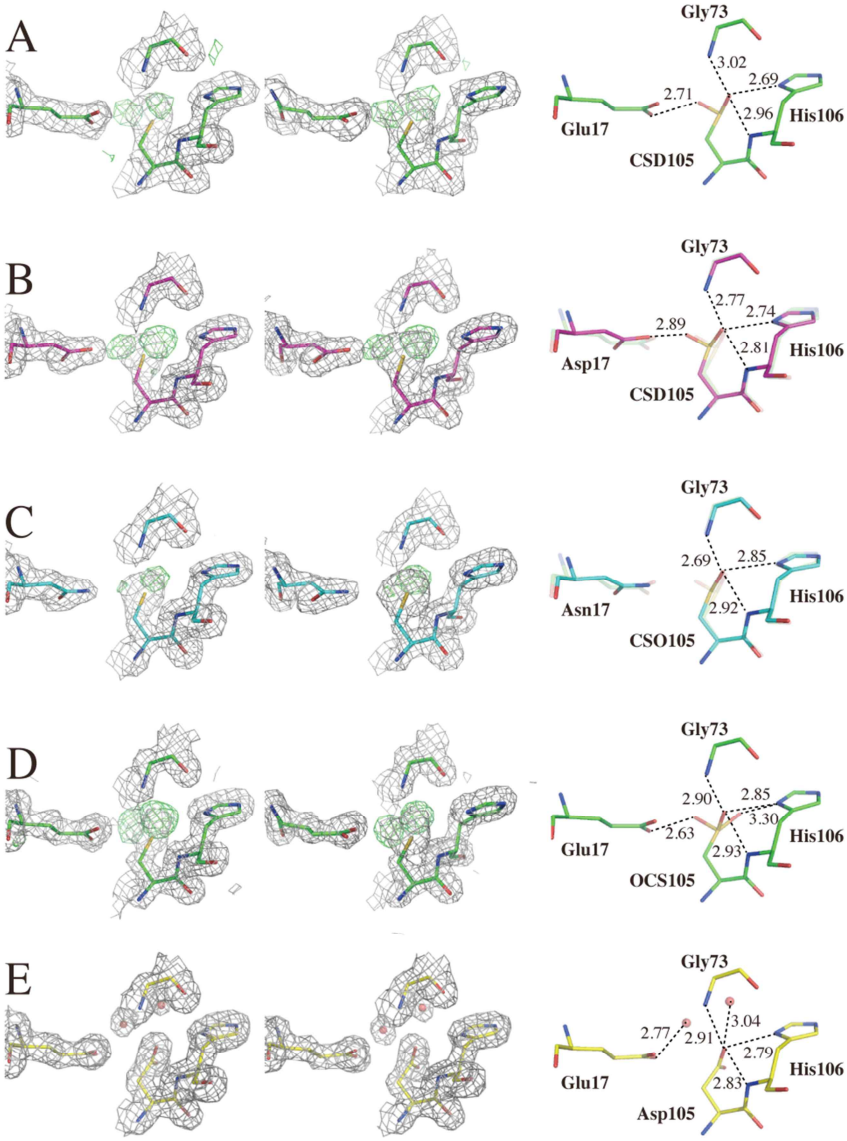

Figure 21. Hydrogen bonds around Cys105

The electron density map of Cys105 before the introduction of oxygen atoms and interacting hydrogen bonds after the introduction. The 2*Fo-Fc* electron density map

contoured at a level of 1.0σ is shown in grey and the *Fo-Fc* electron density map contoured at a level of 3.0σ is illustrated in green. Distances are given in Angstroms. *Left panels*, chain A; *Middle panels*, chain B; *Right panels*, hydrogen bonds are shown. (A) Cys105 in the wild type is oxidized to Cys105-SO_2H. (B) Cys105 in E17D shows Cys105-SO_2H (magenta) and the corresponding region in wild type (light green). (C) Cys105 in E17N shows Cys105-SOH (blue) and the corresponding region in wild type (light green). (D) Cys105 in over-oxidized SAV1875 is oxidized to Cys105-SO_3H, which shows additional density for the sulfonic group in chain A (left), but Cys105-SO_2H in chain B (right). (E) In C105D, Asp105 mimics Cys105-SO_2H, but the geometry of the oxygen atoms is different from that of Cys105-SO_2H. However, Glu17 and Asp105 are stabilized by hydrogen bonds with the introduction of water molecules. Figures were created with PyMOL .

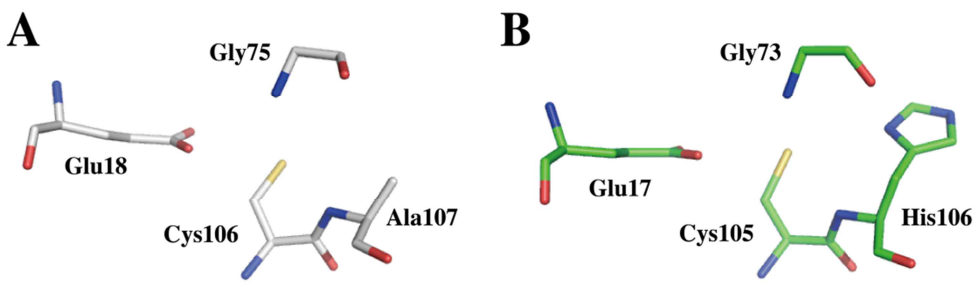

Figure 22. Local difference around the reactive cysteine in DJ-1 (left) and SAV1875 (right).

Histidine at residue 106 in SAV1875, which is an alanine in DJ-1, causes the opposite behavior of cysteine oxidation state in glutamate mutants.

However, in SAV1875, the His106 side chain provides additional strong hydrogen bonding to oxidized Cys105 (Figure 21). Therefore, the oxygen atom of Cys105-

SOH in the E17N mutant is toward the amide pocket. The occupancy of the oxygen atoms of Cys106-SO_2H in E17D mutant is greater toward amide pocket because of this hydrogen bond. Moreover, because there is a greater distance between Cys105 and Asn17 of E17N than Cys105 and Asp17 of E17D mutant, cysteine oxidation to Cys105-SO_2H in E17N SAV1875 remains incomplete (Figure 20B, 20C, 21B, and 21C). Cys105-SO_2H was observed as a main peak in both the E17D and E17N mutants in a mass spectrum that were incubated under H_2O_2 conditions. Therefore, we propose that the E17N mutant is oxidation-impaired, but not oxidation-deficient. Cys105 in wild type SAV1875 under H_2O_2 conditions can form Cys105-SO_3H in chain A. Each oxygen atom is stabilized by a hydrogen bond (Figure 21D). Because the molecular geometries of aspartate and cysteinesulfinic acid are different, the C105D mutant is not topologically the same as wild type SAV1875 (Figure 23). However, the introduction of water molecules, which form hydrogen bonds with Glu17 and Asp105, yields a stable structure (Figure 20E, 21E).

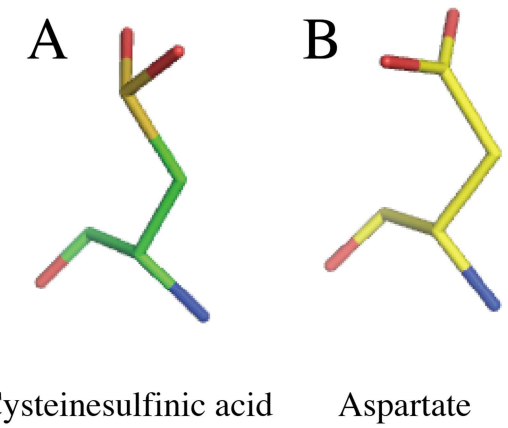

Figure 23. The geometry of cysteinesulfinic acid is not the same as aspartate.

3.3.5. Oxidation propensity of Cys105 in SAV1875

Among all amino acids in a protein, the most oxidation-susceptible residues are the sulfur-containing ones, cysteine and methionine [56-58]. Because recombinant SAV1875 lacks the only methionine residue at position 1 and possesses a single cysteine residue at position 105, the oxidation-reduction state in solution could be conveniently monitored by mass spectrometry and PAGE [57]. Cysteine undergoes oxidation and reduction reactions and results in four different forms: Cys-SH_2, Cys-SOH, Cys-SO_2H, and Cys-SO_3H [59]. The Cys105 in SAV1875 exists as both Cys105-SH_2 and Cys105-SO_2H in solution. One single intense peak with a M_r of 39 kDa in size exclusion chromatography indicates the presence of only dimer molecules of SAV1875 (data not shown). SDS-PAGE shows a single band as a monomer with a M_r of 19 kDa. In contrast, the mass spectrum contained two peaks with M_r values of 19,565 and 19,597 Da, which is +32 Da compared to the first peak. The two main peaks corresponded to SAV1875-Cys105-SH_2 and SAV1875-Cys105-SO_2H, respectively (calculated mass of 19,565.7 Da without methionine residue at position 1). Native PAGE separates SAV1875 into two main bands. Because the charge-to-mass ratio is preserved during native PAGE, SAV1875 can migrate towards the positively charged electrode depending on its overall negative surface charge without dissociation of the structure. This result corroborates the mass spectrometry, which indicated that SAV1875 exists in both reduced (SAV1875-Cys105-SH_2) and oxidized (SAV1875-Cys105-SO_2H) states. The SAV1875 C105D mutant further supports this finding because the C105D mutant, which lacks the only cysteine that can be oxidized (this recombinant C105D SAV1875 lacks the only methionine residue at position 1), has only one band on native PAGE and only one peak in mass spectrometry (Figure 24). Furthermore, the following methods were used to reduce oxidized Cys105: 1) 5 mM DTT was added to all buffers during purification and the protein was handled quickly on ice; 2) 10 mM DTT was introduced to the final buffer (50 mM Tris-HCl, pH 7.5, 200 mM NaCl, 10 mM DTT); and 3) 1 mM phenylethanesulfonylfluoride (PMSF) was

employed during all purification steps and ablated by DTT. Despite these efforts to reduce the oxidized cysteine, mass spectrometry and native PAGE indicated that SAV1875 retained the two distinctive main bands, SAV1875-SH_2 and SAV1875-SO_2H. Therefore, these data imply that the oxidative modification of Cys105 in SAV1875 is very robust.

Mass spectrometry and native PAGE confirmed that both SAV1875-Cys105-SH_2 and SAV1875-Cys105-SO_2H are further oxidized to SAV1875-Cys105-SO_3H when the protein was exposed to H_2O_2 with a molar ratio of SAV1875:H_2O_2 of 1:50. The mass spectrometry showed an enlarged peak at a M_r of 19,612.9 Da (SAV1875-Cys105-SO_3H) after exposure to H_2O_2, which is +48 Da compared to SAV1875-Cys105-SH_2 (Figure 24). This corresponds with the native PAGE result, which has an additional single band below SAV1875-Cys105-SO_2H, indicating SAV1875-Cys105-SO_3H. Circular dichroism data showed that the secondary structure of SAV1875 is not altered, even if SAV1875-Cys105-SO_2H is further oxidized to the over-oxidized state of SAV1875-Cys105-SO_3H (Figure 25). The crystal structure of over-oxidized SAV1875 was determined to a resolution of 1.65 Å. The electron density distribution surrounding the Cys105 residue suggested over oxidation to Cys105-SO_3H. The S^{γ} atom of Cys105 is oxidized to Cys105-SO_3H in subunit A and Cys105-SO_2H in subunit B (Figure 21D).

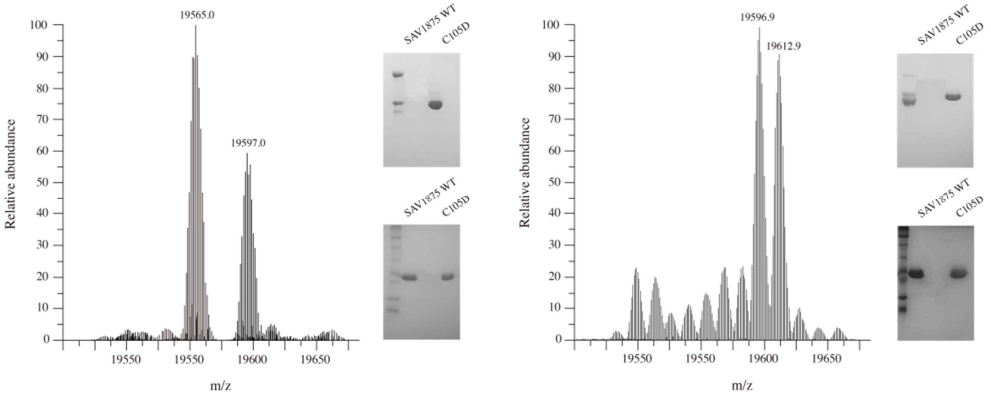

Figure 24. MS spectrometry and PAGE of SAV1875.

Mass spectrometry was used to monitor the oxidation state of SAV1875 in solution. *Left panel* MS analysis of SAV1875. Two major peaks are observed at 19,565.0 and 19,597.0. The calculated mass of SAV1875 is 19,565 Da if the only cysteine, Cys105, is reduced (this recombinant SAV1875 lacks the only methionine residue at position 1). In addition to the first peak, there is another main peak at 19,597 corresponding to two additional oxygen atoms. The right panel corresponds to native PAGE (top) and SDS-PAGE (bottom) analysis. Before exposure to H_2O_2, there were two separate SAV1875 bands in native PAGE. The oxidized band was located in the same region as the C105D. *Right panel* MS analysis of over-oxidized SAV1875. Two main peaks were observed at 19.596.9 and 19612.9, corresponding to SAV1875-Cys105-SO_2H and SAV1875-Cys105-SO_3H, respectively. The right panel corresponds to native PAGE (top) and SDS-PAGE (bottom). For over-oxidized SAV1875, there were three separate bands in native PAGE. One oxidized band is shown at the same region as the C105D and another oxidized band is located underneath the oxidized band. These native PAGE results coincide with the MS analysis.

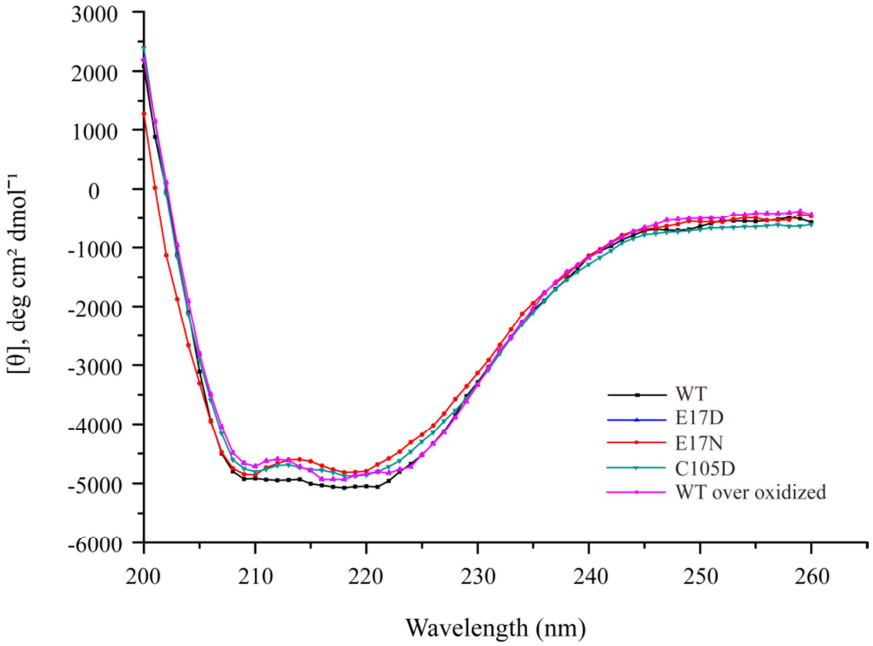

Figure 25. Over-oxidized SAV1875 does not lead to loss of secondary structure. Far-UV CD spectra of wild type (black), E17N (red), E17D (blue), C105D (green) and over oxidized SAV1875 (pink). The spectra were nearly identical, indicating that the E17 or C105 mutations do not affect the overall secondary structure of the protein.

3.3.6. Protease activity of SAV1875 was not detected

SAV1875 has been reported to harbor a *Ph*pI endopeptidase domain, which is found in *Ph*pI from *Pyrococcus horikoshii* (http://www.uniprot.org/uniprot/P0A0K0) [60]. *Ph*pI is an intracellular protease that belongs to the YhbO-type subfamily, and it shows the highest activity in a multimeric complex [14]. Ton1285 is another YhbO-type protein which has proteolytic activity [18]. *Ph*pI and Ton1285 exist as hexamers in solution, converging their catalytic triad towards the solvent accessible center area of the ring-like structure (Figure 26). However, the dimer proteins in the YhbO-type subfamily, recombinant YhbO and DR1199, do not show proteolytic activity

toward peptides or casein [16, 50]. Whereas other type of DJ-1 superfamily, the DJ-1-type protein DJ-1 dimer revealed a greater proteolytic activity toward casein, especially with the deletion of 15 C-terminal residues by enhancing substrate binding affinity [61]. To determine the proteolytic activity, if any, wild type, the SAV1875 mutants, and over-oxidized SAV1875 were used. SAV1875 did not display any significant proteolytic activity towards FITC-casein even after a long incubation time, at a high temperature (more than 37℃) or SAV1875 concentration (up to 50 μM), or in a reducing environment (presence of 1 mM β-mercaptoethanol). A gelatin overlay assay did not show any cleared zones. Therefore, dimeric SAV1875 is surmised not to have a proteolytic function against casein or gelatin (data not shown). If present, the catalytic activity is very low. Although DJ-1-type DJ-1 has proteolytic activity with a catalytic dyad and dimeric state, in YhbO-type proteins, the existence of a catalytic triad and ring-like multimeric structure showed to signify proteolytic function (Figure 26). Moreover, further research is needed on factors that may influence the proteolytic function of DJ-1 superfamily proteins.

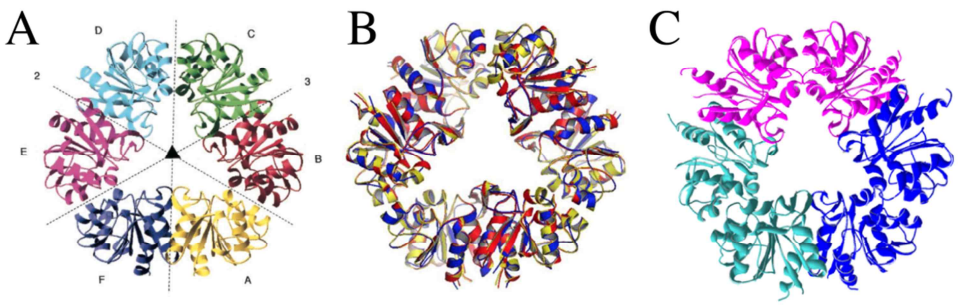

Figure 26. Comparison of oligomeric state in solution of YhbO-type DJ-1 superfamily.

*Ph*pI from *Pyrococcus horikoshii* (A) and Ton1285 from *Thermococcus onnurineus* (B) show hexamer structure in solution, but SAV1875 does not (C).

3.3.7. SAV1875 has chaperone activity

Chaperones are part of a functionally related group of proteins assisting in protein folding under stress conditions or preventing folding defects by binding to unstructured and hydrophobic regions of target proteins. Chaperones in the DJ-1 superfamily, such as Hsp31, work as dimers by forming a canyon and bowl on their dimeric interface [11]. When the surfaces of Hsp31 were viewed, hydrophobic patches were detected around the canyon for the binding of unstructured proteins [40]. DJ-1 and YajL, which are categorized as members of the DJ-1-type subfamily, have also shown chaperone activity. Interestingly, DJ-1 exhibited a greater chaperone activity towards α-synuclein when Cys106 was oxidized to Cys106-SO_2H and lost activity when the cysteine was further oxidized to Cys106-SO_3H, which correlated with a loss in some of its secondary structure [62, 63]. SAV1875 is defined as a member of the YhbO-type subfamily, displaying structural differences from the DJ-1 or Hsp-type subfamily. The YhbO-type proteins with a chaperone function had not yet been identified. However, SAV1875 expresses similar surface patterns of a canyon as Hsp31, DJ-1, and YajL. SAV1875 has a canyon that winds from the dimeric interface to each side of the subunit, and hydrophobic patches are detected around the canyon (Figure 13). These are characteristics of SAV1875 that are distinctive from the YhbO-type proteins. Other YhbO-type proteins are hexamers (*Ph*pI and Ton1285), or dimer YhbO-type proteins (recombinant YhbO and DR1199) lack apparent canyon structure. Furthermore, Cys105 in SAV1875 favors oxidation to Cys105-SO_2H, similar to a DJ-1 protein. Considering these characteristics, SAV1875 is expected to hold unfolded protein, and the oxidation state of Cys105 may play a crucial role in chaperone function.

The wild type, the SAV1875 mutants, and the over-oxidized SAV1875 were tested for chaperone activity using citrate synthase. The observed data shows a chaperone-facilitated renaturation of citrate synthase in the wild type, E17D, E17N,

and C105D mutants. There are no significant differences in the chaperone activity between the wild type and the SAV1875 mutants. However, negative results were obtained with over-oxidized SAV1875, which was previously exposed to a 1:50 molar ratio of SAV1875:H_2O_2. Therefore, we determined that SAV1875 functions as a molecular chaperone with an oxidized Cys105, but it loses chaperone activity when this cysteine is oxidized further to Cys105-SO_3H, even though over-oxidized SAV1875 is structurally stable (Figure 27). Circular dichroism revealed that the secondary structure is well conserved (Figure 25). The native PAGE result showed that the surface charge is preserved in over-oxidized SAV1875 with Cys105-SO_3H (Figure 24) [46]. From this study, we identified SAV1875 as a novel chaperone protein in the YhbO-type subfamily and that the canyon surface structure along with cysteine redox state are the key elements for the chaperone function.

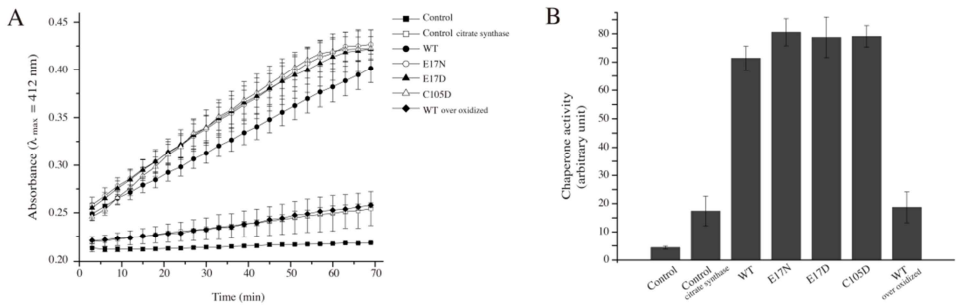

Figure 27. Chaperone activity of SAV1875 depending on cysteine oxidation state. SAV1875 exerts a chaperone function. The chaperone activity was assayed by monitoring an increase in absorbance at 412 nm. (A) The control (■) contained 50 μl of the reaction mixture only, which was 1 mM DTNB, 0.2 mM $MnCl_2$, 0.4 mM oxaloacetic acid, 0.3 mM acetyl-CoA in 100 mM Tris-HCl buffer (pH 8.0). The control with citrate synthase (□) contained an additional 0.75 μg of denatured citrate synthase. A final concentration of 5 μM was used for the wild type (●), E17N (○). E17D (▲), C105D (△), and over-oxidized SAV1875 (◆) and was

added to a citrate synthase reaction mixture. (B) The calculation of chaperone activity at the 70 minutes time point. The data from three scans were averaged.

3.4. Discussion

The cysteine endows proteins with an exceptional biochemistry due to the distinctive characteristics of its thiol group. The thiol group undergoes nucleophilic attack, electron transfer, hydride transfer, hydrogen radical transfer, and oxygen atom transfer reaction [64]. Due to the thiol group, cysteine is involved in redox activity, metal binding properties, catalytic component of enzyme function, and regulation of protein. The properties of thiol group are related with its different structures caused by oxidation. Regarding redox activity and posttranslational modifications, cysteine residues with sulfur in numerous oxidation states are known. The cysteine can form disulfide bond, depending on the cellular location of the protein. These bonds serve mostly to stabilize the protein structure, and the structures of many extracellular proteins are determined by topology of multiple disulfide bonds. There are other oxidative modifications such as sulfenic, sulfinic, and sulfonic acids. Recently, the notion is becoming important since the oxidative modification of cysteine in proteins has been implicated in cellular signaling and regulatory pathways [65, 66].

The DJ-1 superfamily proteins contain absolutely conserved cysteine. From known crystal structures of DJ-1 superfamily proteins, we figured out this cysteine is oxidized from cysteinesulfenic acid (Cys-SOH), cysteinesulfinic acid (Cys-SO_2H), to cysteinesulfonic acid (Cys-SO_3H). Changes in the sulfur oxidation state of cysteine influences the activity of various proteins [64]. Thus, the oxidation status of cysteine and the corresponding structural differences may account for the

function of SAV1875. In addition, study on the DJ-1 superfamily proteins of *S. aureus* is expected to be valuable in better knowledge of stress response mechanism of *S. aureus*, because the DJ-1 superfamily members are mostly known as stress response proteins.

In our crystal structure of wild type SAV1875, Cys105 was oxidized to Cys105-SO_2H, even though it was not intentionally produced. The oxidized Cys105 accepts hydrogen bonds from the Gly73/His106 amide pocket, the His106 side chain, and the protonated O^{ε} atom of Glu17. The residues that are structurally equivalent to Cys105 and Glu17 in SAV1875 are highly conserved in other members of the DJ-1 superfamily, indicating that cysteine and glutamate may play a crucial role in the function of the protein. The influence of Glu17 on the oxidation of Cys105 was verified with the crystal structures of the E17D, E17N, and C105D mutants. In the crystal structures, the hydrogen bond between Cys105 and residue 17 was weakened or eliminated in the glutamate mutants (E17D and E17N). C105D, which mimics cysteinesulfinic acid, had a different configuration of oxygen atoms (O^{ε}) compared to cysteinesulfinic acid, but the hydrogen bonds were maintained due to the introduction of water molecules. Moreover, the cysteine can be further oxidized to Cys105-SO_3H using excess H_2O_2. The crystal structure of over-oxidized SAV1875 revealed a stable formation of Cys105-SO_3H. From our study, we propose that SAV1875 may act as reactive oxygen species scavenger and protect cellular components.

Because the DJ-1 superfamily includes proteins spanning many functions, such as proteases, chaperones, and general stress response proteins, SAV1875 is also predicted to perform similar biological functions. Thus, several functional tests were conducted to determine the function of SAV1875 and the relationship between the oxidation states of cysteine and the differences in protein activity. *Ph*pI, a homolog of SAV1875 in the YhbO-type subfamily, has been identified as a protease [14]. Another YhbO-type protein, Ton1285, also has a proteolytic role [18].

From a structural standpoint, SAV1875 has a sandwich fold and catalytic triad in common but has different in oligomerization states. Unlike dimeric SAV1875, *Ph*pI and Ton1285 exist as a hexamer in solution. On the other hand, DJ-1-type protein DJ-1 shows proteolytic activity as a dimer with the deletion of 15 C-terminus residues [61]. Proteolytic activity was not detected in SAV1875. This analysis indicates that other factors along with oligomeric state are biologically relevant and still require precise characterization.

Hsp31 displays chaperone activity by holding unfolded protein with its canyon and hydrophobic surface. DJ-1 and YajL have shown chaperone activity as well, showing similar surface structure. Interestingly, when Cys106 of DJ-1 was oxidized to Cys106-SO_2H, chaperone activity increased. When the DJ-1 with Cys106-SO_2H was oxidized further, it lost its chaperone activity due to structural perturbation [63]. SAV1875 has similar canyon-shaped surface and oxidized cysteine, suggesting that SAV1875 may work as a chaperone. We discovered that the wild type and SAV1875 mutants assisted in the folding of citrate synthase but over-oxidized SAV1875 did not, even though its structure was maintained. Further detailed studies on diverse substrates and *in vivo* tests are needed to verify the exact mechanism of the SAV1875 chaperone activity.

Here, we predicted the possible functions of SAV1875 and determined that it functions as a chaperone. The characterization of SAV1875 led to the discovery of a new putative chaperone protein in the YhbO-type subfamily. Further research in the DJ-1 superfamily proteins and *in vivo* studies would advance our understanding of the fundamentals of cysteine oxidation and functional events.

Chapter IV. Summary

The cellular stress response is present in all living organisms and it dictates whether the organism adapts, survives, or if injured beyond repair, undergoes death. Thus, the study of stress responses has broad biological applications in microorganisms, plants, animals, and humans in health and disease. Although every cell within an organism is faced with a variety of stresses throughout its life, the detailed mechanism of how it defends from stresses are remain unclear. Resistance is an example of the adaptation of the bacteria to antibiotics. *S. aureus* in a leading cause of nosocomial and community-acquired infections, but mortality rate is increasing because it easily develops antibiotic resistance. Herein, we focused on the structural and functional studies of bacterial stress response proteins. The crystal structure of SAV0551 from Hsp-type DJ-1 subfamily was identified and two different functions of SAV0551 were figured out. It functions as both a chaperone and a glyoxalase III. Cysteine thiol group in SAV0551 is a catalytic nucleophile, which can degrade substrates. Next, the structural and functional changes of YhbO-type DJ-1 subfamily member, SAV1875 were analyzed under oxidative stress condition. SAV1875 accepts oxygen atom through its cysteine residue and forms stable cysteinesulfinic acid (Cys-SO_2H) structure. We discovered a novel chaperone function of SAV1875, but it lost its activity when the protein is oxidized further, to cysteinesulfonic acid (Cys-SO_3H) even though the structure is stable. Further study still needs to be done to verify the exact mechanism, but cysteine is considered to have a role in controlling the activity of protein under stress condition. From our study, we could examine structural changes of cysteine and also, its potential role in catalytic reaction and signaling pathway. This structural and functional study will be helpful for a better understanding of the mechanism of stress response system.

References

1 Archer, G. L. (1998) *Staphylococcus aureus*: a well-armed pathogen. Clinical infectious diseases : an official publication of the Infectious Diseases Society of America. **26**, 1179-1181

2 Dinges, M. M., Orwin, P. M. and Schlievert, P. M. (2000) Exotoxins of *Staphylococcus aureus*. Clinical microbiology reviews. **13**, 16-34, table of contents

3 Becker, K., Harmsen, D., Mellmann, A., Meier, C., Schumann, P., Peters, G. and von Eiff, C. (2004) Development and evaluation of a quality-controlled ribosomal sequence database for 16S ribosomal DNA-based identification of *Staphylococcus* species. Journal of clinical microbiology. **42**, 4988-4995

4 Chambers, H. F. (2001) The changing epidemiology of *Staphylococcus aureus*? Emerging infectious diseases. **7**, 178-182

5 McNicoll, L. and Marsella, M. (2010) The growing problem of methicillin-resistant *Staphylococcus aureus*: will hospitals prevail? Medicine and health, Rhode Island. **93**, 267-270

6 Sieradzki, K. and Tomasz, A. (1996) A highly vancomycin-resistant laboratory mutant of *Staphylococcus aureus*. FEMS microbiology letters. **142**, 161-166

7 Hiramatsu, K. (1998) The emergence of *Staphylococcus aureus* with reduced susceptibility to vancomycin in Japan. The American journal of medicine. **104**, 7S-10S

8 Turco, T. F., Melko, G. P. and Williams, J. R. (1998) Vancomycin intermediate-resistant *Staphylococcus aureus*. The Annals of pharmacotherapy. **32**, 758-760

9 Hanaki, H., Labischinski, H., Sasaki, K., Kuwahara-Arai, K., Inaba, Y. and Hiramatsu, K. (1998) [Mechanism of vancomycin resistance in MRSA strain

Mu50]. The Japanese journal of antibiotics. **51**, 237-247

10 Woods, C. and Colice, G. (2014) Methicillin-resistant *Staphylococcus aureus* pneumonia in adults. Expert review of respiratory medicine. **8**, 641-651

11 Quigley, P. M., Korotkov, K., Baneyx, F. and Hol, W. G. (2003) The 1.6-A crystal structure of the class of chaperones represented by *Escherichia coli* Hsp31 reveals a putative catalytic triad. Proceedings of the National Academy of Sciences of the United States of America. **100**, 3137-3142

12 Subedi, K. P., Choi, D., Kim, I., Min, B. and Park, C. (2011) Hsp31 of *Escherichia coli* K-12 is glyoxalase III. Molecular microbiology. **81**, 926-936

13 Mujacic, M. and Baneyx, F. (2007) Chaperone Hsp31 contributes to acid resistance in stationary-phase *Escherichia coli*. Applied and environmental microbiology. **73**, 1014-1018

14 Du, X., Choi, I. G., Kim, R., Wang, W., Jancarik, J., Yokota, H. and Kim, S. H. (2000) Crystal structure of an intracellular protease from *Pyrococcus horikoshii* at 2 Å resolution. Proceedings of the National Academy of Sciences of the United States of America. **97**, 14079-14084

15 Rawlings, N. D., Morton, F. R. and Barrett, A. J. (2006) MEROPS: the peptidase database. Nucleic acids research. **34**, D270-272

16 Fioravanti, E., Dura, M. A., Lascoux, D., Micossi, E., Franzetti, B. and McSweeney, S. (2008) Structure of the stress response protein DR1199 from *Deinococcus radiodurans*: a member of the DJ-1 superfamily. Biochemistry. **47**, 11581-11589

17 Abdallah, J., Caldas, T., Kthiri, F., Kern, R. and Richarme, G. (2007) YhbO protects cells against multiple stresses. Journal of bacteriology. **189**, 9140-9144

18 Jung, H. J., Kim, S., Kim, Y. J., Kim, M. K., Kang, S. G., Lee, J. H., Kim, W. and Cha, S. S. (2012) Dissection of the dimerization modes in the DJ-1 superfamily. Molecules and cells. **33**, 163-171

19 Wei, Y., Ringe, D., Wilson, M. A. and Ondrechen, M. J. (2007) Identification of functional subclasses in the DJ-1 superfamily proteins. PLoS computational biology. **3**, e10

20 Herrera, F. E., Zucchelli, S., Jezierska, A., Lavina, Z. S., Gustincich, S. and Carloni, P. (2007) On the oligomeric state of DJ-1 protein and its mutants associated with Parkinson Disease. A combined computational and in vitro study. The Journal of biological chemistry. **282**, 24905-24914

21 Ito, G., Ariga, H., Nakagawa, Y. and Iwatsubo, T. (2006) Roles of distinct cysteine residues in S-nitrosylation and dimerization of DJ-1. Biochemical and biophysical research communications. **339**, 667-672

22 Junn, E., Taniguchi, H., Jeong, B. S., Zhao, X., Ichijo, H. and Mouradian, M. M. (2005) Interaction of DJ-1 with Daxx inhibits apoptosis signal-regulating kinase 1 activity and cell death. Proceedings of the National Academy of Sciences of the United States of America. **102**, 9691-9696

23 Mo, J. S., Kim, M. Y., Ann, E. J., Hong, J. A. and Park, H. S. (2008) DJ-1 modulates UV-induced oxidative stress signaling through the suppression of MEKK1 and cell death. Cell death and differentiation. **15**, 1030-1041

24 van Hal, S. J., Jensen, S. O., Vaska, V. L., Espedido, B. A., Paterson, D. L. and Gosbell, I. B. (2012) Predictors of mortality in *Staphylococcus aureus* Bacteremia. Clinical microbiology reviews. **25**, 362-386

25 Gouet, P., Courcelle, E., Stuart, D. I. and Metoz, F. (1999) ESPript: analysis of multiple sequence alignments in PostScript. Bioinformatics. **15**, 305-308

26 Collaborative Computational Project, N. (1994) The CCP4 suite: programs for protein crystallography. Acta crystallographica. Section D, Biological crystallography. **50**, 760-763

27 Dodson, E. J., Winn, M. and Ralph, A. (1997) Collaborative Computational Project, number 4: providing programs for protein crystallography.

Methods in enzymology. **277**, 620-633

28 Vagin, A. and Teplyakov, A. (2010) Molecular replacement with MOLREP. Acta crystallographica. Section D, Biological crystallography. **66**, 22-25

29 Emsley, P. and Cowtan, K. (2004) Coot: model-building tools for molecular graphics. Acta crystallographica. Section D, Biological crystallography. **60**, 2126-2132

30 Murshudov, G. N., Skubak, P., Lebedev, A. A., Pannu, N. S., Steiner, R. A., Nicholls, R. A., Winn, M. D., Long, F. and Vagin, A. A. (2011) REFMAC5 for the refinement of macromolecular crystal structures. Acta crystallographica. Section D, Biological crystallography. **67**, 355-367

31 Brunger, A. T. (1992) Free R value: a novel statistical quantity for assessing the accuracy of crystal structures. Nature. **355**, 472-475

32 Pettersen, E. F., Goddard, T. D., Huang, C. C., Couch, G. S., Greenblatt, D. M., Meng, E. C. and Ferrin, T. E. (2004) UCSF Chimera--a visualization system for exploratory research and analysis. Journal of computational chemistry. **25**, 1605-1612

33 Krissinel, E. and Henrick, K. (2007) Inference of macromolecular assemblies from crystalline state. Journal of molecular biology. **372**, 774-797

34 Lee, G. J. (1995) Assaying proteins for molecular chaperone activity. Methods in cell biology. **50**, 325-334

35 Zhi, W., Landry, S. J., Gierasch, L. M. and Srere, P. A. (1992) Renaturation of citrate synthase: influence of denaturant and folding assistants. Protein science : a publication of the Protein Society. **1**, 522-529

36 Mujacic, M., Bader, M. W. and Baneyx, F. (2004) Escherichia coli Hsp31 functions as a holding chaperone that cooperates with the DnaK-DnaJ-GrpE system in the management of protein misfolding under severe stress conditions. Molecular microbiology. **51**, 849-859

37 Lethanh, H., Neubauer, P. and Hoffmann, F. (2005) The small heat-shock

proteins IbpA and IbpB reduce the stress load of recombinant *Escherichia coli* and delay degradation of inclusion bodies. Microbial cell factories. **4**, 6

38 Sastry, M. S., Korotkov, K., Brodsky, Y. and Baneyx, F. (2002) Hsp31, the *Escherichia coli* yedU gene product, is a molecular chaperone whose activity is inhibited by ATP at high temperatures. The Journal of biological chemistry. **277**, 46026-46034

39 Ben-Zvi, A. P. and Goloubinoff, P. (2001) Review: mechanisms of disaggregation and refolding of stable protein aggregates by molecular chaperones. Journal of structural biology. **135**, 84-93

40 Sastry, M. S., Quigley, P. M., Hol, W. G. and Baneyx, F. (2004) The linker-loop region of *Escherichia coli* chaperone Hsp31 functions as a gate that modulates high-affinity substrate binding at elevated temperatures. Proceedings of the National Academy of Sciences of the United States of America. **101**, 8587-8592

41 Allaman, I., Belanger, M. and Magistretti, P. J. (2015) Methylglyoxal, the dark side of glycolysis. Frontiers in neuroscience. **9**, 23

42 Kizil, G., Wilks, K., Wells, D. and Ala'Aldeen, D. A. (2000) Detection and characterisation of the genes encoding glyoxalase I and II from *Neisseria meningitidis*. Journal of medical microbiology. **49**, 669-673

43 Larkin, M. A., Blackshields, G., Brown, N. P., Chenna, R., McGettigan, P. A., McWilliam, H., Valentin, F., Wallace, I. M., Wilm, A., Lopez, R., Thompson, J. D., Gibson, T. J. and Higgins, D. G. (2007) Clustal W and Clustal X version 2.0. Bioinformatics. **23**, 2947-2948

44 Laemmli, U. K. (1970) Cleavage of structural proteins during the assembly of the head of bacteriophage T4. Nature. **227**, 680-685

45 Louis-Jeune, C., Andrade-Navarro, M. A. and Perez-Iratxeta, C. (2012) Prediction of protein secondary structure from circular dichroism using theoretically derived spectra. Proteins. **80**, 374-381

46 Greenfield, N. J. (2006) Using circular dichroism spectra to estimate

protein secondary structure. Nature protocols. **1**, 2876-2890

47 Twining, S. S. (1984) Fluorescein isothiocyanate-labeled casein assay for proteolytic enzymes. Analytical biochemistry. **143**, 30-34

48 Vandooren, J., Geurts, N., Martens, E., Van den Steen, P. E. and Opdenakker, G. (2013) Zymography methods for visualizing hydrolytic enzymes. Nature methods. **10**, 211-220

49 Morgunov, I. and Srere, P. A. (1998) Interaction between citrate synthase and malate dehydrogenase. Substrate channeling of oxaloacetate. The Journal of biological chemistry. **273**, 29540-29544

50 Abdallah, J., Kern, R., Malki, A., Eckey, V. and Richarme, G. (2006) Cloning, expression, and purification of the general stress protein YhbO from *Escherichia coli*. Protein expression and purification. **47**, 455-460

51 Wilson, M. A., St Amour, C. V., Collins, J. L., Ringe, D. and Petsko, G. A. (2004) The 1.8 Å resolution crystal structure of YDR533Cp from *Saccharomyces cerevisiae*: a member of the DJ-1/ThiJ/*Pf*pI superfamily. Proceedings of the National Academy of Sciences of the United States of America. **101**, 1531-1536

52 Blackinton, J., Lakshminarasimhan, M., Thomas, K. J., Ahmad, R., Greggio, E., Raza, A. S., Cookson, M. R. and Wilson, M. A. (2009) Formation of a stabilized cysteine sulfinic acid is critical for the mitochondrial function of the parkinsonism protein DJ-1. The Journal of biological chemistry. **284**, 6476-6485

53 Wilson, M. A., Ringe, D. and Petsko, G. A. (2005) The atomic resolution crystal structure of the YajL (ThiJ) protein from *Escherichia coli*: a close prokaryotic homologue of the Parkinsonism-associated protein DJ-1. Journal of molecular biology. **353**, 678-691

54 Bandyopadhyay, S. and Cookson, M. R. (2004) Evolutionary and functional relationships within the DJ-1 superfamily. BMC evolutionary biology. **4**, 6

55 Witt, A. C., Lakshminarasimhan, M., Remington, B. C., Hasim, S.,

Pozharski, E. and Wilson, M. A. (2008) Cysteine pK_a depression by a protonated glutamic acid in human DJ-1. Biochemistry. **47**, 7430-7440

56 Rinalducci, S., Murgiano, L. and Zolla, L. (2008) Redox proteomics: basic principles and future perspectives for the detection of protein oxidation in plants. Journal of experimental botany. **59**, 3781-3801

57 Roeser, J., Bischoff, R., Bruins, A. P. and Permentier, H. P. (2010) Oxidative protein labeling in mass-spectrometry-based proteomics. Analytical and bioanalytical chemistry. **397**, 3441-3455

58 Stadtman, E. R. and Levine, R. L. (2003) Free radical-mediated oxidation of free amino acids and amino acid residues in proteins. Amino acids. **25**, 207-218

59 Wani, R., Nagata, A. and Murray, B. W. (2014) Protein redox chemistry: post-translational cysteine modifications that regulate signal transduction and drug pharmacology. Frontiers in pharmacology. **5**, 224

60 Kuroda, M., Ohta, T., Uchiyama, I., Baba, T., Yuzawa, H., Kobayashi, I., Cui, L., Oguchi, A., Aoki, K., Nagai, Y., Lian, J., Ito, T., Kanamori, M., Matsumaru, H., Maruyama, A., Murakami, H., Hosoyama, A., Mizutani-Ui, Y., Takahashi, N. K., Sawano, T., Inoue, R., Kaito, C., Sekimizu, K., Hirakawa, H., Kuhara, S., Goto, S., Yabuzaki, J., Kanehisa, M., Yamashita, A., Oshima, K., Furuya, K., Yoshino, C., Shiba, T., Hattori, M., Ogasawara, N., Hayashi, H. and Hiramatsu, K. (2001) Whole genome sequencing of meticillin-resistant *Staphylococcus aureus*. Lancet. **357**, 1225-1240

61 Chen, J., Li, L. and Chin, L. S. (2010) Parkinson disease protein DJ-1 converts from a zymogen to a protease by carboxyl-terminal cleavage. Human molecular genetics. **19**, 2395-2408

62 Shendelman, S., Jonason, A., Martinat, C., Leete, T. and Abeliovich, A. (2004) DJ-1 is a redox-dependent molecular chaperone that inhibits alpha-synuclein aggregate formation. PLoS biology. **2**, e362

63 Zhou, W., Zhu, M., Wilson, M. A., Petsko, G. A. and Fink, A. L. (2006)

The oxidation state of DJ-1 regulates its chaperone activity toward alpha-synuclein. Journal of molecular biology. **356**, 1036-1048

64 Giles, N. M., Watts, A. B., Giles, G. I., Fry, F. H., Littlechild, J. A. and Jacob, C. (2003) Metal and redox modulation of cysteine protein function. Chemistry & biology. **10**, 677-693

65 Biswas, S., Chida, A. S. and Rahman, I. (2006) Redox modifications of protein-thiols: emerging roles in cell signaling. Biochemical pharmacology. **71**, 551-564

66 Finkel, T. (2000) Redox-dependent signal transduction. FEBS letters. **476**, 52-54

국문초록

Staphylococcus aureus 는 가장 잘 알려진 병원성 균주 중 하나이다. 식중독, 피부감염 등 가벼운 증상부터 심내막염, 패혈증에 이르는 심각한 감염성 질환을 일으키는 균주로 알려져 있지만 환경 변화에 대한 적응력이 뛰어나고 각종 항생제에 내성을 가진 슈퍼박테리아 strain 인 MRSA, VISA, VRSA 가 지속적으로 출현하는 것이 심각한 문제로 대두되고 있다. DJ-1/ThiJ/*Ph*pI superfamily 는 생명체의 모든 계에 분포하는 단백질의 그룹 중 하나로 주로 세포의 스트레스 대응 매커니즘에 관여되어 있다고 알려져 있다. 본 연구에서는 다양한 항생제에 내성을 보이는 VISA 인 *S. aureus* Mu50 유래의 DJ-1/ThiJ/*Ph*pI superfamily 단백질인 SAV0551 과 SAV1875 의 구조와 기능에 대해 연구하였다. SAV0551 은 구조상 Hsp-type DJ-1 subfamily 에 속하며 반응성 높은 Cysteine 이 190 번 위치에 존재한다. Cys190 은 His191, Asp221 과 catalytic triad 를 이루고 있다. catalytic triad 와 그 기능의 차이를 알기 위하여, C190A, C190D 의 mutant 들이 디자인 되었다. 본 연구에서 우리는 SAV0551 이 chaperone 이자 glyoxalase III 임을 밝혔다. 하지만, C190A 와 C190D 는 chaperone 기능은 여전히 가지고 있지만 glyoxalase III 효과를 잃었다. SAV1875 는 그 구조상 YhbO-type DJ-1 subfamily 에 속하며 DJ-1/ThiJ/*Ph*pI superfamily 의 단백질의 공통된 특징인 반응성이 높은 cysteine 을 105 번 위치에 가지고 있다. 이 cysteine 은 His106, Asp77 과 함께 catalytic triad 를 이루고 있다. Cys105 는 크리스탈 구조상에서 산화되어있고, 매우 안정화 되어 있으며 이는 SAV1875 의 mutant 인 E17D, E17N, C105D 으로 확인할 수

있었다. SAV1875 Cys105 는 H_2O_2 상태에서 과산화 시켰을 때, Cys105-SO_3H (cysteinesulfonic acid)로 완전하게 산화되며 이 또한 매우 안정적인 구조를 보이고 있었다. SAV1875 와 mutant 를 이용하여 그 활성을 실험한 결과, SAV1875 는 chaperone 으로 작용하며 그 기능은 Cys105 의 산화상태와 관련이 있음을 알 수 있었다. 본 연구를 바탕으로 우리는 *S. aureus* 에서 chaperone 으로 작용하는 SAV0551 과 SAV1875 의 구조를 규명하였고, SAV0551 의 catalytic triad 와 관련된 glyoxalase III 의 기능을 알 수 있었으며, cysteine 의 다양한 산화상태를 SAV1875 의 변이와 과산화 구조에서 밝혔다. Cysteine 의 산화는 단백질의 기능에서 중요한 역할을 한다는 것을 SAV1875 의 chaperone 실험을 통해 제시하였다.

주요어: DJ-1/ThiJ/*Pf*pI superfamily*, Staphylococcus aureus*, cysteine, oxidation, chaperone

학번: 2011-30503

약학박사학위논문

Structural and functional studies of the DJ-1/ThiJ/*Pf*pI superfamily proteins from *Staphylococcus aureus*

포도상구균 유래의 DJ-1/ThiJ/*Pf*pI superfamily 단백질에 대한 구조와 기능 연구

2016 년 2 월

서울대학교 대학원

약학과 물리약학전공

김 효 정

Abstract

Structural and functional studies of the DJ-1/ThiJ/*Pf*pI superfamily proteins from *Staphylococcus aureus*

Hyo Jung Kim

Physical pharmacy

Department of pharmacy

The Graduate School

Seoul National University

Staphylococcus aureus is one of the most common pathogen that causes various diseases ranging from mild infections, such as skin infections and food poisoning, to life threatening infections, such as sepsis, endocarditis, and toxic shock syndrome. However, *S. aureus* has adapted to circumvent therapeutic strategies by developing resistance to antibiotics and becoming problems. The DJ-1/ThiJ/*Pf*pI superfamily is a group of proteins over diverse organisms. This superfamily includes versatile proteins, such as proteases, chaperones, heat shock proteins and human Parkinson's disease protein. SAV0551 and SAV1875, conserved proteins from *S. aureus*, are members of the DJ-1/ThiJ/*Pf*pI superfamily. However, their

structure and function remain unknown. Thus, to understand the function and activity mechanism of these proteins, the crystal structure of SAV0551 and SAV1875 from *S. aureus* was determined. Their conserved cysteine residue forms a catalytic triad with histidine and aspartate. In particular, cysteine in SAV1875 is spontaneously oxidized to Cys105-SO_2H in the crystal structure. To study the oxidative propensity of Cys105 in SAV1875 and the corresponding functional differences with changes in cysteine oxidation state, the crystal structures of SAV1875 variants, E17N, E17D, C105D, and over-oxidized SAV1875 were determined. The overall fold of SAV1875 and SAV0551 is similar to that observed for the DJ-1/ThiJ/*Pf*pI superfamily. We identified SAV1875 as a novel member of the YhbO-type subfamily exhibiting chaperone function and SAV0551 as a member of Hsp-type subfamily that has chaperone and glyoxalase function. The chaperone activity was based on the surface structure, but if SAV1875 is over-oxidized further with H_2O_2, its chaperone activity is eliminated.

Key words: DJ-1/ThiJ/*Pf*pI superfamily, *Staphylococcus aureus*, cysteine, oxidation, chaperone

Student Number: 2011-30503

Table of Contents

Abstract·····i

Contents·····iv

List of Tables·····viii

List of Figures·····ix

Contents

Chapter I. Introduction

1.1. *Staphylococcus aureus*

1.1.1. Features of *Staphylococcus aureus*·····1

1.1.2. Antibiotic resistance of *Staphylococcus aureus*·····2

1.2. DJ-1/ThiJ/*Pf*pI superfamily

1.2.1. Introduction of DJ-1/ThiJ/*Pf*pI superfamily·····3

1.2.2. Classification of DJ-1/ThiJ/*Pf*pI superfamily·····3

1.2.3. Protein members of DJ-1/ThiJ/*Pf*pI superfamily·····5

1.3. Research goals·····5

Chapter II. The structure and function of SAV0551

2.1. Introduction·····9

2.2. Materials and Methods

2.2.1. Cloning, protein expression, and purification·····11

2.2.2. Crystallization and data collection·····12

2.2.3. Structure determination and refinement·····13

2.2.4. Determination of chaperone activity·····13

2.2.5. Determination of glutathione independent glyoxalase activity·····14

2.3. Results

2.3.1. Structure of SAV0551·····15

2.3.2. Oligomeric state of SAV0551·····17

2.3.3. Catalytic triad of SAV0551·····20

2.3.4. SAV0551 has chaperon activity·····22

2.3.5. SAV0551 has glutathione independent glyoxalase activity·····23

2.4. Discussion·····26

Chapter III. The structure and function of SAV1875

3.1. Introduction·····29

3.2. Materials and Methods

3.2.1. Cloning, protein expression, and purification·····31

3.2.2. Crystallization and data collection·····33

3.2.3. PAGE·····34

3.2.4. Mass spectrometry·····34

3.2.5. Protein oxidation·····35

3.2.6. Circular Dichroism (CD)·····35

3.2.7. Protease activity assay and zymogram·····36

3.2.8. Determination of chaperone activity·····37

3.3. Results

3.3.1. Structure of SAV1875·····37

3.3.2. Oligomeric state of SAV1875·····40

3.3.3. Comparison of SAV1875 with DJ-1 superfamily proteins·····43

3.3.4. Stabilization of oxidized Cys105·····45

3.3.5. Oxidation propensity of Cys105 in SAV1875·····51

3.3.6. Protease activity of SAV1875 was not detected·····55

3.3.7. SAV1875 has chaperon activity·····57

3.4. Discussion·····59

Chapter IV. Summary·····62

References·····63

Korean Abstract (국문초록)·····71

List of Tables

Table 1. Classification of DJ-1/ThiJ/*Pf*pI superfamily·····4

Table 2. Primer design of SAV1875 mutants·····31

List of Figures

Figure 1. Micrograph of *S. aureus*·····1

Figure 2. Comparison of SAV0551 amino acid sequence to other members of the DJ-1/ThiJ/*Pf*pI superfamily·····10

Figure 3. Expression, purification, and crystallization of SAV0551·····15

Figure 4. Ribbon diagram of SAV0551·····17

Figure 5. The SAV0551 dimer·····18

Figure 6. Catalytic triad of SAV0551·····19

Figure 7. Surface structure of SAV0551·····20

Figure 8. The configuration of catalytic triad·····21

Figure 9. No significant difference in chaperone activity in wild type SAV0551 and cysteine mutants·····23

Figure 10. Remaining amount of methylglyoxal at 100 sec of time point·····25

Figure 11. Narrow active site cleft of SAV0551·····26

Figure 12. Comparison of SAV1875 amino acid sequence to other members of DJ-1/ThiJ/*Pf*pI superfamily·····30

Figure 13. Expression, purification, and crystallization of SAV1875·····38

Figure 14. Ribbon diagram of SAV1875·····39

Figure 15. Dimer structure of SAV1875·····40

Figure 16. Ribbon diagram of constrained hexamer SAV1875·····42

Figure 17. Surface structure of SAV1875·····43

Figure 18. The superposition of SAV1875 (cyan) with other members of the DJ-

1/ThiJ/*Pf*pI superfamily YhbO (pink), *Ph*pI (blue), DR1199 (orange), Ton1285 (green), and DJ-1 (Grey)·····44

Figure 19. A hydrogen bond·····46

Figure 20. Oxidation state of cysteine at residue 105·····48

Figure 21. Hydrogen bonds around Cys105·····49

Figure 22. Local difference around the reactive cysteine in DJ-1 (left) and SAV1875 (right)·····50

Figure 23. The geometry of cysteinesulfinic acid is not the same as aspartate··51

Figure 24. MS spectrometry and PAGE of SAV1875·····53

Figure 25. Over-oxidized SAV1875 does not lead to loss of secondary structure·····55

Figure 26. Comparison of oligomeric state in solution of YhbO-type DJ-1 superfamily·····56

Figure 27. Chaperone activity of SAV1875 depending on cysteine oxidation state·····58

Chapter I. Introduction

1.1. *Staphylococcus aureus*

Staphylococcus aureus is a gram positive bacterium that is usually found in the nasal passages and on the skin. This organism is part of the human normal flora, and is primarily found in the nose and skin. However, *S. aureus* is either one of the most common opportunistic pathogen that causes various diseases ranging from mild infections, such as skin infections and food poisoning, to life threatening infections, such as sepsis, endocarditis, and toxic shock syndrome [1]. Several exotoxins, which are secreted from *S. aureus*, are associated with specific diseases [2].

1.1.1. Features of *Staphylococcus aureus*

S. aureus belongs to the *Staphylococcaceae* family. It appears as grape-like clusters when viewed through a microscope, and has large, round, golden-yellow colonies. The spherical cells of *S. aureus* are up to 1 μm in diameter, non-motile, non-spore forming, facultative anaerobes that usually form in clusters [3].

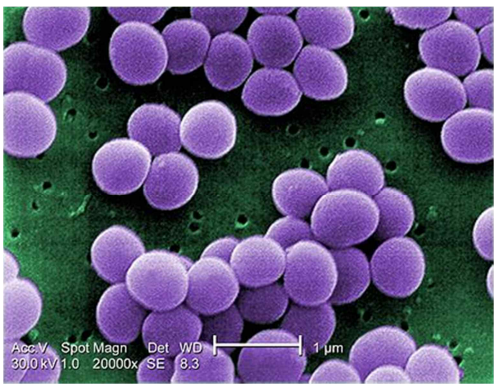

Figure 1. Micrograph of *S. aureus* (Matthew J. Arduino, DRPH Photo Credit)

1.1.2. Antibiotic resistance of *Staphylococcus aureus*

The treatment of choice for *S. aureus* infection was penicillin. Penicillin inhibits the formation of peptidoglycan cross-linkages that provides the rigidity and strength in a bacterial cell wall. However, soon after the advent of penicillin in 1946, 80% of hospital *S. aureus* isolates were penicillin-resistant by 1960 [4]. Nowadays, penicillin resistance is extremely common, and first-line therapy is most commonly a penicillinase-resistant β-lactam antibiotics (oxacillin or flucloxacillin). In many cases, treatment faces difficulties because of the evolution of resistant strains. MRSA, methicillin resistant *S. aureus* emerged. Today, MRSA accounts for over 60% of *S. aureus* infection, including nosocomial and community acquired infection [5]. Combination therapy can be used to treat serious infections, but its use is controversial because of the possibility of kidney damages. Recently, there are even newly emerging strains such as vancomycin resistant *S. aureus* (VRSA). More specifically, vancomycin resistant *S. aureus* bacteria are classified as VISA (vancomycin-intermediate *S. aureus*) if the minimum inhibitory concentration (MIC) against vancomycin is 4-8 μg/ml and classified as VRSA if the MIC is more than 16 μg/ml [6]. For example, *S. aureus* Mu50 (ATCC 700699), which was first isolated from a sternal abscess in a child who had received a prolonged course of vancomycin treatment [7], is classified as VISA because the MIC against vancomycin is 8 μg/ml [8, 9]. Because of this bacterial resistance, the prognosis of a *S. aureus* infection is still poor despite early diagnosis and appropriate treatment [10]. Currently, the spread of resistance in bacterial populations is a major health challenge. Therefore, understanding the detailed mechanism of how bacteria adapt to environmental changes is essential for developing better therapeutics. Thus, researches on the bacterial system under environmental stress condition are emerging as important issues.

1.2. DJ-1/ThiJ/*Pf*pI Superfamily

1.2.1. Introduction of DJ-1/ThiJ/*Pf*pI Superfamily

The DJ-1/ThiJ/*Pf*pI superfamily (DJ-1 superfamily hereafter) is a group of proteins over diverse organisms. This superfamily includes versatile proteins, such as proteases, chaperones, heat shock proteins and human Parkinson's disease protein. Mainly, DJ-1 superfamily proteins function as specific stress response proteins: *Escherichia coli* Hsp31, which is involved in thermal stress protection, acid resistance, and glyoxalase activity [11-13]; *Ph*pI and *Pf*pI, which are heat-endurable proteases from *Pyrococcus horikoshii* [14] and *Pyrococcus furious* [15], respectively; *Deinococcus radiodurans* DR1199, which is a general stress resistance protein [16]; and *E. coli* YhbO, a protein highly sensitive to oxidative, thermal, UV, and pH stresses [17].

Structurally, DJ-1 superfamily proteins share a common fold. Most members of DJ-1 superfamily proteins are oligomers from dimer to hexamer. Each monomer consists of the antiparallel β-strands surrounded by α-helices. This fold is called "α/β sandwich fold". In the core structure, there is a "nucleophilic elbow" is present, a sharp turn of a β-strand and an α-helix, which is common to several hydrolytic enzymes. On its extremely sharp turn, cysteine is located. This cysteine usually is a part of catalytic triad in DJ-1 superfamily proteins.

1.2.2. Classification of DJ-1/ThiJ/*Pf*pI superfamily

The DJ-1 superfamily proteins can be classified into subfamilies based on their quaternary structure; DJ-1-type, YhbO-type, and Hsp-type. Alternative oligomerization modes are a method of generating functional diversity in homologs

with a similar tertiary structure. Each subfamily has different characteristics in the oligomeric state and a catalytic dyad/triad conformation. The DJ-1-type proteins (DJ-1 and YajL) form a dimeric interface consisting of α-helices, β-strands, and loops. The YhbO-type proteins (YhbO, *Ph*pI, DR1199, and Ton1285) interact with the other subunits by three helices. The Hsp-type proteins (Hsp31) form a unique dimerization surface consisting of N terminal β strands and loops [18, 19]. DJ-1, YajL, and YdeA are the members of DJ-1-type DJ-1 subfamily. YhbO, *Pf*pI, DR1199, and Ton1285 are known proteins for YhbO-type DJ-1 subfamily. Hsp31 proteins from *E. coli, Candida albicans, Vibrio cholerae,* and *Saccharomyces cerevisiae* are categorized as Hsp-type DJ-1 subfamily members. In addition to the difference in dimerization modes among these subfamilies, there is also a difference in the architecture of catalytic triad. The DJ-1-type DJ-1 forms catalytic dyad with nearby histidine. The cysteine in the DJ-1-type YajL does not form catalytic dyad/triad. The YhbO-type proteins constitute a catalytic triad with cysteine, the histidine next to cysteine, and an acidic residue from the other subunit [11, 16]. The Hsp-type proteins form a catalytic triad using cysteine, the histidine next to cysteine, and an acidic residue from an intrasubunit from the other domain (cap domain). Consequently, these commonalities and distinctive features suggest that the oligomeric state and the reactive cysteine of DJ-1 superfamily proteins appear to be crucial in the functions of these proteins [20, 21].

	DJ-1-type DJ-1 superfamily	**YhbO-type DJ-1 superfamily**	**Hsp-type DJ-1 superfamily**
Examples	DJ-1	YhbO	*E. coli* Hsp31
	YajL	*Pf*pI	*V. cholerae* Hsp31
		Ton1285	*S. cereviseae* Hsp31
		DR1199	*C. albicans* Hsp31

Dimerization modes		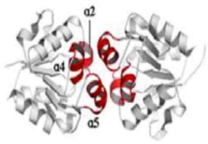	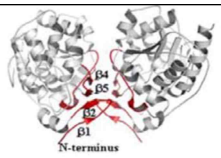

Table 1. Classification of DJ-1/ThiJ/*Pf*pI superfamily. DJ-1 superfamily can be divided into three distinct subfamilies depending on their dimeric interfaces. The DJ-1 dimer, YhbO dimer, and Hsp31 dimer are shown.

1.2.3. Protein members of DJ-1/ThiJ/*Pf*pI superfamily

Many of DJ-1 family proteins are of unknown function, and also are examples of proteins with both sequence and fold similarity that has multiple classes. DJ-1, a representative member of DJ-1-type DJ-1 subfamily protein is associated with Parkinson's disease and cancers. Deletion or mutations in DJ-1 are reported to be responsible for recessive early onset of Parkinson disease. However, the detailed mechanisms are still not fully revealed. DJ-1 plays a protective role against oxidative stress. It functions as a redox sensitive regulator of suppressing the JNK signaling pathways or interacts with Daxx and sequesters in within the nucleus, preventing the initiation of apoptotic signals [22, 23]. It also acts as a chaperone that helps folding of α-syneclin. YhbO-type DJ-1 subfamily members are stress response proteins that protect cells from oxidative, thermal, and pH stresses. Some proteins (*Pf*pI, *Ph*pI, and Ton1285) of YhbO-type DJ-1 subfamily revealed proteolytic activity. Hsp-type DJ-1 proteins are mostly 31 kDa of chaperones and also have glyoxalase III activity.

1.3. Research goals

Bacteria are designed to be adaptable to their circumstance. In the changes in temperature, pH, radiation, oxidation, and other nature of the surrounding support, bacteria adapt to environment. Bacterial surrounding layers, genetic information for resistance, and other structures associated with a bacterium are capable of alteration. Some alterations are reversible, disappearing when the particular pressure is lifted. Other alterations are maintained and can even be passed on to succeeding generations of bacteria. This adaptation is under tight genetic control, involving the expression of multiple genes. The examples are the responses shown by *Helicobacter pylori* to growth in an acidic environment of stomach and *Deinococcus radiodurans* to growth in a harsh radiation. Bacteria also react to sudden changes in their environment by expressing or repressing the expression of a whole list of genes. A well-known example of this adaptation is the heat shock response of *E. coli*. The name derives from the fact that the response was first observed in bacteria suddenly shifted to a higher growth temperature. Another adaptation exhibited by *Vibrio parahaemolyticus* is the formation of adherent populations on solid surfaces. This mode of growth is called a biofilm, involving the expression of previously unexpressed genes. In addition, deactivation of actively expressing genes can occur.

Some harmful bacteria are adapting to drugs faster than cures can be developed. Resistance is an example of adaptation of the bacteria to environment. The introduction of first antibiotic is followed by the development of resistance to the agent. The adaptation of bacteria to an antibacterial agent can occur in two ways. The first method is known as inherent resistance. For example, gram-negative bacteria are often naturally resistant to penicillin. This is because bacteria have another outer membrane, which makes the penetration of penicillin to its target more difficult. The second method is called acquired resistance due to a change in the genetic information of the bacterial genome. Acquired adaptation can occur because of mutation or as a response by the bacteria to the selective pressure

imposed by the bacterial agent. Once the genetic alteration that confers resistance is present, it can be passed on to the subsequent generations.

S. aureus is notorious for its ability to become resistant to many antibiotics. Methicillin-resistant *Staphylococcus aureus* (MRSA) isolates soon after the introduction of methicillin. First, MRSA isolates have been associated with nosocomial infections and rapidly developed resistance to multiple drug classes. In recent years, reservoir of community associated MRSA is rapidly expanding. Compared to nosocomial strains, community-associated MRSA isolates are associated with increased virulence and currently are more likely to be susceptible to a variety of antibiotics. Vancomycin non susceptibility in *S. aureus* is on the increase, requires further complicating therapy. Study of early isolates of MRSA showed that a key genetic component responsible for resistance, *mecA*, is not native to the *S. aureus* genome. This genetic element confers resistance to most currently available β-lactam antibiotics. However, not all *mecA* clones are resistant to methicillin, modulated by a variety of chromosomal factors. In the early MRSA that has the *mecA* gene do not express methicillin resistance, but soon after, mutations on control regulator genes occur and the strains become resistant to methicillin. Today, most MRSA strains are resistant to multi drugs including vancomycin.

S. aureus is one of the well-known pathogens causing many forms of infection ranging from mild to life threatening. The bacteria tend to infect the skin, often cause superficial skin lesions such as boil, furuncle, abscess, and styes. However, the bacteria can travel through the bloodstream and infect organs in the body, particularly lung (pneumonia), heart valves (endocarditis), and bones (osteomyelitis). Among many strains of *S. aureus*, some strains produce toxins that can cause toxic shock syndrome. *S. aureus* infection is an important infection with an incidence rate ranging from 20 to 50 cases/100,000 population per year. The mortality rate due to *S. aureus* infection is between 10% and 30%. Comparatively,

this accounts for a greater number of deaths than for AIDS, tuberculosis, and viral hepatitis combined [24].

Previously, researches have concentrated on developing more powerful antibiotics to cope with the increased resistance. But developing more powerful antibiotics contributes to concerns about antibiotic-resistant bacteria. Researches about fundamental mechanisms of bacterial physiology to adapt varying environment are currently ongoing, but still remain elusive. Thus, our research focused on the alteration of bacterial proteins under stress conditions. Since DJ-1 superfamily proteins are known as stress-response proteins, we expected that these proteins would show defensive roles under stress condition.

Herein, we elucidated the crystal structures of SAV0551, SAV1875, mutants of wild type proteins, and over-oxidized SAV1875. To gain insight on the function, chaperone, protease, and glyoxalase activity tests were conducted. These functional tests revealed SAV0551 and SAV1875 as multi-functional proteins. Since the wild type SAV1875 is oxidized in the crystal structure, this protein is predicted to be related to oxidative stress defense system. The three mutants, E17N, E17D, and C105D, and over-oxidized SAV1875 containing Cys105-SO_3H (cysteinesulfonic acid) were designed to identify the oxidative propensity of Cys105 as well as the corresponding structural and functional differences. The structural and functional research under oxidative condition will promote a better understanding of bacterial physiology and how bacteria defend against oxidative stress.

Chapter II. The structure and function of SAV0551

2.1. Introduction

From the sequence homology among Hsp-type DJ-1 subfamily members, SAV0551 is predicted to be classified into Hsp-type DJ-1 subfamily: Hsp31 from *E.coli* (54% sequence identity), Hsp31 from *Vibrio cholerae* (49% sequence identity), and Hsp31 from *Saccharomyces cerevisiae* (12% sequence identity). A structure-based sequence alignment was acquired using the ClustalW web server tool [25] and viewed using the ESPript web server tool [25]. The sequence alignment of SAV0551 with Hsp31 proteins from *E. coli*, *V. choleae*, and *S. cerevisiae* is shown in Figure 2. Form the sequence information, SAV0551 is predicted to have chaperone and glyoxalase function as well based on similarity to others of Hsp-type DJ-1 subfamily proteins. SAV0551 gene codes 292 amino acids. The estimated molecular weight is 32 kDa and calculated pI is 4.90.

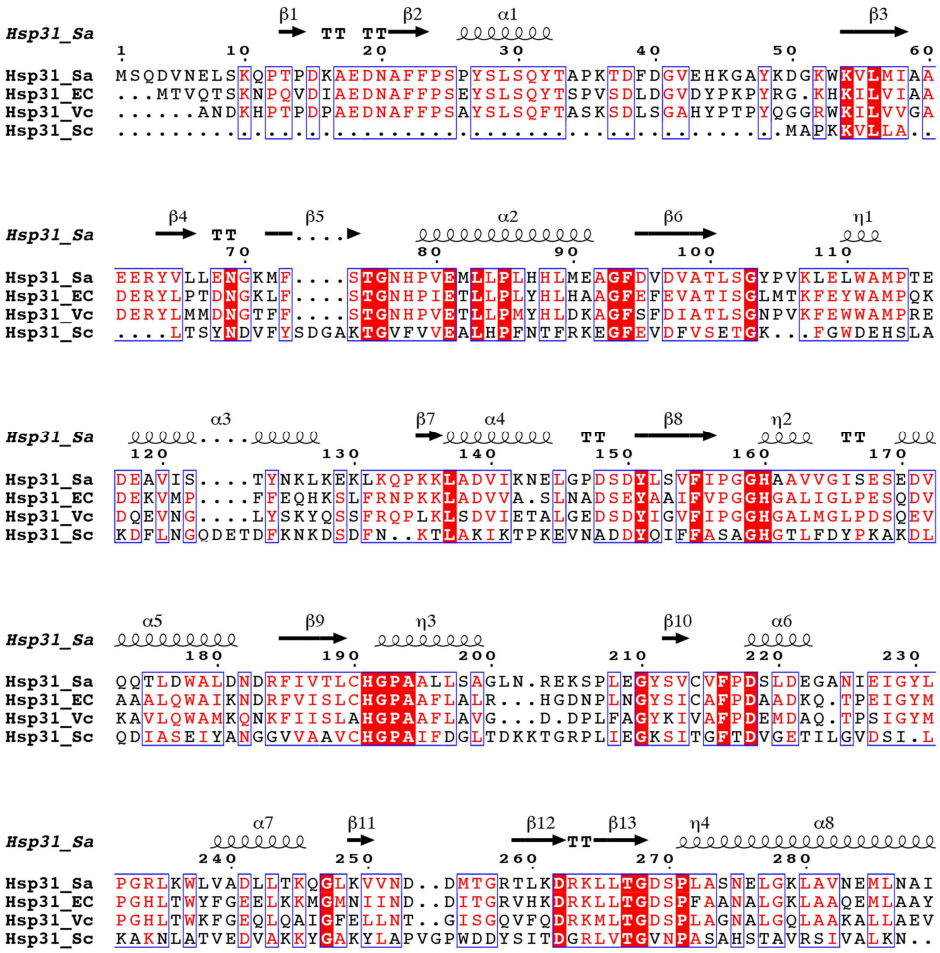

Figure 2. Comparison of SAV0551 amino acid sequence to other members of Hsp-type DJ-1/ThiJ/*Pf*pI superfamily.

Sequence alignment of SAV0551 with *E.coli* Hsp31 (54% sequence identity), *Vibrio cholerae* Hsp31 (49% sequence identity), and *Saccharomyces cerevisiae* Hsp31 (12% sequence identity). Identical residues are colored white on a red background and similar residues are red on a white background. Secondary structure elements (springs, α-helices; arrows, β-strands) are represented above the sequences and are numbered. The figure was constructed using ESPript [25].

2.2. Materials and Methods

3.2.1. Cloning, protein expression, and purification

The predicted ORF of Hsp31 (SAV0551) was amplified from *S. aureus* MU50 genomic DNA using standard PCR methods. The forward and reverse oligonucleotide primers designed using the published genome sequence were 5'-GACTGCATATGTCACAAGATGTAAATGAATTAAG and 5'- GTCACTCGAGT TTATTTTGTATTGCATTTAACAT, respectively, where the bases underlined represent the NdeI and XhoI restriction enzyme cleavage sites. The amplified DNA was inserted into the NdeI/XhoI-digested expression vector pET-21a(+) expression vector (Novagen Inc., USA). The resulting construct contains eight nonnative residues at the C-terminus (LEHHHHHH) that facilitate protein purification. The accuracy of the cloning was confirmed by DNA sequencing. The resulting expression plasmid was then transformed into *E. coli* BL21(DE3) cells (Novagen Inc., USA).

To prepare mutants, the EZchange Site-directed Mutagenesis kit (Enzynomics Inc., Republic of Korea) was used to generate point mutations in the SAV0551 recombinant pET-21a(+) plasmid. The point mutations resulted in separate multiple recombinant plasmids, specifically C190A and C190D. The sequences of the reconstructed mutants were confirmed by DNA sequencing (data not shown).

Wild type and SAV0551 mutants (C190A and C190D) cells were grown at 37°C until the OD600 reached 0.6 and expression was induced by the addition of isopropyl-β-D-thiogalactopyranoside (IPTG) to a final concentration of 0.5 mM. After an additional 4 hr of growth at 37°C, cells were harvested by centrifugation and resuspended in 50 mM Tris-HCl, pH 7.5, 0.5 M NaCl and 20 mM imidazole buffer. Cells were lysed by sonication at 4°C and the supernatant was loaded to Ni^{2+}-NTA column (Qiagen; 3 ml of resin per liter of cell culture) previously

equilibrated with the same buffer. The column was washed extensively with wash buffer (50 mM Tris-HCl, pH 7.5, 0.5 M NaCl, and 50 mM imidazole); then the bound protein was eluted with elution buffer (50 mM Tris-HCl, pH 7.5, 0.5 M NaCl, and 500 mM imidazole) until there was no detectable absorbance at 280 nm in the elutant. Fractions containing protein were concentrated to about 2 ml and applied to a Superdex 75 (10/300 GL) column (GE Healthcare Life Sciences, Germany) column that had been equilibrated with the final buffer (50 mM Tris-HCl, pH 7.5 and 0.15 M NaCl). Purified protein was judged to be over 95% pure by SDS-PAGE. The protein solution was concentrated using 10,000 MWCO spin columns (Millipore, USA). The protein concentration was estimated by measuring the absorbance at 280 nm, employing the calculated extinction coefficient of 35,535 $M^{-1}cm^{-1}$.

2.2.2. Crystallization and data collection

Crystallization was performed at 293 K by the hanging-drop vapor diffusion method using 24-well VDX plates (Hampton Research, USA). Initial crystallization conditions were established using screening kits from Hampton Research (Crystal Screens I and II, Index, PEG/Ion, and MembFac) and from Emerald BioSystems (Wizard I, II, III and IV). For the optimal growth of the SAV0551 crystals, each hanging drop was prepared on a siliconized cover slip by mixing 1 µl of protein solution and 1 µl of precipitant solution (23% (w/v) PEG3350, 100 mM BisTris, pH 6.0), and this drop was equilibrated against a 1 ml reservoir of precipitant solution. These conditions yielded needle-shaped crystals for each protein that grew to dimensions of 1.0 × 0.3 × 0.2 mm in two days. All crystals belonged to space group P212121 and contain eight molecules per asymmetric unit.

For crystal freezing, the crystals were transferred to a cryoprotectant solution with 30% (v/v) ethylene glycol in the crystallization condition for several minutes

before being flash-frozen in a stream of nitrogen gas at 100 K. Diffraction data were collected on beam-lines 5C at the Pohang Light Source, South Korea. The raw data were processed and scaled using the HKL2000 program suite [26]. Further data analysis was carried out using the CCP4 suite [27].

2.2.3. Structure determination and refinement

To determine the structure of wild type SAV0551, molecular replacement was used with the program Molrep [28] within the CCP4 suite [27] using the homologous structure of Hsp31 from *V. cholerae* (PDB code 4I4N) as a search model. Refinement of each crystal structure was done through iterative cycles of model building using COOT [29], followed by refinement of the models with Refmac5 [30]. A 5% portion of the data were set aside prior to refinement for the Rfree calculations for each data set [31]. Solvent molecules became apparent in the later stages of refinement and were added into the model. Further refinement was pursued until no further decrease in Rfree was observed. Structural alignments were carried out using the program PyMOL and Chimera [32], which were then used for the construction and generation of all figures. Protein interfaces, surfaces and assemblies were calculated using the PISA server at the European Bioinformatics Institute [33].

2.2.4. Determination of chaperone activity

To monitor the chaperone activity of wild type and the SAV0551 mutants, citrate synthase was employed as a substrate [34, 35]. Initially, to identify chaperone activity, 75 μg of citrate synthase (Sigma-Aldrich Inc., USA) was mixed with a solution of 100 mM Tris-HCl, pH 8.0, 20 mM dithiothreitol (DTT), 6 M guanidine chloride (GnCl). The citrate synthase mixture (75 μg of citrate synthase, 100 mM Tris-HCl, pH 8.0, 6 M GnCl, 20 mM DTT) was incubated for 1 hr at 25°C; consequently, the citrate synthase in this solution was denatured. After incubation,

refolding of citrate synthase was achieved by 100-fold dilution with a solution of 100 mM Tris-HCl (pH 8.0) containing 5 μM wild type and the SAV0551 mutants. The diluted solution was mixed with acetyl-CoA, oxaloacetate, $MnCl_2$ and 5,5'-dithiobis-(2-nitrobenzoic acid) (DTNB) to detect the activity of citrate synthase (100 mM Tris-HCl, pH 8.0, 1 mM DTNB, 0.2 mM $MnCl_2$, 0.4 mM oxaloacetic acid, 0.3 mM acetyl-CoA). After mixing, only the active, refolded enzyme will break acetyl-CoA into the acetyl group and CoA. The CoA reacts with DTNB, which acts as a coloring agent, and this produces a yellow TNB-CoA-SH compound that is detectable at 412 nm using a Multi-Mode microplate reader (SpectraMax M5e, USA). After a 48 min reaction period, the highest specific activity value obtained for TNB-CoA-SH was considered 100% and the lowest was 0%. The calculated specific activities of the wild type and the SAV0551 mutants were expressed as a percentage of this value.

2.2.5. Determination of glutathione independent glyoxalase activity

The glyoxalase activity assay of wild type and the SAV0551 mutants was performed using the methylglyoxal (Sigma, 40% solution). The reaction was initiated by adding enzyme in reaction buffer (100 mM HEPES, pH 7.5, 50 mM KCl, 2 mM DTT) with 6 mM methylglyoxal. The reaction mixture of methylglyoxal and protein (wild type and the SAV0551 mutants) were incubated at 20°C. The final concentration of protein was 10 μM. The remaining methylglyoxal at each time point was determined by reaction with 2,4-dinitrophenylhydrazine (DNPH) to generate the purple chromophore mehtylglyoxal-bis-2,4,-dinitrophenylhydrazone after alkali treatment.

The assay was performed by removing a 50 μl sample of the reaction at fixed time points after enzyme addition (0 sec, 20 sec, 40 sec, 60 sec, 80 sec, 100 sec, and 120 sec) and rapidly mixing with 0.9 ml of distilled water. To this solution, 0.33 ml of a freshly prepared stock of DNPH reagent (0.2% DNPH dissolved in 2 N HCl) was

immediately added and incubated at 37°C for 15 min. This highly acidic solution stops the enzymatic reaction, whose rate was already greatly diminished by the initial 19-fold dilution into water. The purple color of the hydrazine was developed by addition of 1.67 ml of 3.8 M NaOH and incubation for 5-10 min at room temperature followed by measurement of absorbance at 550 nm in a SpectraMax M5e. All measurements were made in triple times.

2.3. Results

2.3.1. Structure of SAV0551

The SAV0551 sample was prepared as a concentration of 10 mg/ml (Figure 3).

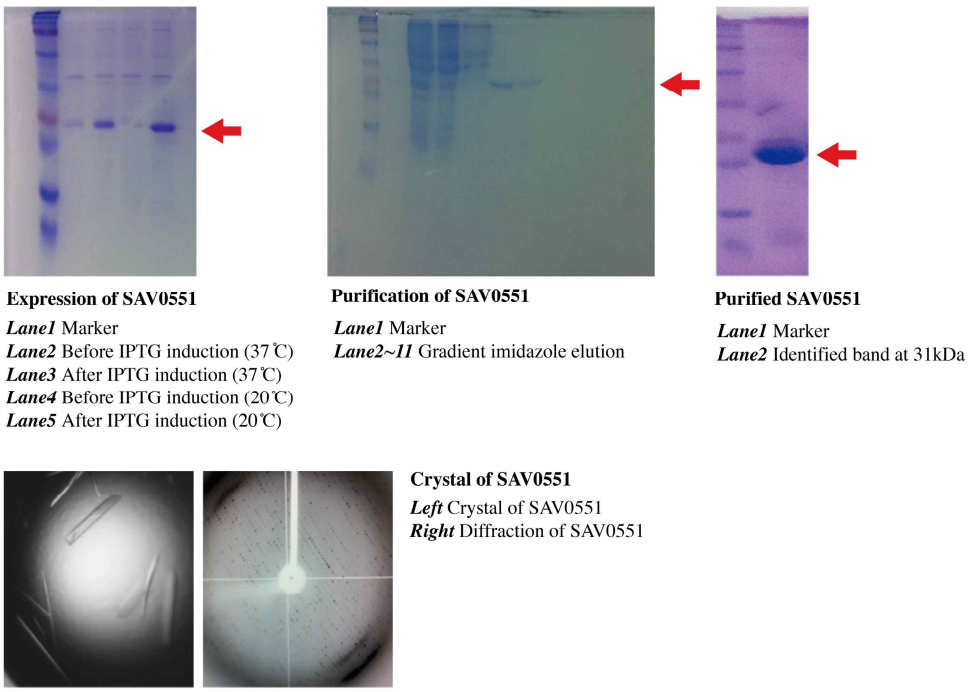

Figure 3. Expression, purification, and crystallization of SAV0551.

SAV0551 sample was prepared to determine the structure and function. The SAV0551 was over expressed by IPTG induction system, and purified using Ni^{2+}-NTA affinity column. Protein purity is measured over 95% based on SDS-PAGE. SAV0551 crystallizes in a condition of 23% (w/v) PEG3350, 100 mM BisTris, pH 6.0. The crystal diffracted to a 2.6 Å of resolution.

SAV0551 crystallizes in a space group P212121, with four dimers in the asymmetric unit. The crystal structure of SAV0551 was determined at 2.6 Å resolution including the additional C-terminal histidine tag. The protein consists of two domains: a core domain whose similarity to DJ-1 superfamily proteins had been expected, and a cap domain, which has also called "P" region. The core domain consists of an α/β sandwich fold with eleven α-helices and eight β-strands. Six β-strands, β4 (residues 93-97), β1 (residues 52-56), β5 (residues 149-154), β6 (residues 183-187), β8 (residues 263-266), and β7 (residues 257-260), are aligned in the center, wherein the latter β7 strand is anti-parallel to the central β-strands. Nine helices surround the core of β-strands. α11 (residues 269-287), α2 (residues 77-89), α3 (residues 108-110), α4 (residues 116-125), α5 (resides 135-142), α6 (residues 158-161), α7 (residues 168-179), α8 (residues 190-196), and α10 (237-243) are around the core in a clockwise direction. In addition, two short α-helices (α1 (resides 135-142) and α9 (resides 135-142)) and two β-strands (β2 (resides 135-142) and β3 (resides 135-142)) form cap domain. These core domain and cap domain are linked via a 22-residue-long-linker (residues 31-51) (Figure 4).

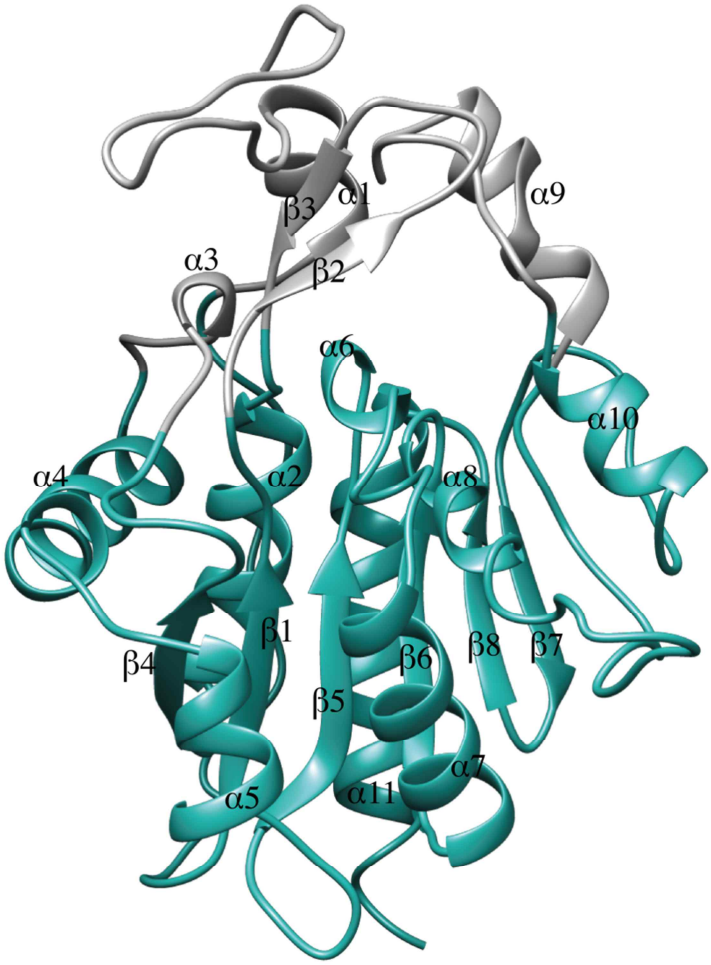

Figure 4. Ribbon diagram of SAV0551.

Ribbon representation of the SAV0551 monomer. Main domain is colored in cyan and additional cap domain is colored in grey. SAV0551 shows a sandwich structure with a α1-β1-β2-β3-α2-β4-α3-α4-β5-α6-α7-β6-α8-α9-α10-β7-β8-α11 topology.

2.3.2. Oligomeric state of SAV0551

The dimer structure of SAV0551 is consistent with the results of size exclusion chromatography indicating an apparent molecular mass of 65 kDa, which is double the size of the monomer. The loops and β-strands from cap domain are responsible

for dimer formation (Figure 5). Each monomer contains catalytic triad consisting of Cys190 and His191 from the core domain and Asp221 from the cap domain. The Cys190 S^{γ} interacts with His191 $N^{\delta 1}$, while the Asp221 carboxylate hydrogen bonds with His191 $N^{\varepsilon 2}$ (Figure 6). This catalytic triad is well conserved in Hsp-type DJ-1 superfamily proteins. In the crystal structure, oxygen atoms are modeled near the S^{γ} atom of Cys190 in chain A, B, D and G. This result is not consistent with the structure of SAV1875, another DJ-1 superfamily protein from the same organism. Although we have identified two oxygen atoms are covalently bound to Cys105 S^{γ} in the crystal structure of two chains in SAV1875 previously, the oxidation state of Cys190 in SAV0551 is not consistent among eight chains. Since this catalytic triad is predicted to have a catalytic function, cysteine mutant C190A was designed. To mimic the oxidized cysteine, C190D mutant was also designed.

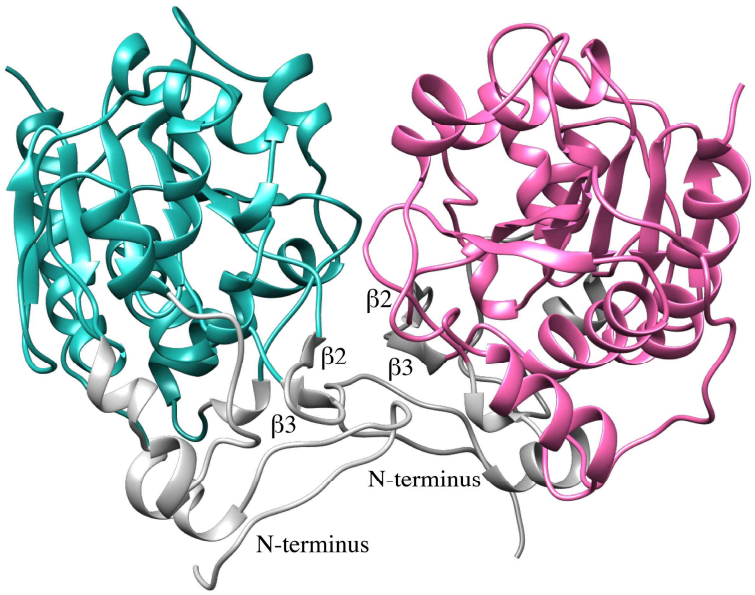

Figure 5. The SAV0551 dimer.

β2, β3, and N-terminus loop of cap domain are mainly involved in dimeric conformation.

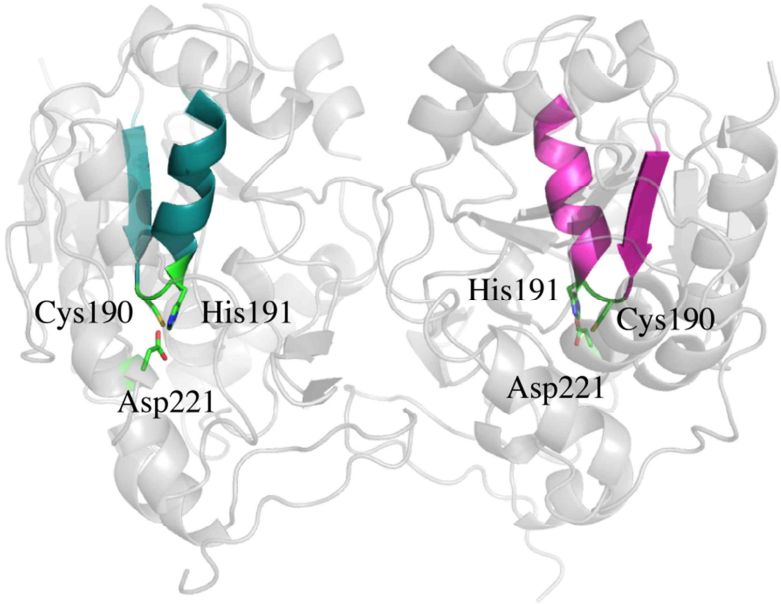

Figure 6. Catalytic triad of SAV0551.

The nucleophilic elbow (strand-nucleophile-helix motif) in each domain is shown in cyan and magenta. The catalytic triad is shown as sticks (Cys190, His191, and Asp221). The catalytic triad is located on the cleft region between main domain and cap domain.

When viewing the surface area, the majority of the surface is negatively charged with the exception of hydrophobic patches. The dimer results in a large concave structure and canyon structure, a hydrophobic bowl that measured ~20 Å in diameter and a canyon ~10 Å in depth. The catalytic triad is exposed toward the solvent accessible area, but the opening is restricted (measured ~6 Å in a diameter) (Figure 7).

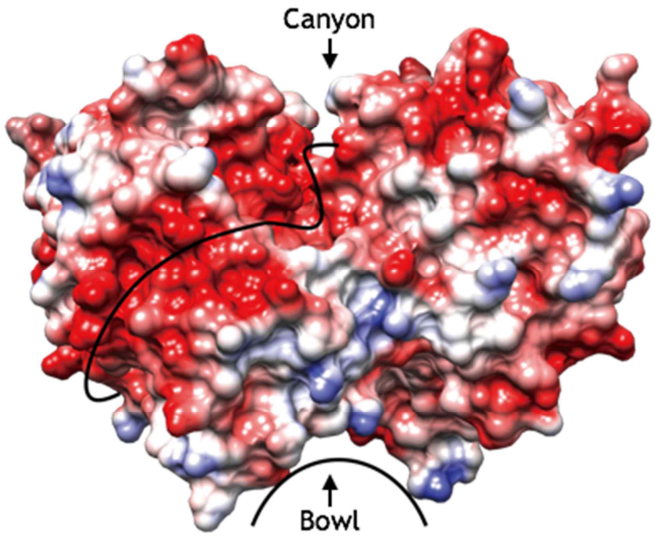

Figure 7. Surface structure of SAV0551.

Potential surface charge of the crystal structure of SAV0551, calculated with Chimera [32], where surfaces are colored between -10 kcal/mol·e (red) and +10 kcal/mole·e (blue). Canyon and bowl are labeled.

2.3.3. Catalytic triad of SAV0551

All the DJ-1 superfamily proteins share the reactive cysteine residue at a sharp turn between a β-strand and an α-helix, a "nucleophilic elbow". Mostly, the cysteine at the nucleophilic elbow forms catalytic triad together with a histidine and an acidic residue. Although the nucleophilic elbow and a cysteine are absolutely conserved in DJ-1 superfamily members, catalytic triad is not strictly conserved. Many of DJ-1-type DJ-1 subfamily proteins dose not contain catalytic triad. DJ-1-type DJ-1 lacks histidine residue next to Cys106, but His126 was found within 5 Å to Cys106, instead, forming catalytic dyad. DJ-1-type YajL lacks histidine residue around reactive cysteine. YhbO-type and Hsp-type DJ-1 subfamily proteins have conserved catalytic triad, but the architecture of the catalytic triad is different.

YhbO-type DJ-1 subfamily has catalytic triad with a cysteine, histidine next to cysteine, and an acidic residue from adjacent subunit. The catalytic triad that was found in Hsp-type DJ-1 subfamily protein consists of cysteine and histidine from the core domain and an acidic residue (Glu/Asp) from cap domain. Furthermore, even though the overall topology is similar, the configuration of the catalytic triad results in an opposite "handedness" between the two subfamilies (Figure 8).

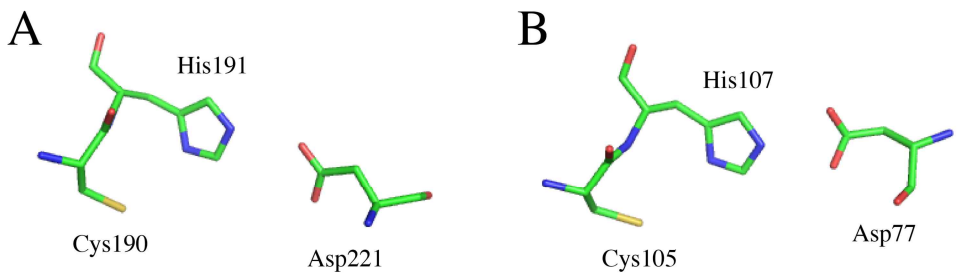

Figure 8. The configuration of catalytic triad.
The configuration of the catalytic triad results in an opposite "handedness".
(A) Catalytic triad in Hsp-type DJ-1 subfamily protein SAV0551. (B) Catalytic triad in YhbO-type DJ-1 subfamily protein SAV1875. This shows an opposite handedness of catalytic triad.

SAV0551 is a Hsp-type DJ-1 subfamily member and it shares the same structural arrangement of catalytic triad as other members of Hsp-type DJ-1 subfamily. Residues 183-196 (α8 and β6) of SAV0551 form the nucleophilic elbow. Cys190 at the nucleophilic acid forms catalytic triad together with His191 and Asp221. One of the dissimilarity in catalytic triad of Hsp31-type proteins is shown for the acidic residue. It can be substituted to glutamate if the origin of Hsp31 protein is yeast. Taken together, the presence of cap domain, the oligomeric interface that is consisted of cap domain loops, and the features of catalytic triad prove SAV0551 is

a member of Hsp-type DJ-1 subfamily [11].

2.3.4. SAV0551 has chaperon activity

Hsp-type DJ-1 subfamily proteins are highly conserved and function as molecular chaperones which facilitate the synthesis and folding of proteins. Under the stress conditions such as heat shock, pH shift, or oxidation, increased expression of chaperone proteins protect cells by stabilizing unfolded proteins, giving cell time to repair or re-synthesize damaged proteins. Molecular chaperones have been divided into three functional subclasses based on their mechanism of action. “Folding” chaperones (DnaK and GroEL) rely on ATP-driven conformational changes to mediate the net refolding of their substrates [36]. “Holding” chaperones (Hsp31, Hsp33, and IbpB) stabilize partially partially folded proteins on their surface and rapidly release them in an active form once the stress has abated. It plays an important role in protecting cells from severe stress condition [37, 38]. The third class of chaperone, “disaggregating” (ClpB) promotes the solubilization of proteins that have been aggregated as a result of stress [39]. Hsp31 proteins are kwon as holdase, a holding molecular chaperone. To hold unfolded substrates, the surface structure of Hsp31 is crucial. Hsp31 from *E.coli*, work as dimers by forming a deep acidic canyon and bowl on their dimeric interface [11]. When the surfaces of Hsp31 from *E. coli* were viewed, hydrophobic patches were detected around the canyon for the binding of unstructured proteins [40]. SAV0551 expresses similar surface patterns of a canyon and bowl as Hsp31 from *E. coli*. SAV0551 has a deep acidic canyon that winds from the dimeric interface to each side of the subunit, and bowl structure is located on the bottom side. The hydrophobic patches are detected around the canyon. This characteristic surface structure is well conserved in other Hsp-type DJ-1 subfamily members. The wild type and the SAV0551 mutants were tested for chaperone activity using citrate synthase. The observed data shows a chaperone-facilitated renaturation of citrate synthase in the wild type and the

SAV0551 mutants. There are no significant differences in the chaperone activity between the wild type and the SAV0551 mutants. From this study, we identified SAV0551 as a chaperone protein from *S. aureus* and that the presence of cysteine is not the key elements for the chaperone function (Figure 9).

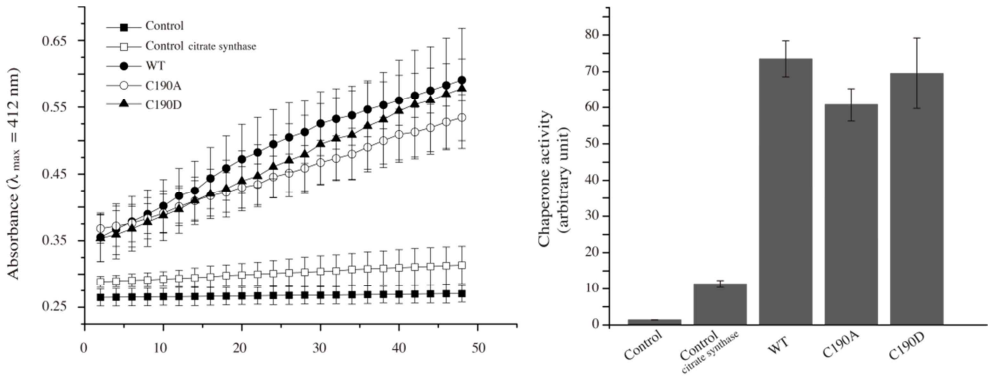

Figure 9. No significant difference in chaperone activity in wild type SAV0551 and the cysteine mutants.

SAV0551 exerts a chaperone function. The chaperone activity was assayed by monitoring an increase in absorbance at 412 nm. (A) The control (■) contained 50 µl of the reaction mixture only, which was 1 mM DTNB, 0.2 mM $MnCl_2$, 0.4 mM oxaloacetic acid, 0.3 mM acetyl-CoA in 100 mM Tris-HCl buffer (pH 8.0). The control with citrate synthase (□) contained an additional 0.75 µg of denatured citrate synthase. A final concentration of 5 µM was used for the wild type (●), C190A (○) and C190D (▲). (B) The calculation of chaperone activity at the 48 minutes time point. The data from three scans were averaged.

2.3.5. SAV0551 has glutathione independent glyoxalase activity

Endogenous methylglyoxal is generated as an unavoidable consequence of glycolysis. It also formed by lipid peroxidation systems, metabolism of acetone,

and the degradation of DNA [41]. Methylglyoxal is a known endogenous and environmental mutagen, which can modify both DNA and proteins. To detoxify methylglyoxal, there is glyoxalase system that converts methylglyoxal to non-toxic D-lactate. The glyoxalase system is accomplished by the sequential action of two thiol-dependent enzymes: glyoxalase I and II in the presence of glutathione (GSH) [42]. Recently, a GSH-independent glyoxalase system of Hsp31 was identified in *E. coli*. In this system, the *E. coli* Hsp31 converts methylglyoxal directly to D-lactate in a single step, independent of GSH [12]. The reactive cysteine and catalytic triad are shown to be responsible for the function, but the detailed mechanism of how Hsp31 executes these functions remains to be determined. To determine the glyoxalase III activity, wild type, the SAV0551 mutants, and SAV1875 were used. SAV1875 is also DJ-1 superfamily protein, which has a catalytic triad and reactive cysteine. The level of methylglyoxal is reduced substantially by the time when it was mixed with wild type SAV0551. However, cysteine mutants C190A and C190D do not show any difference in remaining amount of methylglyoxal. This result indicates that reactive cysteine is crucial for glyoxalase III function. Moreover, SAV1875 shows half of SAV0551's glyoxalase activity (calculated from the amount of remaining methylglyoxal at 100 second time point) (Figure 10). Considering cysteine on catalytic triad is the key component for its action, this result may be due to the local structure of catalytic triad. The surface structure of SAV1875 around catalytic triad is of a great different shape from SAV0551. In the crystal structure of SAV1875, the catalytic triad is exposed to solvent area with about 6 Å in width. On the other hand, the catalytic triad of SAV0551 is positioned deep inside of the surface with narrow opening (3 Å). This structure shows SAV0551 allows only small molecules to access its catalytic triad. Methylglyoxal is a small molecule, which could be a perfect fit inside restricted pocket of SAV0551 (Figure 11). From this study, we can figure out not only just presence of catalytic triad, but the approach to catalytic triad is important for its glyoxalase

function.

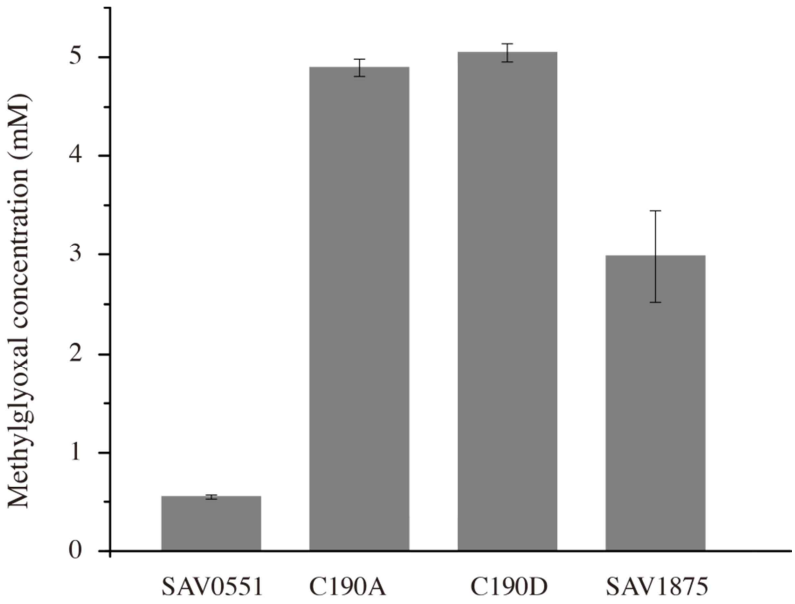

Figure 10. Remaining amount of methylglyoxal at 100 sec of time point.

SAV0551 exerts glyoxalase activity. It degrades methylglyoxal. 6 mM methylglyoxal was used initially. The remaining amount of methylglyoxal at 100 second time point is indicated as a graph.

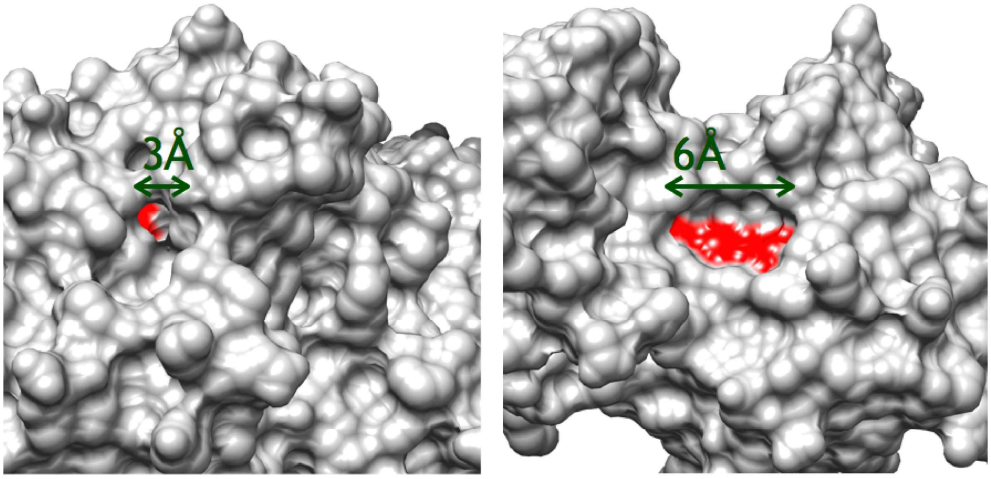

Figure 11. Narrow active site cleft of SAV0551.

The narrow opening of active site is selective for small substrate such as methylglyoxal.

2.4. Discussion

Chaperone is a class of proteins that assist folding or assemble of other macromolecular structures. Chaperones assist folding of newly synthesized proteins, repairing misfolded proteins, and eliminating aggregated proteins. Hsp31, holding chaperone, is known to repair misfolded protein by holding unfolded protein on its surface area. This chaperone function becomes more crucial when the cells are exposed to a harsh condition, such as heat, radiation, and oxidative stress. Chaperones help misfolded proteins, which are damaged by various stresses, to retrieve their normal biological function. Heat shock proteins are expressed when cells are under stress conditions. The structural studies herein confirmed SAV0551 as a member of the Hsp-type DJ-1 superfamily and is has all the pertinent traits of

this group, including the shape of dimerization interface using cap domain and the architecture of catalytic triad. For the interaction of unfolded proteins, hydrophobic bowl, a deep canyon, and hydrophobic patches are known as important characteristics of *E. coli* Hsp31. Similar to Hsp31 of *E. coli*, the quaternary structure of SAV0551 has analogous features. The dimer structure contains about 20 Å width hydrophobic bowl and a deep acidic canyon that winds from one subunit to another. The highly conserved hydrophobic patches are also detected on the surface of SAV0551. Because the Hsp-type DJ-1 superfamily members are well-known as Hsp31, holding chaperone, SAV0551 is also predicted to perform similar biological function. We discovered that the wild type and cysteine mutants of SAV0551 assisted in the folding of citrate synthase regardless of the presence of cysteine. Further detailed studies on diverse substrates and *in vivo* tests are needed to verify the exact mechanism of the SAV0551 chaperone activity.

A recent report indicates that Hsp31 displays glyoxalase III function, a GSH-independent glyoxalase. Accumulation of methylglyoxal, also called dicarbonyl stress, causes endogenous damage by reacting with proteins and DNA. DNA modification results in frameshift mutations and proteins modification is often directed to functional sites. Hsp31 protects cell against methylglyoxal toxicity. Glyoxalase activity was detected in wild type SAV0551, and SAV1875 shows less than half of SAV0551's activity, while cysteine mutants of SAV0551 did not. As predicted, cysteine is revealed as a key residue for the glyoxalase activity. Moreover, compared to the catalytic triad of SAV1875, which has a similar overall structure with SAV0551, the catalytic triad in SAV0551 is more occluded by neighboring α-helices. This may be responsible for the substrate affinity. Small molecules such as methylglyoxal would have high selectivity for active site of SAV0551.

Altogether, the crystal structure of Hsp-type DJ-1 subfamily protein SAV0551 was determined. It shows an activity of chaperone through its surface structure and

glyoxalase III through catalytic triad, which are crucial functions for stress response system of a damaged cell.

Chapter III. The structural and functional study of SAV1875

3.1. Introduction

From the sequence homology among YhbO-type DJ-1 subfamily members, SAV1875 is predicted to be classified into YhbO-type DJ-1 subfamily: YhbO (49% sequence identity), *Ph*pI (42% sequence identity), DR1199 (40% sequence identity), Ton1285 (39% sequence identity), and DJ-1 (29% sequence identity). A structure-based sequence alignment was acquired using the ClustalW web server tool [43] and viewed using the ESPript web server tool [25]. The sequence alignment of YhbO, *Ph*pI, DR1199, Ton1285 and DJ-1 is shown in Figure 12. SAV1875 is an uncharacterized protein coding 171 amino acids. The estimated molecular weight is 19 kDa and calculated pI is 4.59.

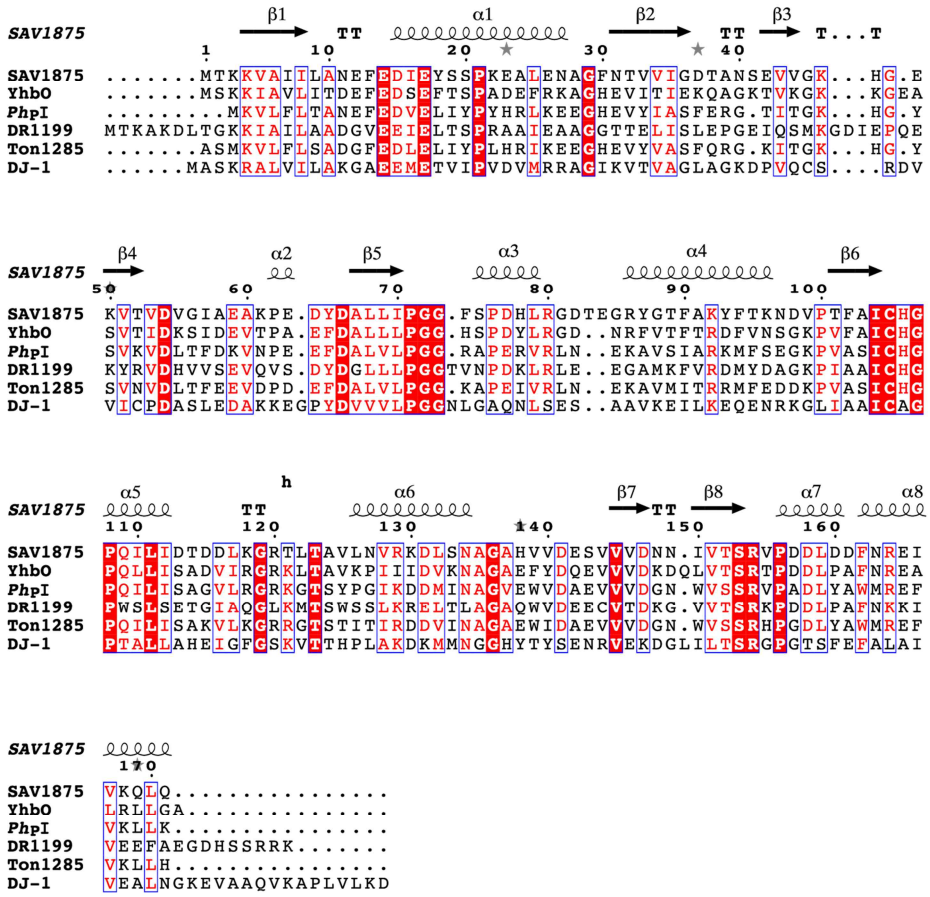

Figure 12. Comparison of SAV1875 to other members of DJ-1/ThiJ/*Pf*pI superfamily.

Sequence alignment of SAV1875 with YhbO (49% sequence identity), *Ph*pI (42% sequence identity), DR1199 (40% sequence identity), Ton1285 (39% of sequence identity) and DJ-1 (29% sequence identity) proteins. Identical residues are colored white on a red background and similar residues are red on a white background. Secondary structure elements (springs, α-helices; arrows, β-strands) are represented above the sequences and are numbered. The figure was constructed using ESPript [25].

3.2. Materials and Methods

3.2.1. Cloning, protein expression, and purification

The ORF encoding SAV1875 was amplified from *S. aureus* Mu50 genomic DNA by PCR using 5'-GACTGCATATGACTAAAAAAGTAGCAATTATTC as the forward primer and 5'-GTACACTCGAGTTGTAATTGTTTAACGATTTCT as the reverse primer. The NdeI and XhoI restriction sites are underlined and were used for cloning into the pET-21a(+) vector (Novagen Inc., USA). The resulting construct has eight additional residues (LEHHHHHH) that encode a C-terminal hexa-histidine tag. For removal of hexa-histidine tag, SAV1875 gene is inserted into a pET-28a(+) (Novagen Inc., USA) vector. The resulting construct in pET-28a(+) comprised residues 1-171 with an additional 20 residues (MGSSHHHHHHSSGLVPRGSH) containing thrombin cleavage site. The sequence of the cloned gene was confirmed by DNA sequencing (data not shown).

To prepare mutants, the EZchange Site-directed Mutagenesis kit (Enzynomics Inc., Republic of Korea) was used to generate point mutations in the SAV1875 recombinant pET-21a(+) plasmid. SAV1875 gene was amplified from recombinant plasmid DNA with the following primer pairs (Table 2).

Mutants	Primer sequence	
E17D	Forward	5'GCAAACGAATTTGAAGATATAGATTATTCAAGTCCTAAAG AGGC-3'
	Reverse	3'GCCTCTTTAGGACTTGAATAATCTATATCTTCAAATTCTGC-5'
E17N	Forward	5'-GCAAACGAATTTGAAGATATAAACTATTCAAGTCCTAAAGA GGC-3'

	Reverse	3'-GCCTCTTTAGGACTTGAATAGTTTATATCTTCAAATTCGTTTGC-5'
C105D	Forward	5'-GATGTACCAACATTTGCCATTGATCATGGGCCACAAATACTAATAG-3'
	Reverse	3'-CTATTAGTATTTGTGGCCCATGATCAATGGCAAATGTTGGTACATC-5'

Table 2. Primer design of SAV1875 mutants.

After digestion of the methylated and non mutated parental DNA template with DpnI, the circular dsDNA was transformed to competent cell. The point mutations resulted in separate multiple recombinant plasmids, specifically E17D, E17N, and C105D. The sequence of the cloned gene were confirmed by DNA sequencing (not shown).

Wild type and SAV1875 mutants (E17D, E17N, and C105D) in pET-21a(+) were overexpressed in *E. coli* BL21(DE3) cells (Novagen Inc., USA) and grown at 37°C in Luria-Bertani (LB) medium supplemented with ampicillin (50 μg/ml) until the OD600 reached 0.5. Recombinant protein expression was induced by the addition of 0.5 mM isopropyl β-D-1-thiogalactopyranoside (IPTG), and the cells were allowed to grow for an additional 4 hr at 37°C. The cells were harvested by centrifugation at 4°C. The cell pellet was resuspended in lysis buffer (50 mM Tris-HCl, pH 7.5, 500 mM NaCl) and disrupted at 4°C using an Ultrasonic processor (Cole Parmer, USA). The cell lysate was centrifuged at 18,000 rpm for 1 hr at 4°C. The cleared supernatant was purified by binding to a Ni^{2+}-NTA affinity column (Qiagen, USA; 3 ml of resin per liter of cell lysate) and eluted with binding buffer

containing 100 mM imidazole. Further purification and buffer exchange were achieved by size exclusion chromatography using a Superdex 75 (10/300 GL) column (GE Healthcare Life Sciences, Germany) that was previously equilibrated with buffer (50 mM Tris-HCl, pH 7.5, 200 mM NaCl). The purities of the hexa-histidine tagged wild type and SAV1875 mutants were estimated to be over 95% by SDS-PAGE. The purified proteins were concentrated to 10 mg/ml by ultrafiltration in 10,000 MWCO spin columns (Millipore, USA). The absorbance at 280 nm was measured, and the calculated extinction coefficient of 5960 $M^{-1}cm^{-1}$ was employed to determine the protein concentration.

3.2.2. Crystallization and data collection

Crystallization was performed at 293 K by the hanging-drop vapor diffusion method using 24-well VDX plates (Hampton Research, USA). Initial crystallization conditions were established using screening kits from Hampton Research (Crystal Screens I and II, Index, PEG/Ion, and MembFac) and from Emerald BioSystems (Wizard I, II, III and IV). For the optimal growth of the SAV1875 crystals, each hanging drop was prepared on a siliconized cover slip by mixing 1 μl of protein solution and 1 μl of precipitant solution (29% (w/v) PEG MME 2000, 100 mM BisTris, pH 6.5), and this drop was equilibrated against a 1 ml reservoir of precipitant solution. The SAV1875 mutants (E17D, E17N, and C105D), and over-oxidized SAV1875 crystals were prepared in the same manner but with different precipitant solutions: for E17D, 44% (w/v) PPG400, 100 mM BisTris, pH 6.0; for E17N, 47.5% (w/v) PPG400, 0.2 M guanidine hydrochloride, 100 mM BisTris, pH 6.0; for C105D, 37.5% (w/v) PPG400, 100 mM BisTris, pH 6.0; and for over-oxidized SAV1875, 47.5% (w/v) PPG400, 100 mM BisTris, pH 5.5. These conditions yielded needle-shaped crystals for each protein that grew to dimensions of 1.0 × 0.4 × 0.4 mm in three days. All crystals belonged to space group P21212 and contain two molecules per asymmetric unit.

For crystal freezing, the crystals were transferred to a cryoprotectant solution with 30% (v/v) glycerol in the crystallization condition for several minutes before being flash-frozen in a stream of nitrogen gas at 100 K. Diffraction data were collected on beam-lines 6C and 5C at the Pohang Light Source, South Korea and BL-17A at the Photon factory, Japan. The raw data were processed and scaled using the HKL2000 program suite [26]. Further data analysis was carried out using the CCP4 suite [27].

3.2.3. PAGE

SDS-PAGE was conducted according to the Laemmli method [44] using a 12% (w/v) polyacrylamide gel. The samples were treated with 1% (w/v) SDS and 5% (v/v) 2-mercaptoethanol at 100°C for 5 min before electrophoresis in a vertical Mini Gel system (Bio-Rad Laboratories, Republic of Korea). The proteins were stained with Coomassie Brilliant Blue R250 (Thermo Scientific, USA). Additionally, for the separation of SAV1875 depending on the charge-to-mass ratio between oxidized and reduced state, native PAGE was performed, and analysis was conducted using a 10% (w/v) polyacrylamide gel with neither SDS nor 2-mercaptoethanol. Native PAGE was performed in a buffer (25 mM Tris-HCl, pH 8.3, 192 mM glycine). The staining was performed as described above for SDS-PAGE.

3.2.4. Mass spectrometry

Mass analyses were performed on a nano-HPLC system (Dionex Ultimate 3000 RSLCnano System, Thermo Scientific, USA) coupled with a hybrid quadrupole-obitrap mass spectrometer (Q-Exactive, Thermo Scientific, USA) at the NICEM (National Instrumentation Center for Environmental Management, Seoul National University, Seoul, Republic of Korea). Protein samples (10 μl) were loaded onto a C8 reverse phase column (INNO5, Young Jin Biochrom., Republic of Korea). A

HPLC was used for room temperature gradient elution at a flow rate of 150 µl/min by using a linear gradient from 0.1% (v/v) formic acid in water (Solvent A) to 0.1% (v/v) formic acid in acetonitrile (Solvent B). The total run time for each sample was 20 min. The molecular mass of protein was generated from several multiply charged peaks using the Xcalibur 2.2 Software (Thermo Scientific, USA).

3.2.5. Protein oxidation

For the complete oxidation of cysteine, the wild type and SAV1875 mutants at 20 mg/ml (1 mM) were incubated for 30 min at room temperature in H_2O_2 (Sigma-Aldrich Inc., USA) with a molar ratio of protein: H_2O_2 of 1:50. After treatment, excess H_2O_2 was removed by extensive dialysis with buffer (50 mM Tris-HCl, pH 7.5). The control consisted of the same protein with H_2O, which was incubated under the same conditions. The oxidation states of Cys105 were determined by mass spectrometry and native PAGE.

3.2.6. Circular Dichroism (CD)

Circular dichroism (CD) spectra were collected with a Chirascan Series spectrometer equipped with a temperature controller (Applied Photophysics, UK). The protein samples were prepared in a buffer (50 mM Tris-HCl, pH 7.5, 200 mM NaCl). The CD Spectra were recorded with a step size of 1.0 nm, a bandwidth of 1 nm and an averaging time of 2.0 sec. Measurements were performed in a 1 mm path length quartz SUPRASIL cell (Hemlla, Germany) using a 10 µM concentration of proteins at room temperature. Three scans were applied continuously and the data were averaged. CD spectra were smoothed and processed after blank subtraction using Pro-Data Viewer software (Applied Photophysics, UK). Furthermore, the secondary structure was analyzed using the K2D3 software (data not shown) [45]. The change in molar ellipticity [θ] was calculated using the following equation [46], where θ is in degrees, length (l) is in millimeters and C is

the molar concentration of protein:

$$[\theta] = \theta / (l \times C \times \text{number of residues})$$

3.2.7. Protease activity assay and zymogram

The protease activity assay of wild type, the SAV1875 mutants, and over-oxidized SAV1875 was performed using the MGT protease assay kit (Marker Gene Technologies, Inc., USA). Fluorescein isothiocyanate (FITC)-labeled casein was cleaved into smaller fragments and highly fluorescent-labeled peptides were released [47]. Fluorescence increase is proportional to protease activity, and this fluorescence was measured in a continuous assay format using a Multi-Mode microplate reader (SpectraMax M5e, USA) with excitation and emission wavelength of 485 and 528 nm, respectively. The FITC-casein was diluted to 1 mg/ml with reaction buffer (100 mM sodium phosphate, pH 7.6, 150 mM NaCl). By mixing FITC-casein with a gradient of protein concentrations (final protein concentration from 1 μM to 15 μM, separately), the protease activity was monitored. The proteins were diluted into the reaction buffer immediately before conducting the test. The mixture of FITC-casein and protein (wild type, the SAV1875 mutants and over-oxidized SAV1875) were sealed and incubated for 2 hr at 37 °C under protection from UV light.

For zymogram analysis, 0.1% (v/v) gelatin copolymerized with the acrylamide gels were used. Electrophoresis was performed at 4 °C at a constant voltage of 100 V. The gels were washed in 2.5% (w/v) Triton X-100 solution at room temperature for 40 min. Following washing, gels were incubated for 20 hr at 37°C in a buffer (50 mM Tris-HCl, pH 8.0, 5 mM $CaCl_2$, 0.02% NaN_3) for proteolytic activity. Staining with Coomassie Brilliant Blue shows the proteolytically cleaved sites as a clear band on a dark background [48].

3.2.8. Determination of chaperone activity

To monitor the chaperone activity of wild type, the SAV1875 mutants and over-oxidized SAV1875, citrate synthase was employed as a substrate [34, 35]. Initially, to identify chaperone activity, 75 μg of citrate synthase (Sigma-Aldrich Inc., USA) was mixed with a solution of 100 mM Tris-HCl, pH 8.0, 20 mM dithiothreitol (DTT), 6 M guanidine chloride (GnCl). The citrate synthase mixture (75 μg of citrate synthase, 100 mM Tris-HCl, pH 8.0, 6 M GnCl, 20 mM DTT) was incubated for 1 hr at 25°C; consequently, the citrate synthase in this solution was denatured. After incubation, refolding of citrate synthase was achieved by 100-fold dilution with a solution of 100 mM Tris-HCl (pH 8.0) containing 5 μM wild type, the SAV1875 mutants or over-oxidized SAV1875. The diluted solution was mixed with acetyl-CoA, oxaloacetate, $MnCl_2$ and 5,5'-dithiobis-(2-nitrobenzoic acid) (DTNB) to detect the activity of citrate synthase (100 mM Tris-HCl, pH 8.0, 1 mM DTNB, 0.2 mM $MnCl_2$, 0.4 mM oxaloacetic acid, 0.3 mM acetyl-CoA). After mixing, only the active, refolded enzyme will break acetyl-CoA into the acetyl group and CoA. The CoA reacts with DTNB, which acts as a coloring agent, and this produces a yellow TNB-CoA-SH compound that is detectable at 412 nm using a Multi-Mode microplate reader (SpectraMax M5e, USA) [49]. After a 70 min reaction period, the highest specific activity value obtained for TNB-CoA-SH was considered 100% and the lowest was 0%. The calculated specific activities of the wild type, the SAV1875 mutants, and over-oxidized SAV1875 were expressed as a percentage of this value.

3. 3. Results

3.3.1. Structure of SAV1875

The SAV0551 sample was prepared as a concentration of 10 mg/ml (Figure 13).

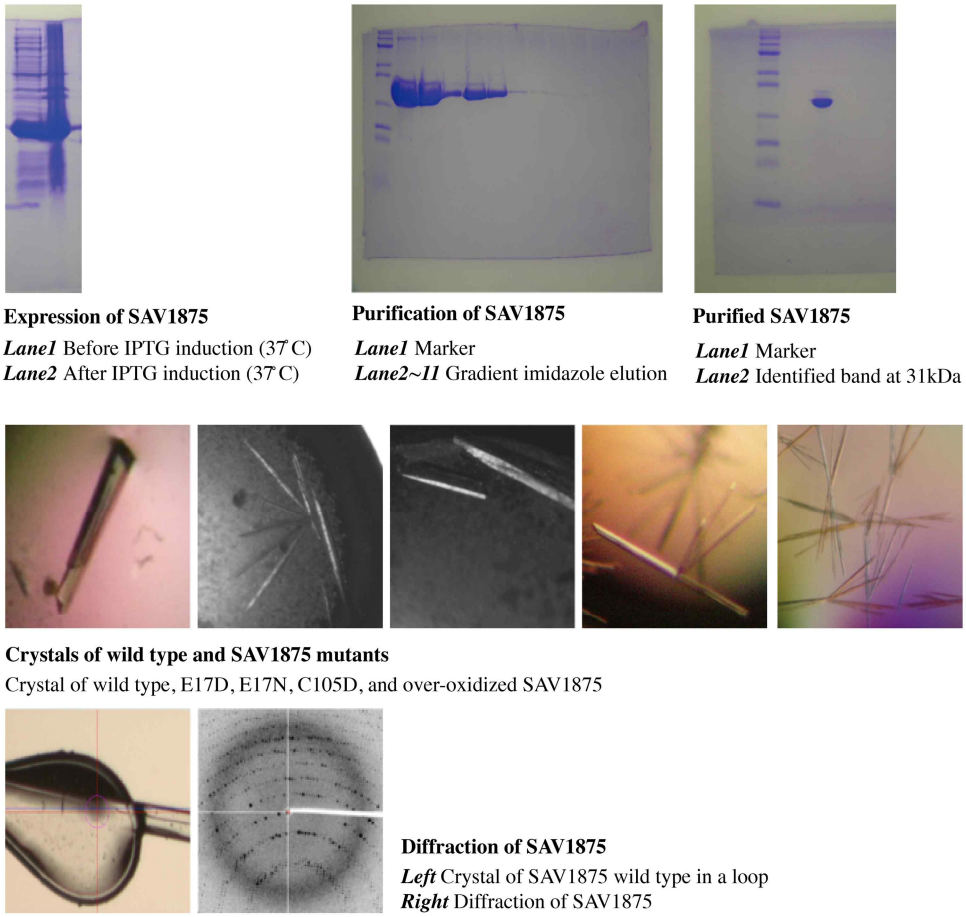

Figure 13. Expression, purification, and crystallization of SAV1875.

Wild type and mutants SAV1875 samples were prepared to determine the structure and function. The wild type and mutants SAV1875 were over expressed by IPTG induction system, and purified using Ni^{2+}-NTA affinity column. Protein purity is measured over 95% based on SDS-PAGE. SAV1875 wild type crystallizes in a condition of 29% (w/v) PEG MME 2000, 100 mM BisTris, pH 6.5. The crystal diffracted to a 1.8 Å of resolution.

The 2.1 Å crystal structure of SAV1875 has clear electron density for 171 amino

acids including the additional C-terminal tag and lacks the methionine residue at position 1. The protein consists of an α/β sandwich fold with eight α-helices and eight β-strands. Six β-strands, β2 (residues 31-35), β1 (residues 4-8), β5 (residues 67-70), β6 (residues 101-104), β8 (residues 150-153), and β7 (residues 145-147), are aligned in the center, wherein the latter β7 strand is anti-parallel to the central β-strands. Eight α-helices surround the core of β-strands. Both sides of the β-strands are covered with α-helices (α1 (residues 15-27), α7 (residues 156-158), and α8 (residues 160-171) are located on one side and α2 (residues 62-64), α3 (residues 75-81), α4 (residues 86-96), α5 (residues 107-113), and α6 (residues 126-134) are on the other side). Additionally, anti-parallel strands β3 (residues 42-44) and β4 (residues 50-52) are located on top of the sandwich structure (Figure 14).

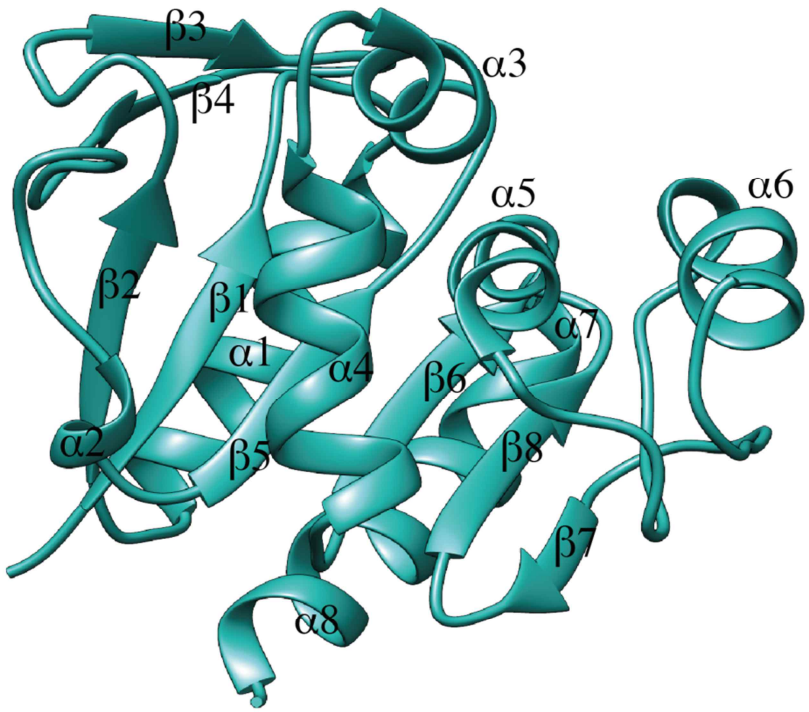

Figure 14. Ribbon diagram of SAV1875.

Ribbon representation of the SAV1875 monomer.

3.3.2. Oligomeric state of SAV1875

The crystal structure revealed that SAV1875 exists as a compact homodimer with an interface that buries about 828 $Å^2$ per subunit (12.3% of the subunit surface). The dimer involves contacts between three helices (α3, α5, and α6) on each monomer (Figure 15). On its dimeric interface, there are 3 salt bridge pairs between Asp77 and His106, Asp115 and Lys130, and Asp131 and Arg80. Numerous hydrophobic residues are also found in the dimeric interface, including Gly73, Phe74, His78, Gly81, Ile112, Leu126, Val128, and Leu132. On the basis of its quaternary structure, SAV1875 was classified as a new member of YhbO-type subfamily.

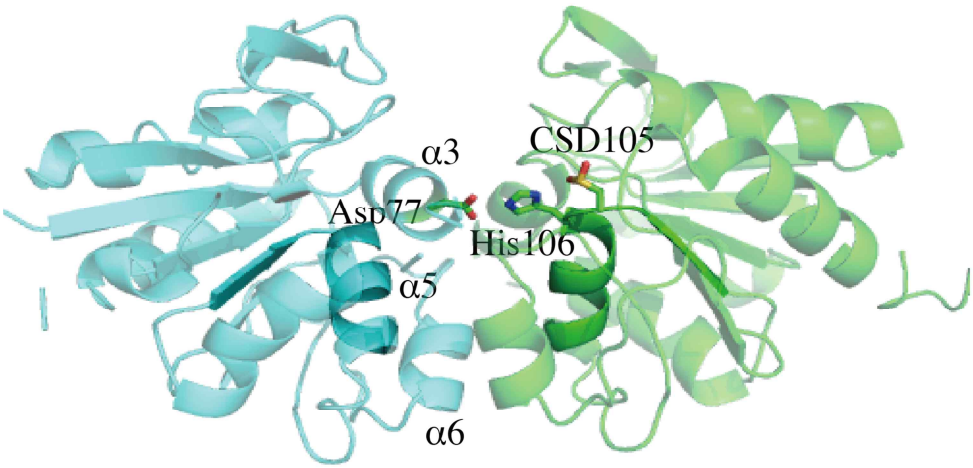

Figure 15. Dimer structure of SAV1875.

The SAV1875 dimer is shown in a ribbon representation from side view. Chain A is colored in cyan and chain B is in green. Three helices (α3, α5, and α6) are involved in dimeric interface. The nucleophilic elbow (strand-nucleophile-helix motif) in each domain is shown in darker color. Cysteine is positioned in the turn of the

nucleophilic elbow, and the catalytic triad is shown as sticks (CSD105, His106, and Asp77 from the adjacent monomer). The oxidized Cys105 is denoted as CSD105.

The dimer crystal structure of SAV1875 is consistent with the results of size exclusion chromatography, which indicates a dimeric state of SAV1875 with an apparent molecular mass of 39 kDa in solution. However, the YhbO-type dimer proteins can form a ring-like hexamer in solution by trimerization. With the exception of DR1199, which has a long protruded loop toward the center, other YhbO-type proteins, including *Ph*pI, YhbO, and Ton1285, can exist as hexamers in a solution [18, 50]. Because an additional terminal amino acid extension alters the oligomerization modes of YhbO, we prepared a variant of SAV1875, a histidine-tag removed SAV1875. Both forms of histidine-tagged and tag-removed SAV1875 proteins form only dimers in a solution. This may be because of the wider dimerization mode of the two subunits in SAV1875 compared with *Ph*pI. If SAV1875 were to make the same trimerization as *Ph*pI, the helices and loops, which form DJ-1-type dimeric interface, would sterically inhibit each other (Figure 16).

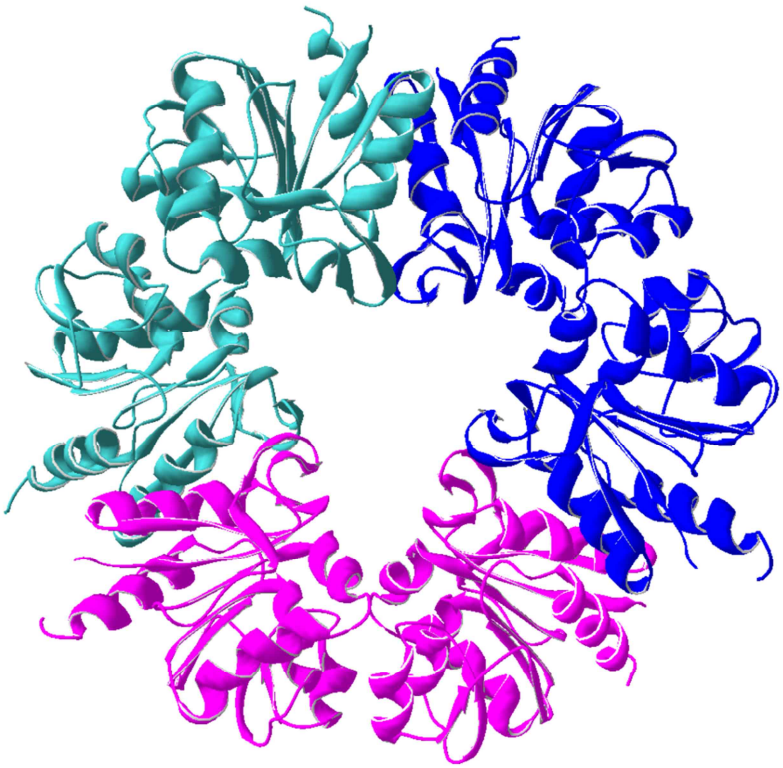

Figure 16. Ribbon diagram of constrained hexamer SAV1875.

If SAV1875 makes the same hexamerization, helices and loop would crash each other. This is because of the wide dimerization mode of two subunits in SAV1875.

When viewing the surface area, the electrostatic distribution of SAV1875 reveals several characteristics. The majority of the surface is negatively charged with several exceptions that indicate hydrophobic patches on the surface area which are dominated by Ile16, Ala28, Gly29, Ala39, Val44, His47, Gly48, Ala58, His78, Gly85, Gly119, Leu126, Arg129, His138, Val146, Ala148, and Pro156. The dimeric interface of SAV1875 shows a deep canyon and this spans over the dimer (Figure 17). These characteristics are similar to those of Hsp31 [11], known chaperone proteins in the DJ-1 superfamily. Therefore, these findings suggest that SAV1875 may function as a chaperone.

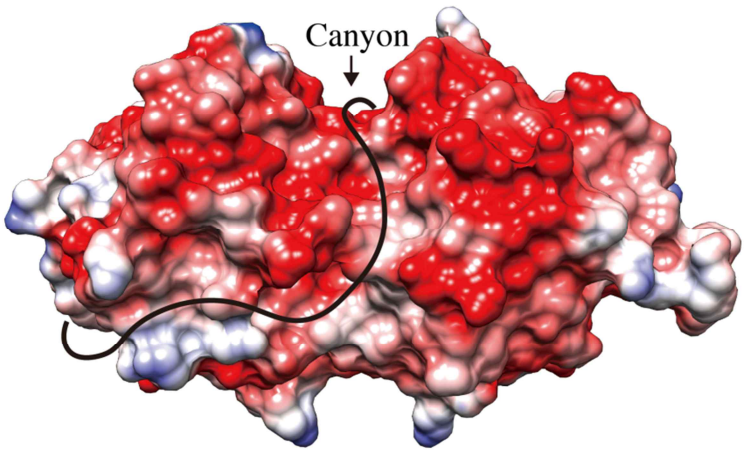

Figure 17. Surface structure of SAV1875.

Potential surface charge of the crystal structure of SAV1875, calculated with Chimera [32], where surfaces are colored between -10 kcal/mol•e (red) and +10 kcal/mole•e (blue). Most of the surface is negatively charged. Canyon is labeled.

3.3.3. Comparison of SAV1875 with DJ-1 superfamily proteins

The overall fold of SAV1875 shows structural similarity to other members of DJ-1 superfamily proteins, as predicted by sequence homology. The superposition of SAV1875 with the structures of YhbO, *Ph*pI, DR1199, Ton1285, and DJ-1 are shown in Figure 18.

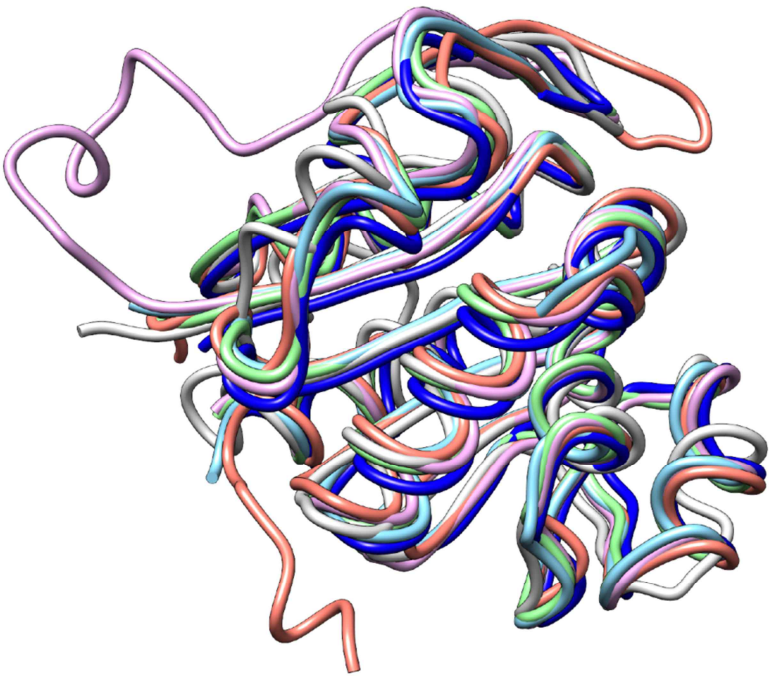

Figure 18. The superposition of SAV1875 (cyan) with other members of the DJ-1/ThiJ/*Pf*pI superfamily YhbO (pink), *Ph*pI (blue), DR1199 (orange), Ton1285 (green), and DJ-1 (Grey).

The overall fold of the core domain of SAV1875 is similar to other members of the DJ-1/ThiJ/*Pf*pI superfamily.

In addition to the similarity of the overall fold within the DJ-1 superfamily proteins, all the DJ-1 superfamily proteins share the reactive cysteine residue at a sharp turn between a β-strand and α-helix. This strand-nucleophile-helix motif is defined as a "nucleophilic elbow". Residues 101-113 (α5 and β6) of SAV1875 form the nucleophilic elbow. Cys105 lies at the sharp turn between the α5 helix and the β6 strand (Figure 15). In nearly all the DJ-1 superfamily proteins, except the DJ-1-type subfamily, the cysteine forms a catalytic triad with a neighboring histidine and an acidic residue. However, the structural features of the catalytic triad vary between the different DJ-1 subfamilies. The YhbO-type proteins constitute a

catalytic triad with cysteine, the histidine next to cysteine, and an acidic residue from the other subunit [14, 16]. The Hsp-type proteins form a catalytic triad using cysteine, the histidine next to cysteine, and an acidic residue from an intrasubunit from the other domain (cap domain) [11, 51].

The catalytic triad that was found in SAV1875 consists of Cys105, His106, and Asp77 (from the adjacent monomer) and was located in its dimeric interface, specifically on the depressed area (Figure 15). The catalytic triad shares the same handedness with the YhbO-type proteins. Cys105 interacts with N^{δ} His106, and Asp77 interacts with N^{ε} of His106. However, Cys105 is oxidized to Cys105-SO_2H in the crystal structure of SAV1875 and is denoted as CSD105. Similar results were previously observed in the homologous cysteine residues from the DJ-1 superfamily proteins, in which the involved cysteine residue was very sensitive to oxidation, forming either Cys-SOH or Cys-SO_2H. In the crystal structure of DJ-1 (DJ-1-type), the cysteine is oxidized to Cys-SO_2H. YajL (DJ-1-type) exhibits both Cys-SOH and Cys-SO_2H modification on each subunit. The crystal structure of DR1199 (YhbO-type) shows a Cys-SOH modification, and the cysteine in YDR533Cp (Hsp-type) exists as Cys-SO_2H [16, 51-53]. These oxidized cysteines are stabilized by specific surrounding residues near the cysteine, including an acidic residue which is analogous to Glu17 in SAV1875.

3.3.4. Stabilization of oxidized Cys105

The cysteine residue at the nucleophilic elbow is absolutely conserved in the DJ-1 superfamily proteins, and is considered a critical residue for their catalytic function [54]. In addition to the cysteine, another highly conserved acidic residue in the DJ-1 superfamily is glutamate, which donates hydrogen bonds to the oxidized cysteine. A hydrogen bond is formed between and electronegative atom (the hydrogen acceptor) and a hydrogen atom that attaches with another electronegative atom (the hydrogen donor) (Figure 19). The hydrogen atom in a hydrogen bond is shared by

two electronegative atoms such as oxygen and nitrogen. The hydrogen bond plays very important roles in protein structure because it stabilizes the tertiary and quaternary structure. In protein structure, the most usual cases of hydrogen bond are between two alcohols, an alcohol and an acid, two acids, or and alcohol and an amine or amide.

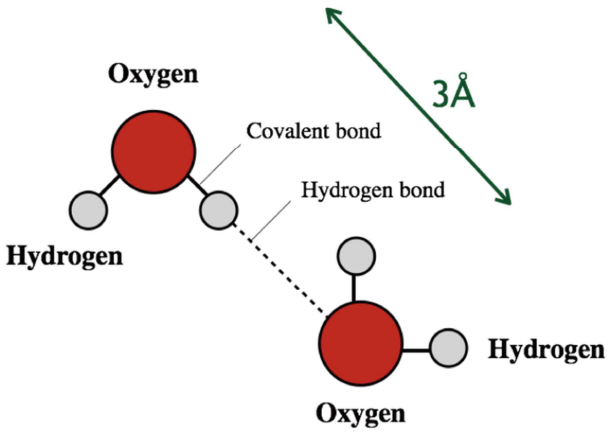

Figure 19. A hydrogen bond.

A single hydrogen atom bound to a electronegative oxygen atoms. The mean donor-acceptor distance in protein is about 3.0 Å.

SAV1875 has a conserved acidic glutamate residue at residue 17. In the crystal structure of SAV1875, oxidized Cys105 acts as another acidic residue and makes hydrogen bonds with Glu17 (2.71 Å), His106 (2.69 Å), and the Gly73/His106 amide pocket (3.02 Å and 2.96 Å, respectively; Figure 21A). Considering the mean donor-acceptor distance in protein is close to 3.0 Å, these hydrogen bonds are responsible for stabilization of oxidized Cys105. Because the O^{δ} of oxidized Cys105 and the O^{ε} of Glu17 form hydrogen bonds, we speculated that a glutamate substitution at position 17 would alter the cysteine oxidation status without disturbing the catalytic triad. Thus, aspartate and asparagine mutants (E17D and E17N, respectively) were designed because these amino acids have shorter carbon chains (one carbon) than glutamate. In particular, asparagine is the amide of

aspartate, which does not carry a formal charge under biologically relevant pH conditions. Cys105 was mutated to aspartate, which mimics Cys-SO_2H, to generate the solely oxidized form of SAV1875. The crystal structure of each mutant was identified and showed distinct differences in their cysteine oxidation states (Figure 20). In the crystal structure of wild type and E17D SAV1875, Cys105 is oxidized to Cys105-SO_2H, and Cys-SOH is observed in E17N SAV1875. In the crystal structure of E17D, the hydrogen bond between oxidized Cys105 and Asp17 is retained, showing a distance of 2.81 Å (Figure 21B). The E17N crystal structure showed a disruption of the hydrogen bonds between Cys105 and Asn17 (Figure 21C). However, the oxidized cysteines of the SAV1875 mutants still maintain hydrogen bonds with His106 and with the Gly73/His106 amide pocket.

These results are not consistent with a similar study on the DJ-1 protein [52, 55]. To stabilize the oxidation state of Cys106 in the DJ-1 protein, Glu18 and the Gly75/Ala107 amide pocket are required. In the crystal structures, Cys106 of the DJ-1 E18N mutant is oxidized to Cys106-SO_2H, and Cys106 of DJ-1 E18D mutant is modified to Cys106-SOH, which indicates minor oxidation toward the Gly75/Ala107 amide pocket (Figure 21). The opposite behavior was observed in the SAV1875 mutants and is due to the local structural difference around Cys105. In detail, Gly73 and His106 are shown to form an amide pocket as Gly75/Ala107 in DJ-1 (Figure 22).

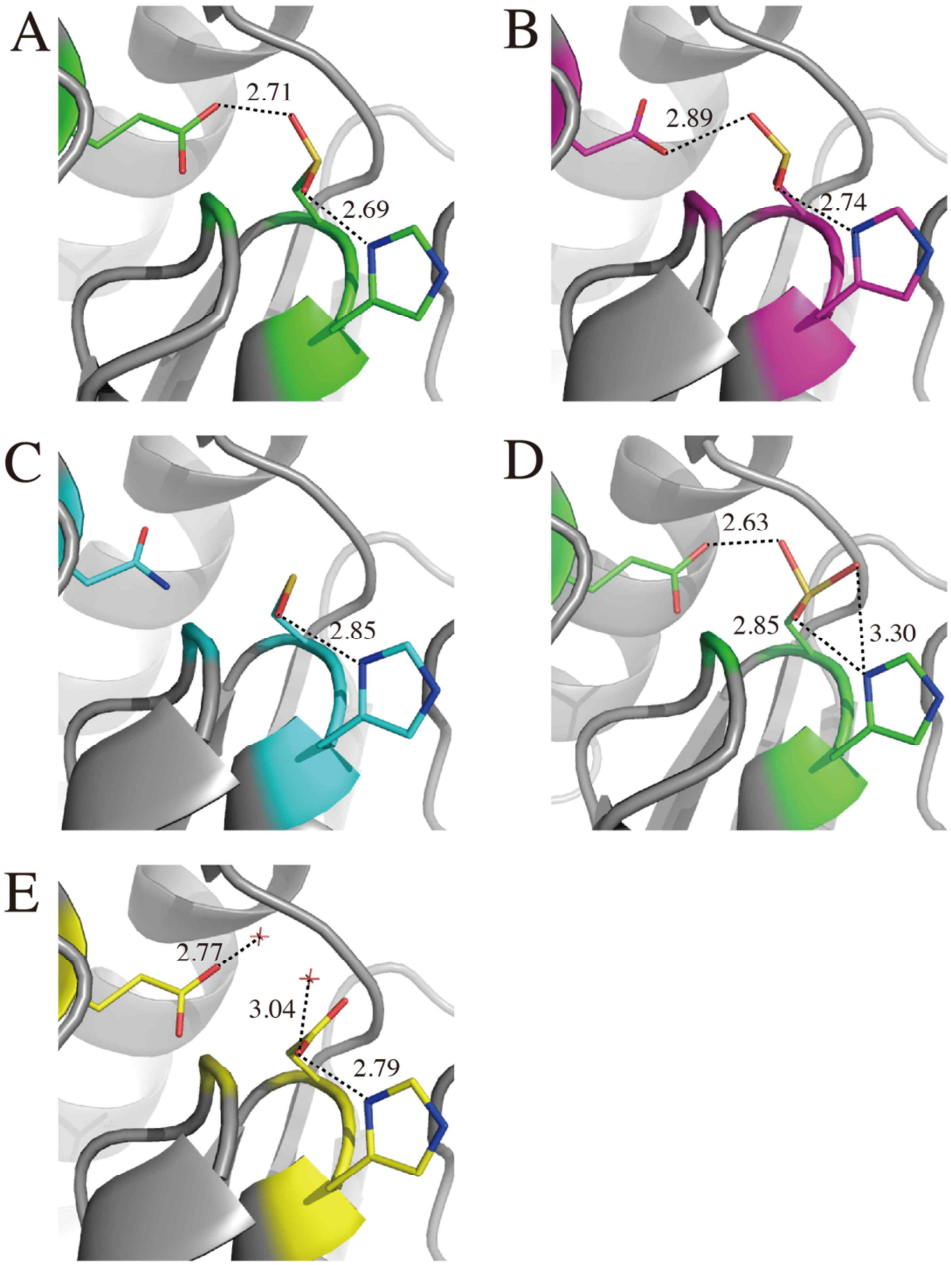

Figure 20. Oxidation state of cysteine at residue 105.

(A) Cys105 in wild type SAV1875 is oxidized to Cys105-SO_2H in the crystal structure. (B) Cys105 in E17D SAV1875 is oxidized to Cys105-SO_2H in the crystal structure. (C) Cys105 in E17N SAV1875 is oxidized to Cys105-SOH in the crystal structure. (D) Cys105 in over-oxidized SAV1875 is oxidized to Cys105-SO_3H in

the crystal structure. (E) In the crystal structure of C105D, two water molecules are inserted. Asp105 and Glu17 form hydrogen bond with each of water molecules.

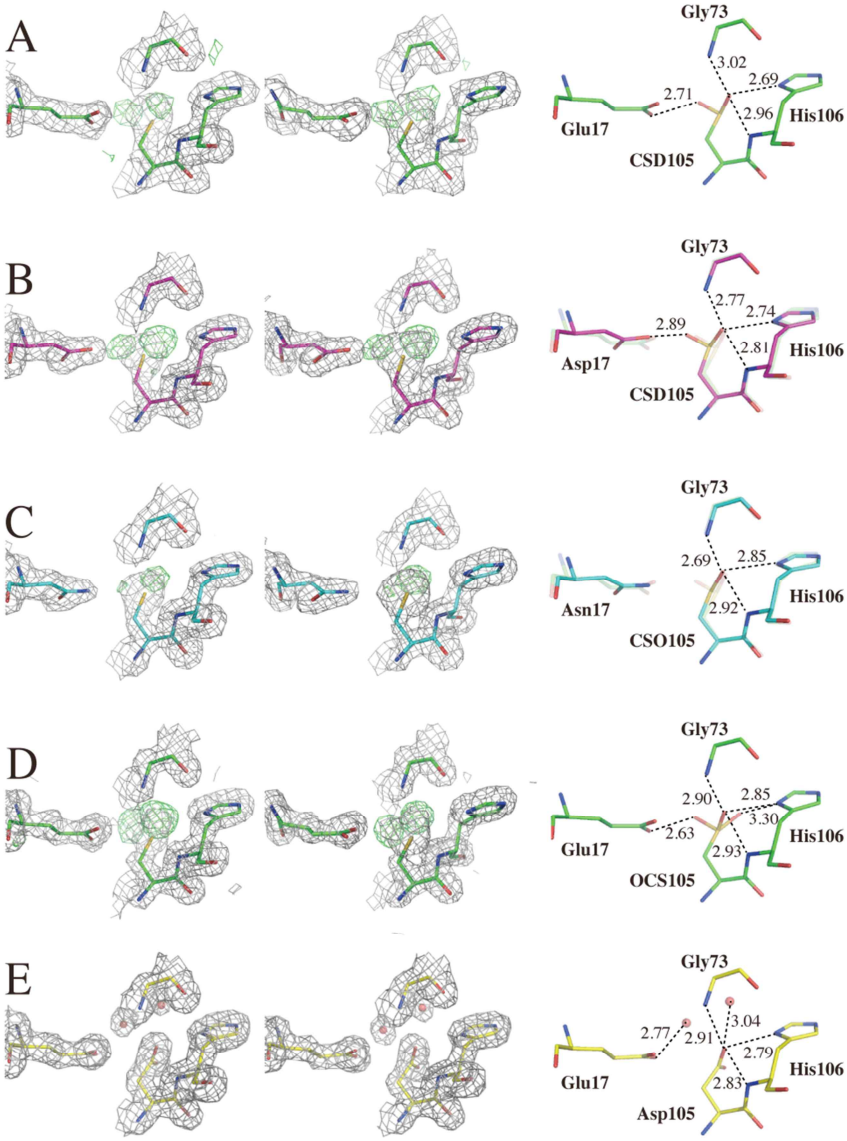

Figure 21. Hydrogen bonds around Cys105

The electron density map of Cys105 before the introduction of oxygen atoms and interacting hydrogen bonds after the introduction. The 2*Fo-Fc* electron density map

contoured at a level of 1.0σ is shown in grey and the *Fo-Fc* electron density map contoured at a level of 3.0σ is illustrated in green. Distances are given in Angstroms. *Left panels*, chain A; *Middle panels*, chain B; *Right panels*, hydrogen bonds are shown. (A) Cys105 in the wild type is oxidized to Cys105-SO_2H. (B) Cys105 in E17D shows Cys105-SO_2H (magenta) and the corresponding region in wild type (light green). (C) Cys105 in E17N shows Cys105-SOH (blue) and the corresponding region in wild type (light green). (D) Cys105 in over-oxidized SAV1875 is oxidized to Cys105-SO_3H, which shows additional density for the sulfonic group in chain A (left), but Cys105-SO_2H in chain B (right). (E) In C105D, Asp105 mimics Cys105-SO_2H, but the geometry of the oxygen atoms is different from that of Cys105-SO_2H. However, Glu17 and Asp105 are stabilized by hydrogen bonds with the introduction of water molecules. Figures were created with PyMOL .

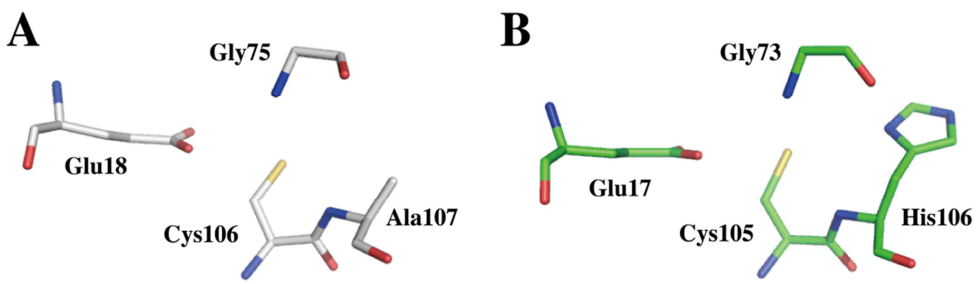

Figure 22. Local difference around the reactive cysteine in DJ-1 (left) and SAV1875 (right).

Histidine at residue 106 in SAV1875, which is an alanine in DJ-1, causes the opposite behavior of cysteine oxidation state in glutamate mutants.

However, in SAV1875, the His106 side chain provides additional strong hydrogen bonding to oxidized Cys105 (Figure 21). Therefore, the oxygen atom of Cys105-

SOH in the E17N mutant is toward the amide pocket. The occupancy of the oxygen atoms of Cys106-SO_2H in E17D mutant is greater toward amide pocket because of this hydrogen bond. Moreover, because there is a greater distance between Cys105 and Asn17 of E17N than Cys105 and Asp17 of E17D mutant, cysteine oxidation to Cys105-SO_2H in E17N SAV1875 remains incomplete (Figure 20B, 20C, 21B, and 21C). Cys105-SO_2H was observed as a main peak in both the E17D and E17N mutants in a mass spectrum that were incubated under H_2O_2 conditions. Therefore, we propose that the E17N mutant is oxidation-impaired, but not oxidation-deficient. Cys105 in wild type SAV1875 under H_2O_2 conditions can form Cys105-SO_3H in chain A. Each oxygen atom is stabilized by a hydrogen bond (Figure 21D). Because the molecular geometries of aspartate and cysteinesulfinic acid are different, the C105D mutant is not topologically the same as wild type SAV1875 (Figure 23). However, the introduction of water molecules, which form hydrogen bonds with Glu17 and Asp105, yields a stable structure (Figure 20E, 21E).

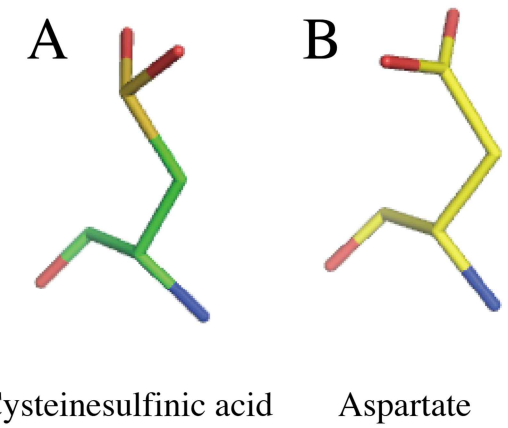

Figure 23. The geometry of cysteinesulfinic acid is not the same as aspartate.

3.3.5. Oxidation propensity of Cys105 in SAV1875

Among all amino acids in a protein, the most oxidation-susceptible residues are the sulfur-containing ones, cysteine and methionine [56-58]. Because recombinant SAV1875 lacks the only methionine residue at position 1 and possesses a single cysteine residue at position 105, the oxidation-reduction state in solution could be conveniently monitored by mass spectrometry and PAGE [57]. Cysteine undergoes oxidation and reduction reactions and results in four different forms: Cys-SH_2, Cys-SOH, Cys-SO_2H, and Cys-SO_3H [59]. The Cys105 in SAV1875 exists as both Cys105-SH_2 and Cys105-SO_2H in solution. One single intense peak with a M_r of 39 kDa in size exclusion chromatography indicates the presence of only dimer molecules of SAV1875 (data not shown). SDS-PAGE shows a single band as a monomer with a M_r of 19 kDa. In contrast, the mass spectrum contained two peaks with M_r values of 19,565 and 19,597 Da, which is +32 Da compared to the first peak. The two main peaks corresponded to SAV1875-Cys105-SH_2 and SAV1875-Cys105-SO_2H, respectively (calculated mass of 19,565.7 Da without methionine residue at position 1). Native PAGE separates SAV1875 into two main bands. Because the charge-to-mass ratio is preserved during native PAGE, SAV1875 can migrate towards the positively charged electrode depending on its overall negative surface charge without dissociation of the structure. This result corroborates the mass spectrometry, which indicated that SAV1875 exists in both reduced (SAV1875-Cys105-SH_2) and oxidized (SAV1875-Cys105-SO_2H) states. The SAV1875 C105D mutant further supports this finding because the C105D mutant, which lacks the only cysteine that can be oxidized (this recombinant C105D SAV1875 lacks the only methionine residue at position 1), has only one band on native PAGE and only one peak in mass spectrometry (Figure 24). Furthermore, the following methods were used to reduce oxidized Cys105: 1) 5 mM DTT was added to all buffers during purification and the protein was handled quickly on ice; 2) 10 mM DTT was introduced to the final buffer (50 mM Tris-HCl, pH 7.5, 200 mM NaCl, 10 mM DTT); and 3) 1 mM phenylethanesulfonylfluoride (PMSF) was

employed during all purification steps and ablated by DTT. Despite these efforts to reduce the oxidized cysteine, mass spectrometry and native PAGE indicated that SAV1875 retained the two distinctive main bands, SAV1875-SH_2 and SAV1875-SO_2H. Therefore, these data imply that the oxidative modification of Cys105 in SAV1875 is very robust.

Mass spectrometry and native PAGE confirmed that both SAV1875-Cys105-SH_2 and SAV1875-Cys105-SO_2H are further oxidized to SAV1875-Cys105-SO_3H when the protein was exposed to H_2O_2 with a molar ratio of SAV1875:H_2O_2 of 1:50. The mass spectrometry showed an enlarged peak at a M_r of 19,612.9 Da (SAV1875-Cys105-SO_3H) after exposure to H_2O_2, which is +48 Da compared to SAV1875-Cys105-SH_2 (Figure 24). This corresponds with the native PAGE result, which has an additional single band below SAV1875-Cys105-SO_2H, indicating SAV1875-Cys105-SO_3H. Circular dichroism data showed that the secondary structure of SAV1875 is not altered, even if SAV1875-Cys105-SO_2H is further oxidized to the over-oxidized state of SAV1875-Cys105-SO_3H (Figure 25). The crystal structure of over-oxidized SAV1875 was determined to a resolution of 1.65 Å. The electron density distribution surrounding the Cys105 residue suggested over oxidation to Cys105-SO_3H. The S^{γ} atom of Cys105 is oxidized to Cys105-SO_3H in subunit A and Cys105-SO_2H in subunit B (Figure 21D).

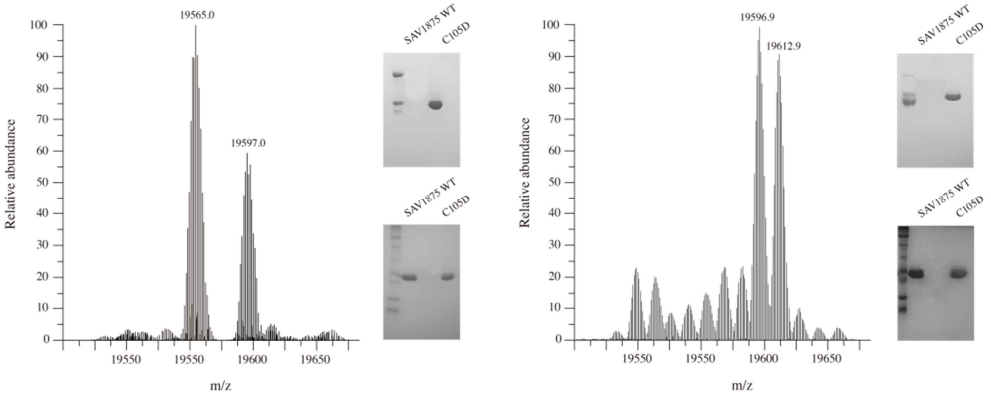

Figure 24. MS spectrometry and PAGE of SAV1875.

Mass spectrometry was used to monitor the oxidation state of SAV1875 in solution. *Left panel* MS analysis of SAV1875. Two major peaks are observed at 19,565.0 and 19,597.0. The calculated mass of SAV1875 is 19,565 Da if the only cysteine, Cys105, is reduced (this recombinant SAV1875 lacks the only methionine residue at position 1). In addition to the first peak, there is another main peak at 19,597 corresponding to two additional oxygen atoms. The right panel corresponds to native PAGE (top) and SDS-PAGE (bottom) analysis. Before exposure to H_2O_2, there were two separate SAV1875 bands in native PAGE. The oxidized band was located in the same region as the C105D. *Right panel* MS analysis of over-oxidized SAV1875. Two main peaks were observed at 19.596.9 and 19612.9, corresponding to SAV1875-Cys105-SO_2H and SAV1875-Cys105-SO_3H, respectively. The right panel corresponds to native PAGE (top) and SDS-PAGE (bottom). For over-oxidized SAV1875, there were three separate bands in native PAGE. One oxidized band is shown at the same region as the C105D and another oxidized band is located underneath the oxidized band. These native PAGE results coincide with the MS analysis.

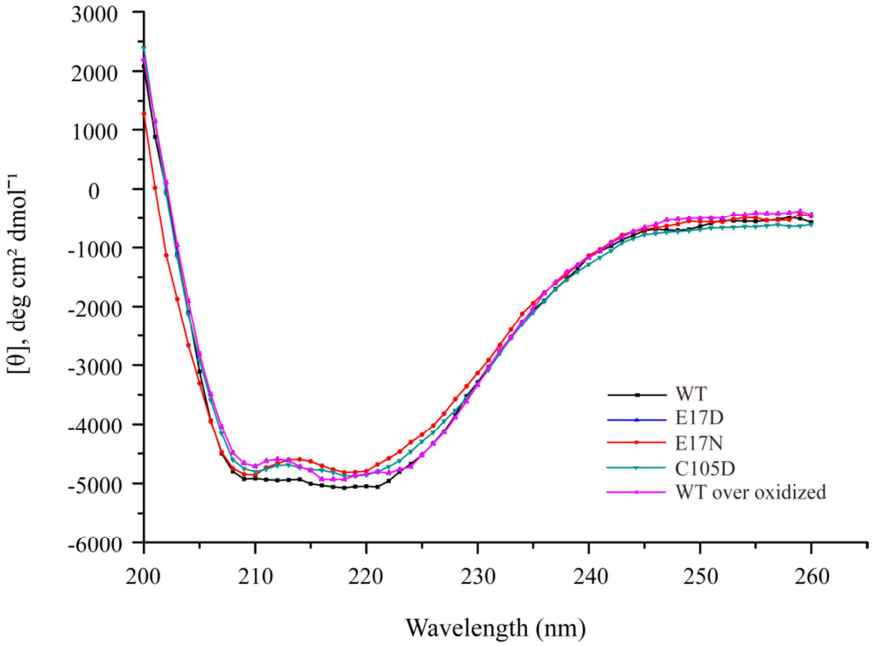

Figure 25. Over-oxidized SAV1875 does not lead to loss of secondary structure. Far-UV CD spectra of wild type (black), E17N (red), E17D (blue), C105D (green) and over oxidized SAV1875 (pink). The spectra were nearly identical, indicating that the E17 or C105 mutations do not affect the overall secondary structure of the protein.

3.3.6. Protease activity of SAV1875 was not detected

SAV1875 has been reported to harbor a *Ph*pI endopeptidase domain, which is found in *Ph*pI from *Pyrococcus horikoshii* (http://www.uniprot.org/uniprot/P0A0K0) [60]. *Ph*pI is an intracellular protease that belongs to the YhbO-type subfamily, and it shows the highest activity in a multimeric complex [14]. Ton1285 is another YhbO-type protein which has proteolytic activity [18]. *Ph*pI and Ton1285 exist as hexamers in solution, converging their catalytic triad towards the solvent accessible center area of the ring-like structure (Figure 26). However, the dimer proteins in the YhbO-type subfamily, recombinant YhbO and DR1199, do not show proteolytic activity

toward peptides or casein [16, 50]. Whereas other type of DJ-1 superfamily, the DJ-1-type protein DJ-1 dimer revealed a greater proteolytic activity toward casein, especially with the deletion of 15 C-terminal residues by enhancing substrate binding affinity [61]. To determine the proteolytic activity, if any, wild type, the SAV1875 mutants, and over-oxidized SAV1875 were used. SAV1875 did not display any significant proteolytic activity towards FITC-casein even after a long incubation time, at a high temperature (more than 37℃) or SAV1875 concentration (up to 50 μM), or in a reducing environment (presence of 1 mM β-mercaptoethanol). A gelatin overlay assay did not show any cleared zones. Therefore, dimeric SAV1875 is surmised not to have a proteolytic function against casein or gelatin (data not shown). If present, the catalytic activity is very low. Although DJ-1-type DJ-1 has proteolytic activity with a catalytic dyad and dimeric state, in YhbO-type proteins, the existence of a catalytic triad and ring-like multimeric structure showed to signify proteolytic function (Figure 26). Moreover, further research is needed on factors that may influence the proteolytic function of DJ-1 superfamily proteins.

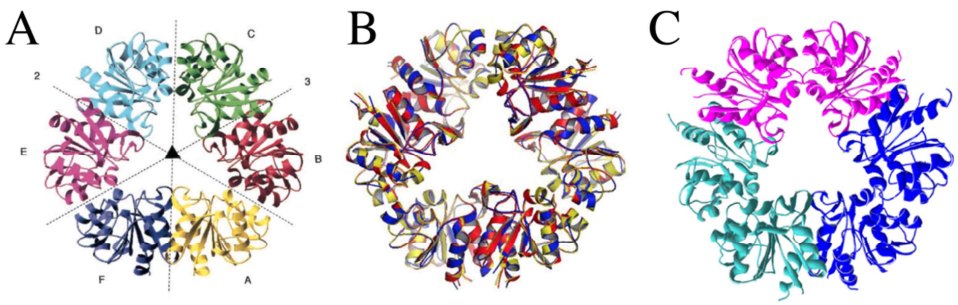

Figure 26. Comparison of oligomeric state in solution of YhbO-type DJ-1 superfamily.

*Ph*pI from *Pyrococcus horikoshii* (A) and Ton1285 from *Thermococcus onnurineus* (B) show hexamer structure in solution, but SAV1875 does not (C).

3.3.7. SAV1875 has chaperone activity

Chaperones are part of a functionally related group of proteins assisting in protein folding under stress conditions or preventing folding defects by binding to unstructured and hydrophobic regions of target proteins. Chaperones in the DJ-1 superfamily, such as Hsp31, work as dimers by forming a canyon and bowl on their dimeric interface [11]. When the surfaces of Hsp31 were viewed, hydrophobic patches were detected around the canyon for the binding of unstructured proteins [40]. DJ-1 and YajL, which are categorized as members of the DJ-1-type subfamily, have also shown chaperone activity. Interestingly, DJ-1 exhibited a greater chaperone activity towards α-synuclein when Cys106 was oxidized to Cys106-SO_2H and lost activity when the cysteine was further oxidized to Cys106-SO_3H, which correlated with a loss in some of its secondary structure [62, 63]. SAV1875 is defined as a member of the YhbO-type subfamily, displaying structural differences from the DJ-1 or Hsp-type subfamily. The YhbO-type proteins with a chaperone function had not yet been identified. However, SAV1875 expresses similar surface patterns of a canyon as Hsp31, DJ-1, and YajL. SAV1875 has a canyon that winds from the dimeric interface to each side of the subunit, and hydrophobic patches are detected around the canyon (Figure 13). These are characteristics of SAV1875 that are distinctive from the YhbO-type proteins. Other YhbO-type proteins are hexamers (*Ph*pI and Ton1285), or dimer YhbO-type proteins (recombinant YhbO and DR1199) lack apparent canyon structure. Furthermore, Cys105 in SAV1875 favors oxidation to Cys105-SO_2H, similar to a DJ-1 protein. Considering these characteristics, SAV1875 is expected to hold unfolded protein, and the oxidation state of Cys105 may play a crucial role in chaperone function.

The wild type, the SAV1875 mutants, and the over-oxidized SAV1875 were tested for chaperone activity using citrate synthase. The observed data shows a chaperone-facilitated renaturation of citrate synthase in the wild type, E17D, E17N,

and C105D mutants. There are no significant differences in the chaperone activity between the wild type and the SAV1875 mutants. However, negative results were obtained with over-oxidized SAV1875, which was previously exposed to a 1:50 molar ratio of SAV1875:H_2O_2. Therefore, we determined that SAV1875 functions as a molecular chaperone with an oxidized Cys105, but it loses chaperone activity when this cysteine is oxidized further to Cys105-SO_3H, even though over-oxidized SAV1875 is structurally stable (Figure 27). Circular dichroism revealed that the secondary structure is well conserved (Figure 25). The native PAGE result showed that the surface charge is preserved in over-oxidized SAV1875 with Cys105-SO_3H (Figure 24) [46]. From this study, we identified SAV1875 as a novel chaperone protein in the YhbO-type subfamily and that the canyon surface structure along with cysteine redox state are the key elements for the chaperone function.

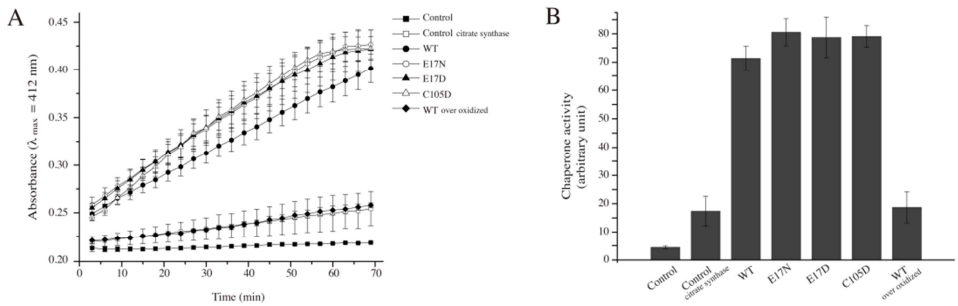

Figure 27. Chaperone activity of SAV1875 depending on cysteine oxidation state. SAV1875 exerts a chaperone function. The chaperone activity was assayed by monitoring an increase in absorbance at 412 nm. (A) The control (■) contained 50 μl of the reaction mixture only, which was 1 mM DTNB, 0.2 mM $MnCl_2$, 0.4 mM oxaloacetic acid, 0.3 mM acetyl-CoA in 100 mM Tris-HCl buffer (pH 8.0). The control with citrate synthase (□) contained an additional 0.75 μg of denatured citrate synthase. A final concentration of 5 μM was used for the wild type (●), E17N (○). E17D (▲), C105D (△), and over-oxidized SAV1875 (◆) and was

added to a citrate synthase reaction mixture. (B) The calculation of chaperone activity at the 70 minutes time point. The data from three scans were averaged.

3.4. Discussion

The cysteine endows proteins with an exceptional biochemistry due to the distinctive characteristics of its thiol group. The thiol group undergoes nucleophilic attack, electron transfer, hydride transfer, hydrogen radical transfer, and oxygen atom transfer reaction [64]. Due to the thiol group, cysteine is involved in redox activity, metal binding properties, catalytic component of enzyme function, and regulation of protein. The properties of thiol group are related with its different structures caused by oxidation. Regarding redox activity and posttranslational modifications, cysteine residues with sulfur in numerous oxidation states are known. The cysteine can form disulfide bond, depending on the cellular location of the protein. These bonds serve mostly to stabilize the protein structure, and the structures of many extracellular proteins are determined by topology of multiple disulfide bonds. There are other oxidative modifications such as sulfenic, sulfinic, and sulfonic acids. Recently, the notion is becoming important since the oxidative modification of cysteine in proteins has been implicated in cellular signaling and regulatory pathways [65, 66].

The DJ-1 superfamily proteins contain absolutely conserved cysteine. From known crystal structures of DJ-1 superfamily proteins, we figured out this cysteine is oxidized from cysteinesulfenic acid (Cys-SOH), cysteinesulfinic acid (Cys-SO_2H), to cysteinesulfonic acid (Cys-SO_3H). Changes in the sulfur oxidation state of cysteine influences the activity of various proteins [64]. Thus, the oxidation status of cysteine and the corresponding structural differences may account for the

function of SAV1875. In addition, study on the DJ-1 superfamily proteins of *S. aureus* is expected to be valuable in better knowledge of stress response mechanism of *S. aureus*, because the DJ-1 superfamily members are mostly known as stress response proteins.

In our crystal structure of wild type SAV1875, Cys105 was oxidized to Cys105-SO_2H, even though it was not intentionally produced. The oxidized Cys105 accepts hydrogen bonds from the Gly73/His106 amide pocket, the His106 side chain, and the protonated O^{ε} atom of Glu17. The residues that are structurally equivalent to Cys105 and Glu17 in SAV1875 are highly conserved in other members of the DJ-1 superfamily, indicating that cysteine and glutamate may play a crucial role in the function of the protein. The influence of Glu17 on the oxidation of Cys105 was verified with the crystal structures of the E17D, E17N, and C105D mutants. In the crystal structures, the hydrogen bond between Cys105 and residue 17 was weakened or eliminated in the glutamate mutants (E17D and E17N). C105D, which mimics cysteinesulfinic acid, had a different configuration of oxygen atoms (O^{ε}) compared to cysteinesulfinic acid, but the hydrogen bonds were maintained due to the introduction of water molecules. Moreover, the cysteine can be further oxidized to Cys105-SO_3H using excess H_2O_2. The crystal structure of over-oxidized SAV1875 revealed a stable formation of Cys105-SO_3H. From our study, we propose that SAV1875 may act as reactive oxygen species scavenger and protect cellular components.

Because the DJ-1 superfamily includes proteins spanning many functions, such as proteases, chaperones, and general stress response proteins, SAV1875 is also predicted to perform similar biological functions. Thus, several functional tests were conducted to determine the function of SAV1875 and the relationship between the oxidation states of cysteine and the differences in protein activity. *Ph*pI, a homolog of SAV1875 in the YhbO-type subfamily, has been identified as a protease [14]. Another YhbO-type protein, Ton1285, also has a proteolytic role [18].

From a structural standpoint, SAV1875 has a sandwich fold and catalytic triad in common but has different in oligomerization states. Unlike dimeric SAV1875, *Ph*pI and Ton1285 exist as a hexamer in solution. On the other hand, DJ-1-type protein DJ-1 shows proteolytic activity as a dimer with the deletion of 15 C-terminus residues [61]. Proteolytic activity was not detected in SAV1875. This analysis indicates that other factors along with oligomeric state are biologically relevant and still require precise characterization.

Hsp31 displays chaperone activity by holding unfolded protein with its canyon and hydrophobic surface. DJ-1 and YajL have shown chaperone activity as well, showing similar surface structure. Interestingly, when Cys106 of DJ-1 was oxidized to Cys106-SO_2H, chaperone activity increased. When the DJ-1 with Cys106-SO_2H was oxidized further, it lost its chaperone activity due to structural perturbation [63]. SAV1875 has similar canyon-shaped surface and oxidized cysteine, suggesting that SAV1875 may work as a chaperone. We discovered that the wild type and SAV1875 mutants assisted in the folding of citrate synthase but over-oxidized SAV1875 did not, even though its structure was maintained. Further detailed studies on diverse substrates and *in vivo* tests are needed to verify the exact mechanism of the SAV1875 chaperone activity.

Here, we predicted the possible functions of SAV1875 and determined that it functions as a chaperone. The characterization of SAV1875 led to the discovery of a new putative chaperone protein in the YhbO-type subfamily. Further research in the DJ-1 superfamily proteins and *in vivo* studies would advance our understanding of the fundamentals of cysteine oxidation and functional events.

Chapter IV. Summary

The cellular stress response is present in all living organisms and it dictates whether the organism adapts, survives, or if injured beyond repair, undergoes death. Thus, the study of stress responses has broad biological applications in microorganisms, plants, animals, and humans in health and disease. Although every cell within an organism is faced with a variety of stresses throughout its life, the detailed mechanism of how it defends from stresses are remain unclear. Resistance is an example of the adaptation of the bacteria to antibiotics. *S. aureus* in a leading cause of nosocomial and community-acquired infections, but mortality rate is increasing because it easily develops antibiotic resistance. Herein, we focused on the structural and functional studies of bacterial stress response proteins. The crystal structure of SAV0551 from Hsp-type DJ-1 subfamily was identified and two different functions of SAV0551 were figured out. It functions as both a chaperone and a glyoxalase III. Cysteine thiol group in SAV0551 is a catalytic nucleophile, which can degrade substrates. Next, the structural and functional changes of YhbO-type DJ-1 subfamily member, SAV1875 were analyzed under oxidative stress condition. SAV1875 accepts oxygen atom through its cysteine residue and forms stable cysteinesulfinic acid (Cys-SO_2H) structure. We discovered a novel chaperone function of SAV1875, but it lost its activity when the protein is oxidized further, to cysteinesulfonic acid (Cys-SO_3H) even though the structure is stable. Further study still needs to be done to verify the exact mechanism, but cysteine is considered to have a role in controlling the activity of protein under stress condition. From our study, we could examine structural changes of cysteine and also, its potential role in catalytic reaction and signaling pathway. This structural and functional study will be helpful for a better understanding of the mechanism of stress response system.

References

1 Archer, G. L. (1998) *Staphylococcus aureus*: a well-armed pathogen. Clinical infectious diseases : an official publication of the Infectious Diseases Society of America. **26**, 1179-1181

2 Dinges, M. M., Orwin, P. M. and Schlievert, P. M. (2000) Exotoxins of *Staphylococcus aureus*. Clinical microbiology reviews. **13**, 16-34, table of contents

3 Becker, K., Harmsen, D., Mellmann, A., Meier, C., Schumann, P., Peters, G. and von Eiff, C. (2004) Development and evaluation of a quality-controlled ribosomal sequence database for 16S ribosomal DNA-based identification of *Staphylococcus* species. Journal of clinical microbiology. **42**, 4988-4995

4 Chambers, H. F. (2001) The changing epidemiology of *Staphylococcus aureus*? Emerging infectious diseases. **7**, 178-182

5 McNicoll, L. and Marsella, M. (2010) The growing problem of methicillin-resistant *Staphylococcus aureus*: will hospitals prevail? Medicine and health, Rhode Island. **93**, 267-270

6 Sieradzki, K. and Tomasz, A. (1996) A highly vancomycin-resistant laboratory mutant of *Staphylococcus aureus*. FEMS microbiology letters. **142**, 161-166

7 Hiramatsu, K. (1998) The emergence of *Staphylococcus aureus* with reduced susceptibility to vancomycin in Japan. The American journal of medicine. **104**, 7S-10S

8 Turco, T. F., Melko, G. P. and Williams, J. R. (1998) Vancomycin intermediate-resistant *Staphylococcus aureus*. The Annals of pharmacotherapy. **32**, 758-760

9 Hanaki, H., Labischinski, H., Sasaki, K., Kuwahara-Arai, K., Inaba, Y. and Hiramatsu, K. (1998) [Mechanism of vancomycin resistance in MRSA strain

Mu50]. The Japanese journal of antibiotics. **51**, 237-247

10 Woods, C. and Colice, G. (2014) Methicillin-resistant *Staphylococcus aureus* pneumonia in adults. Expert review of respiratory medicine. **8**, 641-651

11 Quigley, P. M., Korotkov, K., Baneyx, F. and Hol, W. G. (2003) The 1.6-A crystal structure of the class of chaperones represented by *Escherichia coli* Hsp31 reveals a putative catalytic triad. Proceedings of the National Academy of Sciences of the United States of America. **100**, 3137-3142

12 Subedi, K. P., Choi, D., Kim, I., Min, B. and Park, C. (2011) Hsp31 of *Escherichia coli* K-12 is glyoxalase III. Molecular microbiology. **81**, 926-936

13 Mujacic, M. and Baneyx, F. (2007) Chaperone Hsp31 contributes to acid resistance in stationary-phase *Escherichia coli*. Applied and environmental microbiology. **73**, 1014-1018

14 Du, X., Choi, I. G., Kim, R., Wang, W., Jancarik, J., Yokota, H. and Kim, S. H. (2000) Crystal structure of an intracellular protease from *Pyrococcus horikoshii* at 2 Å resolution. Proceedings of the National Academy of Sciences of the United States of America. **97**, 14079-14084

15 Rawlings, N. D., Morton, F. R. and Barrett, A. J. (2006) MEROPS: the peptidase database. Nucleic acids research. **34**, D270-272

16 Fioravanti, E., Dura, M. A., Lascoux, D., Micossi, E., Franzetti, B. and McSweeney, S. (2008) Structure of the stress response protein DR1199 from *Deinococcus radiodurans*: a member of the DJ-1 superfamily. Biochemistry. **47**, 11581-11589

17 Abdallah, J., Caldas, T., Kthiri, F., Kern, R. and Richarme, G. (2007) YhbO protects cells against multiple stresses. Journal of bacteriology. **189**, 9140-9144

18 Jung, H. J., Kim, S., Kim, Y. J., Kim, M. K., Kang, S. G., Lee, J. H., Kim, W. and Cha, S. S. (2012) Dissection of the dimerization modes in the DJ-1 superfamily. Molecules and cells. **33**, 163-171

19 Wei, Y., Ringe, D., Wilson, M. A. and Ondrechen, M. J. (2007) Identification of functional subclasses in the DJ-1 superfamily proteins. PLoS computational biology. **3**, e10

20 Herrera, F. E., Zucchelli, S., Jezierska, A., Lavina, Z. S., Gustincich, S. and Carloni, P. (2007) On the oligomeric state of DJ-1 protein and its mutants associated with Parkinson Disease. A combined computational and in vitro study. The Journal of biological chemistry. **282**, 24905-24914

21 Ito, G., Ariga, H., Nakagawa, Y. and Iwatsubo, T. (2006) Roles of distinct cysteine residues in S-nitrosylation and dimerization of DJ-1. Biochemical and biophysical research communications. **339**, 667-672

22 Junn, E., Taniguchi, H., Jeong, B. S., Zhao, X., Ichijo, H. and Mouradian, M. M. (2005) Interaction of DJ-1 with Daxx inhibits apoptosis signal-regulating kinase 1 activity and cell death. Proceedings of the National Academy of Sciences of the United States of America. **102**, 9691-9696

23 Mo, J. S., Kim, M. Y., Ann, E. J., Hong, J. A. and Park, H. S. (2008) DJ-1 modulates UV-induced oxidative stress signaling through the suppression of MEKK1 and cell death. Cell death and differentiation. **15**, 1030-1041

24 van Hal, S. J., Jensen, S. O., Vaska, V. L., Espedido, B. A., Paterson, D. L. and Gosbell, I. B. (2012) Predictors of mortality in *Staphylococcus aureus* Bacteremia. Clinical microbiology reviews. **25**, 362-386

25 Gouet, P., Courcelle, E., Stuart, D. I. and Metoz, F. (1999) ESPript: analysis of multiple sequence alignments in PostScript. Bioinformatics. **15**, 305-308

26 Collaborative Computational Project, N. (1994) The CCP4 suite: programs for protein crystallography. Acta crystallographica. Section D, Biological crystallography. **50**, 760-763

27 Dodson, E. J., Winn, M. and Ralph, A. (1997) Collaborative Computational Project, number 4: providing programs for protein crystallography.

Methods in enzymology. **277**, 620-633

28 Vagin, A. and Teplyakov, A. (2010) Molecular replacement with MOLREP. Acta crystallographica. Section D, Biological crystallography. **66**, 22-25

29 Emsley, P. and Cowtan, K. (2004) Coot: model-building tools for molecular graphics. Acta crystallographica. Section D, Biological crystallography. **60**, 2126-2132

30 Murshudov, G. N., Skubak, P., Lebedev, A. A., Pannu, N. S., Steiner, R. A., Nicholls, R. A., Winn, M. D., Long, F. and Vagin, A. A. (2011) REFMAC5 for the refinement of macromolecular crystal structures. Acta crystallographica. Section D, Biological crystallography. **67**, 355-367

31 Brunger, A. T. (1992) Free R value: a novel statistical quantity for assessing the accuracy of crystal structures. Nature. **355**, 472-475

32 Pettersen, E. F., Goddard, T. D., Huang, C. C., Couch, G. S., Greenblatt, D. M., Meng, E. C. and Ferrin, T. E. (2004) UCSF Chimera--a visualization system for exploratory research and analysis. Journal of computational chemistry. **25**, 1605-1612

33 Krissinel, E. and Henrick, K. (2007) Inference of macromolecular assemblies from crystalline state. Journal of molecular biology. **372**, 774-797

34 Lee, G. J. (1995) Assaying proteins for molecular chaperone activity. Methods in cell biology. **50**, 325-334

35 Zhi, W., Landry, S. J., Gierasch, L. M. and Srere, P. A. (1992) Renaturation of citrate synthase: influence of denaturant and folding assistants. Protein science : a publication of the Protein Society. **1**, 522-529

36 Mujacic, M., Bader, M. W. and Baneyx, F. (2004) Escherichia coli Hsp31 functions as a holding chaperone that cooperates with the DnaK-DnaJ-GrpE system in the management of protein misfolding under severe stress conditions. Molecular microbiology. **51**, 849-859

37 Lethanh, H., Neubauer, P. and Hoffmann, F. (2005) The small heat-shock

proteins IbpA and IbpB reduce the stress load of recombinant *Escherichia coli* and delay degradation of inclusion bodies. Microbial cell factories. **4**, 6

38 Sastry, M. S., Korotkov, K., Brodsky, Y. and Baneyx, F. (2002) Hsp31, the *Escherichia coli* yedU gene product, is a molecular chaperone whose activity is inhibited by ATP at high temperatures. The Journal of biological chemistry. **277**, 46026-46034

39 Ben-Zvi, A. P. and Goloubinoff, P. (2001) Review: mechanisms of disaggregation and refolding of stable protein aggregates by molecular chaperones. Journal of structural biology. **135**, 84-93

40 Sastry, M. S., Quigley, P. M., Hol, W. G. and Baneyx, F. (2004) The linker-loop region of *Escherichia coli* chaperone Hsp31 functions as a gate that modulates high-affinity substrate binding at elevated temperatures. Proceedings of the National Academy of Sciences of the United States of America. **101**, 8587-8592

41 Allaman, I., Belanger, M. and Magistretti, P. J. (2015) Methylglyoxal, the dark side of glycolysis. Frontiers in neuroscience. **9**, 23

42 Kizil, G., Wilks, K., Wells, D. and Ala'Aldeen, D. A. (2000) Detection and characterisation of the genes encoding glyoxalase I and II from *Neisseria meningitidis*. Journal of medical microbiology. **49**, 669-673

43 Larkin, M. A., Blackshields, G., Brown, N. P., Chenna, R., McGettigan, P. A., McWilliam, H., Valentin, F., Wallace, I. M., Wilm, A., Lopez, R., Thompson, J. D., Gibson, T. J. and Higgins, D. G. (2007) Clustal W and Clustal X version 2.0. Bioinformatics. **23**, 2947-2948

44 Laemmli, U. K. (1970) Cleavage of structural proteins during the assembly of the head of bacteriophage T4. Nature. **227**, 680-685

45 Louis-Jeune, C., Andrade-Navarro, M. A. and Perez-Iratxeta, C. (2012) Prediction of protein secondary structure from circular dichroism using theoretically derived spectra. Proteins. **80**, 374-381

46 Greenfield, N. J. (2006) Using circular dichroism spectra to estimate

protein secondary structure. Nature protocols. **1**, 2876-2890

47 Twining, S. S. (1984) Fluorescein isothiocyanate-labeled casein assay for proteolytic enzymes. Analytical biochemistry. **143**, 30-34

48 Vandooren, J., Geurts, N., Martens, E., Van den Steen, P. E. and Opdenakker, G. (2013) Zymography methods for visualizing hydrolytic enzymes. Nature methods. **10**, 211-220

49 Morgunov, I. and Srere, P. A. (1998) Interaction between citrate synthase and malate dehydrogenase. Substrate channeling of oxaloacetate. The Journal of biological chemistry. **273**, 29540-29544

50 Abdallah, J., Kern, R., Malki, A., Eckey, V. and Richarme, G. (2006) Cloning, expression, and purification of the general stress protein YhbO from *Escherichia coli*. Protein expression and purification. **47**, 455-460

51 Wilson, M. A., St Amour, C. V., Collins, J. L., Ringe, D. and Petsko, G. A. (2004) The 1.8 Å resolution crystal structure of YDR533Cp from *Saccharomyces cerevisiae*: a member of the DJ-1/ThiJ/*Pf*pI superfamily. Proceedings of the National Academy of Sciences of the United States of America. **101**, 1531-1536

52 Blackinton, J., Lakshminarasimhan, M., Thomas, K. J., Ahmad, R., Greggio, E., Raza, A. S., Cookson, M. R. and Wilson, M. A. (2009) Formation of a stabilized cysteine sulfinic acid is critical for the mitochondrial function of the parkinsonism protein DJ-1. The Journal of biological chemistry. **284**, 6476-6485

53 Wilson, M. A., Ringe, D. and Petsko, G. A. (2005) The atomic resolution crystal structure of the YajL (ThiJ) protein from *Escherichia coli*: a close prokaryotic homologue of the Parkinsonism-associated protein DJ-1. Journal of molecular biology. **353**, 678-691

54 Bandyopadhyay, S. and Cookson, M. R. (2004) Evolutionary and functional relationships within the DJ-1 superfamily. BMC evolutionary biology. **4**, 6

55 Witt, A. C., Lakshminarasimhan, M., Remington, B. C., Hasim, S.,

Pozharski, E. and Wilson, M. A. (2008) Cysteine pK_a depression by a protonated glutamic acid in human DJ-1. Biochemistry. **47**, 7430-7440

56 Rinalducci, S., Murgiano, L. and Zolla, L. (2008) Redox proteomics: basic principles and future perspectives for the detection of protein oxidation in plants. Journal of experimental botany. **59**, 3781-3801

57 Roeser, J., Bischoff, R., Bruins, A. P. and Permentier, H. P. (2010) Oxidative protein labeling in mass-spectrometry-based proteomics. Analytical and bioanalytical chemistry. **397**, 3441-3455

58 Stadtman, E. R. and Levine, R. L. (2003) Free radical-mediated oxidation of free amino acids and amino acid residues in proteins. Amino acids. **25**, 207-218

59 Wani, R., Nagata, A. and Murray, B. W. (2014) Protein redox chemistry: post-translational cysteine modifications that regulate signal transduction and drug pharmacology. Frontiers in pharmacology. **5**, 224

60 Kuroda, M., Ohta, T., Uchiyama, I., Baba, T., Yuzawa, H., Kobayashi, I., Cui, L., Oguchi, A., Aoki, K., Nagai, Y., Lian, J., Ito, T., Kanamori, M., Matsumaru, H., Maruyama, A., Murakami, H., Hosoyama, A., Mizutani-Ui, Y., Takahashi, N. K., Sawano, T., Inoue, R., Kaito, C., Sekimizu, K., Hirakawa, H., Kuhara, S., Goto, S., Yabuzaki, J., Kanehisa, M., Yamashita, A., Oshima, K., Furuya, K., Yoshino, C., Shiba, T., Hattori, M., Ogasawara, N., Hayashi, H. and Hiramatsu, K. (2001) Whole genome sequencing of meticillin-resistant *Staphylococcus aureus*. Lancet. **357**, 1225-1240

61 Chen, J., Li, L. and Chin, L. S. (2010) Parkinson disease protein DJ-1 converts from a zymogen to a protease by carboxyl-terminal cleavage. Human molecular genetics. **19**, 2395-2408

62 Shendelman, S., Jonason, A., Martinat, C., Leete, T. and Abeliovich, A. (2004) DJ-1 is a redox-dependent molecular chaperone that inhibits alpha-synuclein aggregate formation. PLoS biology. **2**, e362

63 Zhou, W., Zhu, M., Wilson, M. A., Petsko, G. A. and Fink, A. L. (2006)

The oxidation state of DJ-1 regulates its chaperone activity toward alpha-synuclein. Journal of molecular biology. **356**, 1036-1048

64 Giles, N. M., Watts, A. B., Giles, G. I., Fry, F. H., Littlechild, J. A. and Jacob, C. (2003) Metal and redox modulation of cysteine protein function. Chemistry & biology. **10**, 677-693

65 Biswas, S., Chida, A. S. and Rahman, I. (2006) Redox modifications of protein-thiols: emerging roles in cell signaling. Biochemical pharmacology. **71**, 551-564

66 Finkel, T. (2000) Redox-dependent signal transduction. FEBS letters. **476**, 52-54

국문초록

Staphylococcus aureus 는 가장 잘 알려진 병원성 균주 중 하나이다. 식중독, 피부감염 등 가벼운 증상부터 심내막염, 패혈증에 이르는 심각한 감염성 질환을 일으키는 균주로 알려져 있지만 환경 변화에 대한 적응력이 뛰어나고 각종 항생제에 내성을 가진 슈퍼박테리아 strain 인 MRSA, VISA, VRSA 가 지속적으로 출현하는 것이 심각한 문제로 대두되고 있다. DJ-1/ThiJ/*Ph*pI superfamily 는 생명체의 모든 계에 분포하는 단백질의 그룹 중 하나로 주로 세포의 스트레스 대응 매커니즘에 관여되어 있다고 알려져 있다. 본 연구에서는 다양한 항생제에 내성을 보이는 VISA 인 *S. aureus* Mu50 유래의 DJ-1/ThiJ/*Ph*pI superfamily 단백질인 SAV0551 과 SAV1875 의 구조와 기능에 대해 연구하였다. SAV0551 은 구조상 Hsp-type DJ-1 subfamily 에 속하며 반응성 높은 Cysteine 이 190 번 위치에 존재한다. Cys190 은 His191, Asp221 과 catalytic triad 를 이루고 있다. catalytic triad 와 그 기능의 차이를 알기 위하여, C190A, C190D 의 mutant 들이 디자인 되었다. 본 연구에서 우리는 SAV0551 이 chaperone 이자 glyoxalase III 임을 밝혔다. 하지만, C190A 와 C190D 는 chaperone 기능은 여전히 가지고 있지만 glyoxalase III 효과를 잃었다. SAV1875 는 그 구조상 YhbO-type DJ-1 subfamily 에 속하며 DJ-1/ThiJ/*Ph*pI superfamily 의 단백질의 공통된 특징인 반응성이 높은 cysteine 을 105 번 위치에 가지고 있다. 이 cysteine 은 His106, Asp77 과 함께 catalytic triad 를 이루고 있다. Cys105 는 크리스탈 구조상에서 산화되어있고, 매우 안정화 되어 있으며 이는 SAV1875 의 mutant 인 E17D, E17N, C105D 으로 확인할 수

있었다. SAV1875 Cys105 는 H_2O_2 상태에서 과산화 시켰을 때, Cys105-SO_3H (cysteinesulfonic acid)로 완전하게 산화되며 이 또한 매우 안정적인 구조를 보이고 있었다. SAV1875 와 mutant 를 이용하여 그 활성을 실험한 결과, SAV1875 는 chaperone 으로 작용하며 그 기능은 Cys105 의 산화상태와 관련이 있음을 알 수 있었다. 본 연구를 바탕으로 우리는 *S. aureus* 에서 chaperone 으로 작용하는 SAV0551 과 SAV1875 의 구조를 규명하였고, SAV0551 의 catalytic triad 와 관련된 glyoxalase III 의 기능을 알 수 있었으며, cysteine 의 다양한 산화상태를 SAV1875 의 변이와 과산화 구조에서 밝혔다. Cysteine 의 산화는 단백질의 기능에서 중요한 역할을 한다는 것을 SAV1875 의 chaperone 실험을 통해 제시하였다.

주요어: DJ-1/ThiJ/*Pf*pI superfamily*, Staphylococcus aureus*, cysteine, oxidation, chaperone

학번: 2011-30503